UNIVERSITY OF LONDON THESIS

Degree PhD Year 2005 Name of Author NIELSEN, T. A.

Glutamate diffusion and AMPA receptor activation in the cerebellar glomerulus

Thomas Aagaard Nielsen

Department of Physiology

University College London

A thesis submitted to the University of London

for the degree of Doctor of Philosophy

January 2005

ProQuest LLC
789 East Eisenhower Parkway
P.O. Box 1346
Ann Arbor, MI 48106-1346

Abstract

Glutamate release onto α-amino-3-hydroxy-5-methyl-4-isoxazolepropionic acid receptors (AMPARs) is the primary mechanism of fast synaptic transmission in the mammalian brain. Previous studies have revealed that at the cerebellar mossy-fibre to granule cell synapse, the AMPAR mediated synaptic current consists of a fast-rising and a slow-rising component. The aim of this thesis is to examine the properties of release, diffusion and receptor activation underlying these two components.

Two plausible mechanisms could underlie the slow-rising current: spillover of glutamate from neighbouring synaptic contacts and prolonged local release of glutamate via a narrow fusion pore. Using simulations of glutamate diffusion and receptor activation, I show that lowering the diffusion coefficient of glutamate in the synaptic cleft (D_{glut}), which is unknown but can be modulated with macromolecules, has different effects on currents mediated by these two mechanisms. Recordings of the effect of perfusion of dextran (43 kDa) are consistent with the spillover model and also indicate that D_{glut} is approximately 3-fold lower than in free solution.

I show using simulations that linear diffusion cannot alone account for the acceleration of the decay of the synaptic current observed at this synapse in lower release probability, but that it can result from non-linear activation of AMPARs. Evidence is presented that diffusion is linear and only one vesicle is released per active zone. In addition, I have extended the diffusion-reaction model of the synapse to develop a framework for examining properties of synaptic AMPARs using glutamate uncaging. I demonstrate that certain kinetic properties of synaptic receptors can be measured using this technique and derive a kinetic model based on preliminary data.

Together, these data fill shortcomings in our understanding of synaptic function. Based on the present results, I construct a model of synaptic transmission

that explains previous observations.

CONTENTS

LIST OF FIGURES

LIST OF TABLES

List of Abbreviations

$[Ca^{2+}]$	Calcium concentration
$[Ca^{2+}]_o$	Extracellular calcium concentration
$[glut]_{cleft}$	Glutamate concentration in the synaptic cleft
ACh	Acetylcholine
ACSF	Artificial cerebrospinal fluid
AMPA	α-amino-3-hydroxy-5-methyl-4-isoxazolepropionate
AMPAR	α-amino-3-hydroxy-5-methyl-4-isoxazolepropionate receptor
AP	Action potential
APV	2-amino-5-phosponovalerate
BAPTA	1,2-bis(2-aminophenoxy)ethane-N,N,N′,N′-tetraacetic acid
Con	Control
Dex	Dextran
D_{glut}	Diffusion coefficient of glutamate in the synaptic cleft
EM	Electron microscopy
EPP	End-plate potential
EPSC	Excitatory potsynaptic current
EPSP	Excitatory potsynaptic potential
FWHM	Full width at half maximum
GABA	γ-aminobutyric acid

GC	Granule cell
HRP	Horse-radish peroxidase
Kyn	Kynurenic acid
LTD	Long-term depression
LTP	Long-term potentiation
mEPP	Miniature end-plate potential
mEPSC	Miniature excitatory postsynaptic current
MF	Mossy fibre
mGluR	Metabotropic glutamate receptor
MNI	4-methoxy-7-nitroindolinyl
NA	Numerical aperture
NMDA	N-methyl-D-aspartate
NMDAR	N-methyl-D-aspartate receptor
NMJ	Neuromuscular junction
PLR	Prolonged local release
P_{open}	Open probability
$P_{open}(t)$	Open probability waveform
PSD	Postsynaptic density
RLR	Rapid local release
τ_n	n^{th} time constant
τ_w	Weighted time constant
UV	Ultraviolet
TBOA	DL-threo-β-benzyloxyaspartate

List of Publications

T.A. Nielsen, D.A. DiGregorio & R.A. Silver (2003): Release probability dependent changes of the AMPA receptor EPSC waveform at the rat cerebellar mossy fibre to granule cell synapse. *J. Physiol.*, **547P** C33.

T.A. Nielsen, D.A. DiGregorio & R.A. Silver (2003): Slowed Glutamate Diffusion Distinguishes Between EPSCs Mediated by Prolonged Local Release and those Arising from Spillover of Neurotransmitter. *Society for Neuroscience Abstracts*, **29**: 903.16.

P.B. Sargent, T. Nielsen, D.A. DiGregorio & R.A. Silver (2003): Time Course of Uniquantal Release at the Cerebellar Mossy Fiber-Granule Cell Synapse. *Society for Neuroscience Abstracts*, **29**: 686.12.

T.A. Nielsen, D.A. DiGregorio & R.A. Silver (2004): Modulation of glutamate mobility reveals the mechanism underlying slow-rising AMPA receptor EPSCs and the diffusion coefficient in the synaptic cleft. *Neuron*, **42 (5)**, 757-71.

D.A. DiGregorio, T.A. Nielsen & R.A. Silver (2004): Investigation of Synaptic AMPA Receptors with Glutamate Uncaging using a Diffraction-Limited UV Spot. *Society for Neuroscience Abstracts*, **30**: 404.4.

Acknowledgements

I find it difficult to imagine a better place to learn synaptic physiology than Angus Silver's laboratory. I would like to express my profound gratitude for the many hours Angus spent explaining the minutiae of neuroscience and listening to my often ill-conceived ideas. Angus's encouragement of creative thinking made my research both enlightening and enjoyable.

I would like to thank David DiGregorio, both in his capacity as a teacher and a close collaborator. His insistence on thoroughness, and on understanding every angle of a result or a theory, improved my work immeasurably.

I would also like to thank the various people who have worked in Angus's lab over the last three years. Simon Mitchell's patience was very helpful in my first weeks on the rig, and we had many good discussions since then. It was a privilege to share the experience of learning slice physiology with Peter Sargent. I have also learned a lot from many insightful discussions with Volker Steuber and Chiara Saviane. Jason Rothman deserves many thanks for his enormous effort in making experiments and analysis more accessible. I would like to thank Padraig Gleeson, Laurance Cathala and Ingo Kleppe for their contribution to both science and morale. I also thank Izumi Fukunaga for her artistic abilities.

I am grateful to the organising committee for PhD programme in Neuroscience at UCL. The advice I received from David Attwell and Alasdair Gibb was

useful throughout my PhD. I would also like to thank Søren Christensen, Wolfgang Mittmann, Pablo Monsivais and Michael Hausser for helpful discussions. The contributions of Alan Hogben and Duncan Farquharson were essential to the success of my experiments.

Much of the theory I have learned over the last years has come from attending the EU Advanced Course in Computational Neuroscience in Trieste, the Optical Techniques for Cell Physiology in Plymouth and the single-channel course run by David Colquhoun at UCL. I am grateful to the faculty, tutors and fellow students at these courses.

I am endebted to my wife, Antonia, for her patience, love and wisdom.

This work was supported by the Wellcome Trust 4-year PhD Programme in Neuroscience.

CHAPTER

ONE

Introduction

The work in this thesis examines the diffusion of neurotransmitter in the synaptic cleft and the activation of postsynaptic receptors. These topics lie at the centre of the field of synaptic physiology. I will therefore first consider the historical developments in the investigation of synaptic function.

1.1 Early developments in synaptic physiology

1.1.1 The neuron doctrine

Synaptic physiology grew out of one of the first large controversies in the history of modern neuroscience. The debate was that between the reticularists, who thought that the nervous system was cytoplasmically continuous, and those who formulated the neuron doctrine, stating that the nervous system, like the rest of an animal organism, consisted of individual and physically separated cells. Convincing evidence for the latter position provided in the late 19^{th} century led many physiologists to abandon the reticular view. This evidence included the wide variety of axo-dendritic structures revealed by Ramón y Cajal's studies of the ner-

vous system, in particular of the cerebellum, using the Golgi stain method and His's studies of neuronal migration, differentiation and process growth in development (Bennett, 2001). It became clear, then, that the site of contact between an axon and a dendrite must contain a specialised structure for communication between two apposing cells. The name "synapse" for this structure was suggested by the physiologist Charles Sherrington on the advice of the Euripidean scholar Arthur W. Verrall (Bennett, 2001; Kuno, 1994).

In addition, Sherrington made several scientific contributions to the new field. Most importantly, his studies of the spinal cord led him to conclude that each synaptic contact had only a small effect on the postsynaptic neuron such that postsynaptic activity is determined by the summed activity of many synapses, and that synapses can have both excitatory and inhibitory effects. He also suggested that transmission across a synapse is associated with an irreducible delay which cannot be attributed to the axonal conduction.

1.1.2 Chemical or electrical transmission?

The investigation of the physiology of synapses then turned to elucidating the mechanisms mediating synaptic transmission. Two possible mechanisms were proposed: chemical signalling involving a neurotransmitter or electrical coupling between cells. Distinguishing between these two mechanisms would take more than 30 years and became the next large controversy in neuroscience; it became known as 'the soup versus the spark' debate. The most direct evidence in favour of chemical transmission is the isolation of the neurotransmitter itself, a task which occupied early 20^{th} century physiologists and pharmacologists such as Henry Dale and Otto Loewi. Several preparations were used in the early studies of synaptic physiology, of which the neuromuscular junction (NMJ) and the

vagus nerve terminal are arguably the most important. The toxin curare had been known to block neuromuscular excitation from Claude Bernard's experiments in 1844 (Kuffler *et al.*, 1984). Stimulation of the vagus nerve decreases the frequency of cardiac action potentials (APs) and thereby slows the heartbeat. This slowing can be blocked with atropine.

Acetylcholine was synthesised by Hunt and Taveau in 1906, who noted its powerful effect on blood pressure, and that this effect can be blocked by atropine (Bennett, 2001). Henry Dale then carried out a systematic study of the effect of acetylcholine on synaptic transmission in 1914, which led him to conclude that acetylcholine had the same effect as vagus nerve stimulation. Otto Loewi provided conclusive evidence that vagus nerve transmission was chemical in 1921. His experiment consisted of perfusing isolated hearts with Ringer's solution before stimulating the vagus nerve. After the slowing of the heart beat rate was observed, the perfused solution was collected and applied to a second isolated heart, which then slowed its rate. A control experiment determined that this effect was blocked by atropine. Loewi called the chemical responsible for vagus transmission "vagusstoff." Furthermore, Dale isolated acetylcholine from the spleen, indicating that this compound was endogenous to biological tissue (Dale & Dudley, 1929).

However, the time scale of the chemical transmission at the vagus nerve led other physiologists to doubt the applicability of chemical transmission at other synapses. John Eccles determined the timecourse of vagus inhibition of cardiac cycle in 1934 and showed that the effect manifested itself on a timescale of hundreds of milliseconds. On the contrary, neuromuscular excitation was at least an order of magnitude faster. Eccles in particular continued to consider electrical transmission the dominating mechanism, based on the timing of synaptic transmission, until the 1950s. Investigations turned to the neuromuscular junction in

the 1930s. Stephen Kuffler measured the synaptic delay, originally proposed by Sherrington, and found it to be on the order of 0.5 msec (Kuffler *et al.*, 1984). This in itself was a problem for an electrical theory, which would predict no delay if the synapse is effectively a resistor. In 1938, Gopfert and Schaefer recorded the potential across the muscle cell membrane, and applied curare to the muscle in a dose that reduces the synaptic strength to below the threshold for action potential generation. Under these conditions, nerve stimulation induced a slower local depolarisation in the muscle, which became known as the end-plate potential (EPP). Experiments over the next few years by Eccles, Katz and Kuffler indicated that the EPP is essential in generating the postsynaptic action potential and that the EPP is graded in it intensity unlike the all-or-none AP. These experiments led to the hypothesis that at the NMJ, innervation of the AP in the presynaptic terminal initiates a process that eventually leads to release of acetylcholine. Acetylcholine diffuses to receptors on the muscle surface, producing a current which depolarises the muscle. However, the most convincing evidence for chemical transmission came from Katz's elucidation of the mechanism of acetylcholine release.

1.1.3 The quantal hypothesis of synaptic transmission

When investigating the EPP, Fatt & Katz (1952) discovered that when amplifying the membrane potential of the curarized muscle with a high gain, small spontaneous EPPs appeared in the absence of stimulation of the presynaptic fibre. These events, which they called miniature EPPs (mEPPs), occurred at random, and had a timecourse similar to the presynaptically evoked EPP, although it was smaller in amplitude. Fatt and Katz considered whether this could be due to leakage of individual ACh molecules from the synaptic terminal. This hypothesis seemed

unlikely, because they estimated that the size of the mEPP corresponds to the response to an order of thousands of ACh molecules. In addition, perfusion of small concentrations did not increase the frequency of mEPPs. Using an extracellular recording electrode, they determined that mEPPs could be confined to localised active spots on the muscle. Fatt and Katz also investigated the effect of removing the ions Na^+ and Ca^{2+} from the extracellular solution. Na^+ removal decreased both the evoked EPP and the mEPP, whereas Ca^{2+} removal reduced the evoked EPP but had little effect on the mEPP. These experiments indicated that the mEPPs were caused by the simultaneous release of a relatively large amount of ACh in a packet. Since the mEPP shared some properties of the evoked EPP, it raised the possibility that the evoked EPP in fact was the sum of several mEPPs.

Del Castillo & Katz (1954) explored this possibility. They outlined the following hypothesis: that the presynaptic fibre contains a large number n of packets, or 'quanta,' of neurotransmitter that each, upon a presynaptic AP, can be released with probability p, and that p is regulated by the extracellular Ca^{2+} concentration ($[Ca^{2+}]_o$). If p is small and n is large, such that the average number of vesicle released per trial (the quantal content) is m=np, the number of released quanta on a given trial will follow a Poisson distribution, such that the probability of seeing j quanta on a particular trial is equal to

$$P_j = \frac{e^{-\mathrm{m}}(\mathrm{m})^{\mathrm{j}}}{j!} \tag{1.1}$$

i.e. $P_0 = e^{-\mathrm{m}}$, or $\mathrm{m} = \ln \frac{\text{trials}}{\text{failures}}$. If the quantum underlying the evoked EPP is the same as that underlying the mEPP, m will also equal the ratio of the amplitudes of the evoked EPP and the mEPP. Del Castillo and Katz recorded a large number of trials of evoked EPPs under low $[Ca^{2+}]_o$ and found a good agreement between

the values for m predicted from Poisson theory and from the size of the mEPP. In further tests of the quantal hypothesis, they found that the histogram of evoked EPP amplitudes could be fit well by the multimodal distribution predicted by a Poisson distribution with release of integral numbers of quantal, when taking into account the variance of unitary quantal events. In addition, the Poisson distribution predicts a coefficient of variation of $\frac{1}{\sqrt{m}}$, which was consistent with recordings where $m < 10$. This number is likely to provide a limit for applicability of the Poisson description to synaptic transmission, as expected from this distribution.

Before detailing the developments in synaptic physiology after the "soup vs spark" debate, it is worth mentioning that in fact, electrical transmission does occur at some synapses. For instance, the crayfish NMJ, as suggested by Paul Fatt and shown by Furshpan & Potter (1957), is electrical: transmission is bidirectional and has a short latency. Superthreshold stimulation of the presynaptic fibre is also not necessary for inducing a current in the muscle. Electrical synapses are found throughtout the mammalian brain (Connors & Long, 2004).

1.1.4 The role of calcium in neurotransmitter release

The experiments of Del Castillo & Katz (1954), which showed that the probability of release of a quantum is dependent on the extracellular calcium concentration, raised the question of the mechanism of calcium involvement in transmitter release. This issue was addressed by first examining the quantitative relationship between transmitter release and extracellular calcium. Del Castillo and Katz postulated that calcium binds a carrier molecule X to form the complex CaX, which induces transmitter release. Jenkinson (1957) found that this formalism predicted the relationship between $[Ca^{2+}]_o$ and transmitter release only in the high range of $[Ca^{2+}]_o$. The timing of the Ca^{2+} dependence of transmitter release was examined

by Katz & Miledi (1967), in which $[Ca^{2+}]_o$ was rapidly increased by iontophoresis with specific timing with respect to a pulse to the presynaptic nerve. It was found that Ca^{2+} raised the level of transmitter release only if it was applied before, rather than after, the presynaptic pulse, indicating that the presence of Ca^{2+} is essential during or immediately after the presynaptic depolarisation, rather than during the postsynaptic conductance. Dodge & Rahamimoff (1967) examined transmitter release in the low range of $[Ca^{2+}]_o$, and found that in this region the amount of transmitter release is best predicted by assuming that approximately four Ca^{2+} ions must bind to the X molecule to induce release at the neuromuscular junction. When repeating this experiment at the squid stellate ganglion, Katz and Miledi found that approximately three Ca^{2+} ions were necessary to induce transmitter release. Thus, while it is clear that binding of multiple Ca^{2+} ions are necessary for release, the exact number may differ across preparations.

These studies did not reveal whether the Ca^{2+} sensor was located extracellularly, or whether Ca^{2+} crossed the cell membrane to activate an intracellular sensor. Evidence for the latter hypothesis was provided by Llinas *et al.* (1972), who injected aequorin, a jellyfish protein for which the luminescent properties depend on the local $[Ca^{2+}]$, into the squid stellate ganglion. Stimulation of the presynaptic fibre was associated with an increase in luminescence, indicating an influx of Ca^{2+} ions into the presynaptic terminal. Miledi (1973) then provided evidence that direct injection of Ca^{2+} into the presynaptic terminal induced transmitter release, even in the presence of extracellular manganese ions, which block transmission evoked by electrical stimulation of the presynaptic fibre. Conversely, diminishing the AP-induced intracellular Ca^{2+} signal with the Ca^{2+} chelator BAPTA, which has rapid Ca^{2+}-binding kinetics, reduces the EPSC amplitude (Adler *et al.*, 1991). Taken together, these experiments indicate that depolarisation of the presynaptic fibre leads to an influx of Ca^{2+} ions that bind to a sensor.

1.1.5 The vesicle hypothesis

Anatomical investigation of synaptic ultrastructure was initially difficult due to the size of some structures. Both the synaptic cleft and the neurotransmitter-containing vesicles are on the order of 10-100 nm, well below the resolution of the light microscope. The application of high-resolution electron microscopy (EM) to synaptic preparations in 1954-5, coincidental with the quantal hypothesis, thus allowed the visualisation of these structures for the first time. Firstly, the identification of the synaptic cleft, provided incontrovertible evidence against the reticularist view of the nervous system. Secondly, De Robertis & Bennett (1954) observed a small "granular or vesicular component ... on the presynaptic side of the synapse..." which they called 'synaptic vesicles.' Del Castillo & Katz (1956) suggested that these vesicles were the structural correlates of the quantum.

John Heuser and Thomas Reese, and the group of Bruno Ceccarelli investigated this hypothesis throughout the 1970s. Vesicle depletion can be observed in EM micrographs of tissue fixed after stimulation (Heuser & Reese, 1973) or application of black widow toxin, which causes release at the NMJ (Ceccarelli *et al.*, 1973). The density of vesicles is particularly high near regions that are electrodense both pre- and postsynaptically, known as the active zone. Heuser & Reese (1973) showed that after stimulation, omega-shapes that appeared to be the result of fusion of vesicles with the presynaptic membrane could be observed near the active zone. Further away, larger invaginations were observed in the presynaptic membrane. Heuser and Reese showed that horse-radish peroxidase (HRP) from the extracellular solution could be taken up by the presynaptic terminal if applied during stimulation and was found in synaptic vesicles after fixation. Furthermore, HRP-containing vesicles would disappear following further stimulation. These experiments indicated that after complete fusion of vesicles with the

presynaptic terminal, membrane could be retrieved at a distance from the active zone and recycled into new vesicles.

Ceccarelli *et al.* (1973), based on experiments that used the same experimental paradigm but with prolonged stimulation durations, suggested that rather than full fusion, synaptic vesicles could form a reversible pore with the presynaptic membrane, by which acetylcholine could escape and HRP could diffuse into the vesicle, followed by a closure of the fusion pore. This possibility was suggested based on the abundance of vesicles with thin connections to the presynaptic membrane and the presence of HRP-containing vesicles close to the active zone. This mode of vesicle recycling was called 'kiss-and-run' and contrasted to full exocytosis followed by endocytosis at the periphery of the synapse, as suggested by Heuser and Reese.

The study of the timing of synaptic transmission with EM was made possible with the invention of the rapid freeze technique, where the entire preparation is frozen to 15°K by a copper-plate with millisecond precision following nerve stimulation. Using this technique, Torri-Tarelli *et al.* (1985) was able to demonstrate the temporal coincidence of vesicle fusion with electrophysiological recordings of quanta.

1.1.6 Concepts of postsynaptic receptors

The modern concept of ligand-receptor interaction as the basis for drug action was independently and contemporaneously formed by John Langley and Paul Ehrlich at the end of the 19^{th} century. Ehrlich, an organic chemist, systematically investigated the relationship between chemical structure and biological action of compounds, and Langley studied the effect of plant alkaloids (including nicotine and atropine) on the autonomic nervous system, concluded that drugs formed

compounds with "receptive substances." Ehrlich introduced the analogy of the ligand as "key" and the receptor as a "lock" that opened upon binding with the ligand. Using a sewing thread soaked in nicotine, Langley was able to investigate the distribution of these receptive substances on the muscle surface, and showed that after denervation, nicotine sensitivity spread to the entire muscle surface (Bennett, 2001).

The quantitative study of receptor-ligand interaction was initiated by A.V. Hill's application of the law of mass action, that is

$$A + R \rightleftharpoons AR \tag{1.2}$$

where A is an agonist and R a receptor, to receptor pharmacology. If K is the equilibrium constant for this reaction, it follows that at equilibrium, the occupancy (defined as the proportion of bound receptors) is equal to

$$\frac{[A]}{K + [A]} \tag{1.3}$$

which is the Hill-Langmuir equation. This equation can often fit dose-response curves, that is, plots of biological activity against applied ligand concentration. However, a more general equation which fits a wider range of dose-response curves is the Hill Equation

$$\frac{[A]^n}{[A]^n + EC_{50}^n} \tag{1.4}$$

where n is the Hill coefficient and EC_{50} the agonists concentration that gives the half-maximal response. The Hill equation can be derived assuming

$$nA + R \rightleftharpoons A_nR \tag{1.5}$$

i.e. that simultaneous binding of n ligand molecules per receptor is necessary for biological activity.

Del Castillo & Katz (1957) suggested, for acetylcholine activation of muscle receptors, an intermediary inactive step, such that:

$$A + R \rightleftharpoons AR \rightleftharpoons AR^* \tag{1.6}$$

where the AR^* state signifies the active state of the receptor that depolarises the muscle. The advantage of this formalism is that antagonism (which they called 'inhibition') can be explained by an agent having an equilibrium for the first reaction shifted to the right, but for the second reaction shifted to the left. Katz & Miledi (1972) further developed the concept of the active state. They discovered that perfusion of acetylcholine led to an increase in the membrane noise. They suggested that the noise could originate from the same process as depolarisation by activating conductances with short duration at a frequency related to the local concentration of acetylcholine. By examining the power spectrum of membrane noise in the presence of acetylcholine, they tentatively calculated that the unitary conductance was 100 pS, and that the mEPP was mediated by activation of 1000 such unitary conductances. Anderson & Stevens (1973), using the voltage clamp technique (see chapter 2), arrived at an estimate of 20.5 pS for the single-channel conductance. Neher & Sakmann (1976), using the patch clamp technique to resolve openings of single acetylcholine-gated channels, found an average single channel conductance of 28 pS, and thus provided firm evidence for synaptic receptors acting through the gating of an ionic channel by ligand binding.

1.1.7 Independence of synaptic contacts

Del Castillo & Katz (1954) had shown that under conditions of low release probability, a Poisson model provided a good description of the statistics of neurotransmitter release at the NMJ. One assumption of the Poisson distribution is that fundamental events act independently. However, the release probability was so low that out of perhaps hundreds of available quanta, at most one to three were released per trial. It is therefore possible that under physiological conditions, where the density of released vesicles is higher, quantal events are not independent and therefore do not summate linearly. It is also possible that under conditions of high release probability, two vesicles can be released from the same active zone. These possibilities were explored by Hartzell *et al.* (1975) in a voltage-clamp study of the snake NMJ. They replicated the finding of Katz & Thesleff (1957) that the dose-response curve has a foot in the lower region where supralinear summation occurs (i.e. the Hill coefficient is larger than one). When ACh was focally applied from two pipettes placed less than two μm apart, the peak currents showed linear summation, but the decay of the current caused by stimulation by both pipettes was prolonged compared to the arithmetic sum of the responses to either pipette. This effect could be replicated synaptically by stimulating the presynaptic fibre in the presence of cholinesterase inhibitors. Under these conditions, increasing the release probability and thereby the density of released vesicles prolonged the decay of the postsynaptic current. In contrast, under physiological condition of cholinesterase activity, there was no such dependence of the waveform on the release probability. The authors concluded cholinestrase activity isolates each released quanta to prevent interactions with its neighbours. It is therefore also likely that the release of more than one quanta in the same location happens rarely, if ever, at the NMJ. The same study investigated the pos-

sibility that postsynaptic receptors are saturated by released acetylcholine. Since exogenous application of small concentrations of acetylcholine summate linearly with the nerve-evoked response, saturation of receptors following synaptically released acetylcholine is unlikely.

The hypothesis that released quanta are spatially segregated was further examined by Korn *et al.* (1981). They showed that the statistics of inhibitory synapses onto the goldfish Mauthner cell fit binomial statistics better than Poisson statistics, where binomial statistics describe n independent all-or-none events occurring with probability p, with no restrictions in n or p. In addition, this preparation allows the stimulation and staining with dye of a single presynaptic afferent. Histological analysis of this fibre revealed that the number of presynaptic terminals closely predicts n derived from the binomial fit of the amplitude distribution. Korn *et al.* (1981) proposed what they later called the 'one-vesicle hypothesis,' that even at high release probabilities (up to 0.62 for the inhibitory inputs to the Mauthner cell), at most one vesicle can be released from an active zone. Thus, the parameter n derived from binomial fits can be interpreted as the number of 'release sites.'

1.2 Central glutamatergic synapses

1.2.1 Evidence for glutamate as a neurotransmitter.

Glutamate was shown as early as the 1950s to have excitatory effects when applied to neurons of the central nervous system, and to be present in high concentrations in the brain (Hayashi, 1952; van Harreveld & Mendelson, 1959; Robbins, 1959). However, the acceptance of glutamate as a central excitatory neurotransmitter was more reluctant than for other transmitters. Glutamate is an amino

acid required for protein synthesis, and is synthesised in every cell in the body, not just neurons. This precludes the evidence for glutamate as a neurotransmitter based on its synthesis and presence in neurons. Glutamate also appeared to have a general excitatory effect on almost every neural preparation tested, which seemed difficult to reconcile with the specific actions required of a neurotransmitter. Lastly, Lucas & Newhouse (1957) discovered that application of glutamate to the retina had neurotoxic effects, which at the time seemed an unlikely property of an endogenous neurotransmitter.

However, Logan & Snyder (1971) showed that a glutamate uptake mechanism existed in the brain, later shown to be present in glial cells (Fagg & Lane, 1979). Such an uptake mechanism was known to exist for the accepted neurotransmitters GABA and glycine, and so provided one mechanism whereby glutamate as a putative neurotransmitter could be removed from the synaptic cleft. A second line of evidence for glutamate as a neurotransmitter came from the methodical study by Jeffrey Watkins and his collaborators of the effects of chemical analogues of glutamate on neural activity. By examining the effect of N-methyl-D-aspartate (NMDA), kainic acid and quisqualate, and the antagonism to these effects provided by a range of compounds including 2-amino-5-phosponovalerate (APV) and Mg^{2+} ions Watkins & Evans (1981) were able to distinguish two classes of glutamate-sensitive receptors, NMDA and non-NMDA receptors. Finally, strong evidence for glutamate as a neurotransmitter came from the analysis of isolated synaptic vesicles, which have estimated contents of at least 60 mM (Burger *et al.*, 1989) or 1000 molecules of glutamate (Riveros *et al.*, 1986). The true amount of glutamate per synaptic vesicle is likely to be higher, since these studies were unable to isolate glutamatergic vesicles over synaptic vesicles containing other neurotransmitters. As I will show in chapter four, the amount of glutamate in synaptic vesicles, which is still unknown, has important implications for synap-

tic function and the measurement of unknown synaptic parameters.

1.2.2 Main glutamate receptor types

Glutamate receptors can be divided into three main subtypes based on cloned gene sequences and pharmacological profile: metabotropic, NMDA, and non-NMDA ionotropic receptors, with the latter being futher divided into α-amino-3-hydroxy-5-methyl-4-isoxazolepropionate (AMPA) and kainate receptors. Metabotropic glutamate receptors (mGluRs) are 7-transmembrane domain G-protein coupled receptors divided into three subtypes, namely groups I-III. Activation of group I mGluRs is linked to phosphoinositide hydrolysis, whereas group II and III receptors are coupled to adenylyl cyclase inhibition (Conn & Pin, 1997). All mGluR groups can function as autoreceptors, that is, be expressed on presynaptic glutamatergic terminals where they are activated by glutamate released from the same terminal (Macek *et al.*, 1996; White *et al.*, 2003). Blocking mGluRs can have a small (von Gersdorff *et al.*, 1997) or large effect on release from glutamatergic synapses. MGluRs can also be expressed on GABAergic terminals, where they can be activated by glutamate released from neighbouring glutamatergic synapses (Semyanov & Kullmann, 2000; Mitchell & Silver, 2000b), or postsynaptically, as on Purkinje cells in the cerebellum (Kinney & Slater, 1992; Batchelor *et al.*, 1994).

There are six cloned genes for NMDA receptor subunits, namely NR1, NR2A to D and NR3. The stoichiometry of functional NMDA receptors is controversial, but it may be a tetramer (Schorge & Colquhoun, 2003; Laube *et al.*, 1998) or a pentamer (Hawkins *et al.*, 1999) comprising two NR1 and at least two NR2 subunits (Dingledine *et al.*, 1999). The functional receptor has binding sites for both glycine and glutamate, both of which must be occupied for the receptor to

open. The current-voltage relationship for the NMDA receptor shows a strong outward rectification, such that at hyperpolarized potentials, the conductance of the receptor is small, whereas it increases non-linearly with increasing depolarisation. This non-linearity has been attributed to block of the NMDA pore by extracellular Mg2+ (Nowak *et al.*, 1984). The NMDA current evoked by synaptic release mediates a slow component of the synaptic current (Forsythe & Westbrook, 1988; Perkel & Nicoll, 1993; Hestrin, 1992; Silver *et al.*, 1992), with a rise time of ~8 ms at room temperature (Lester *et al.*, 1990).

There are nine cloned mammalian genes for non-NMDA receptors, called GluR1-7 and KA1-2 in rats and humans. Of these, GluR1-4 (A-D in mouse) are classified as AMPA receptors (AMPARs) and GluR5-7 and KA1-2 as kainate receptors, based on their pharmacological profile (Dingledine *et al.*, 1999). Non-NMDA receptors are likely to be tetramers (Rosenmund *et al.*, 1998; Mano & Teichberg, 1998), with each subunit consisting of four membrane-spanning regions M1-4. The response of AMPA receptors has a rapid rise time (see below) with decay time courses of variable durations (Raman *et al.*, 1994; Mosbacher *et al.*, 1994) and mediates the fast component of glutamatergic transmission (Vignes & Collingridge, 1997). There is recent evidence that kainate receptors have a metabotropic, as well as an ionotropic, role in signalling (Lerma, 2003). In the cerebellum, kainate receptors are expressed on presynaptic terminals, where they can regulate neurotransmitter release (Delaney & Jahr, 2002). The properties of AMPA receptors, which play a central role in this thesis, will be discussed in detail below.

Detailed receptor kinetics have principally been investigated using two methodologies: macroscopic current responses to rapidly perfused agonist (Franke *et al.*, 1987) and single-channel recordings (Neher & Sakmann, 1976; Colquhoun & Hawkes, 1982). Both of these techniques rely on investigating

patches of membrane that have been excised from the cell surface. The relevance of these data to synaptic function is complicated by two potential problems: firstly, it is possible that damage to the receptors or the cytoskeleton can occur during patch excision. Secondly, excised patches are pulled from extrasynaptic regions on the cell surface, whereas released neurotransmitter activates receptors in the synaptic cleft (Nusser, 2000), and synaptic and extrasynaptic receptors may have different properties.

1.2.3 Glutamate transporters

Glutamate is a non-essential amino acid that can be synthesised from glucose via α-oxoglutarate. In the presynaptic cytoplasm, it is present in concentrations of $\sim$10mM (Ishikawa *et al.*, 2002). Three genes have been cloned that encode proteins, VGLUT1-3, responsible for the transport of glutamate from the cytoplasm into synaptic vesicles. Of these, VGLUT1 expression dominates in the cerebral and cerebellar cortex, and VGLUT2 in the brainstem and spinal cord. In the cerebellar granule cell layer, there is evidence for a developmental switch from VGLUT2 to VGLUT1 after postnatal day 21 in mice (Miyazaki *et al.*, 2003). VGLUT3 is expressed in non-glutamatergic cells, including striatal cholinergic interneurons, where its function is unclear (Gras *et al.*, 2002). Vesicular glutamate transporters rely on a proton gradient across the vesicle membrane established by an ATP-driven proton pump, which can be inhibited by Bafilomycin A1. Application of this drug to the presynaptic terminal decreases amplitude and frequency of miniature excitatory postsynaptic currents (mEPSCs) in cultured hippocampal neurons without changing the release probability as measured with destaining of the lipophilic dye FM1-43, or the sensitivity to exogenous application of glutamate (Zhou *et al.*, 2000). However, studies of the effect of VGLUT1 knockout on

quantal size have provided inconsistent results (Fremeau *et al.*, 2004; Wojcik *et al.*, 2004). The molecular mechanisms for regulation of vesicular glutamate content are therefore still controversial.

Unlike for acetylcholine, there is no mechanism for the hydrolysis of glutamate once released into the synaptic cleft. The two mechanisms for the removal of released glutamate from the synaptic cleft are therefore diffusion and uptake by glutamate transporters, which can be located on glial cells or the pre- or postsynaptic neuron (Shigeri *et al.*, 2004). Five genes for membrane-spanning glutamate transporters have been cloned in humans, called EAAT1-5. The rodent homologues of EAAT1 and EAAT2 are called GLAST and GLT-1, respectively. Glutamate uptake by transporters require cotransport of one H^+ and three Na^+ ions, and the countertransport of one K^+ ion (Erecinska & Silver, 1990). Glutamate can be taken up by the presynaptic terminal into the cytoplasm where it can be taken up by vesicular glutamate transporters into synaptic vesicles. However, glutamate taken up by glial cells is first converted to glutamine by glutamate dehydrogenase and then transported to the presynaptic terminal where it is converted back to glutamate (Erecinska & Silver, 1990).

The duration of the transport cycle is controversial. Initial estimates reported that the transport cycle takes 70 ms at room temperature (Wadiche & Kavanaugh, 1998). In addition, glutamate transporters mediate an anion current, which is not thermodynamically coupled to glutamate transport, but nevertheless is increased with higher extracellular glutamate concentrations. More recent data suggest that at least in Purkinje cells, EAAT4 can remove glutamate from the synaptic cleft with a time constant of 8 ms at room temperature (Auger & Attwell, 2000), and that a rapid current, carried by glutamate and Na^+, can be recorded postsynaptically. Although a later study showed that this current may not be entirely mediated by glutamate transporters, the residual transporter-mediated glutamate cur-

rent is still likely to have a fast timecourse (Brasnjo & Otis, 2004). These results can be reconciled if the transport cycle is not the rate-limiting step in removal of glutamate through transporters.

A number of studies have addressed the physiological effect of glutamate transporters on the excitatory postsynaptic current (EPSC). In cultured hippocampal neurons, evidence of a slow clearance of glutamate from the synaptic cleft comes from the slowing of the mEPSC rise time with the rapidly equilibrating low-affinity competitive antagonist kynurenic acid (Kyn; Diamond & Jahr, 1997). For this class of agent, the block of EPSCs is inversely related to the concentration of synaptically released glutamate in the cleft, because the antagonist competes with glutamate for the binding sites on glutamate receptors. In these neurons, blocking glutamate transporters slows the rise time of the mEPSC in Kyn, indicating that glutamate transporters buffer glutamate from the synaptic cleft on a sub-millisecond timescale. However, Kyn has no effect on the rise time of the mEPSC at other synapses, indicating that glutamate clearance can be faster (Smith *et al.*, 2003).

The role of glutamate transporters in synaptic signalling is an actively pursued branch of synaptic physiology. At the cerebellar parallel-fibre to Purkinje cell synapse, the distribution of glutamate transporters and mGluRs overlap at the periphery of synaptic contacts, and transporters regulate the activation of mGluRs (Brasnjo & Otis, 2001). There also appears to be some variability in the effect of glutamate transporters on the decay of the EPSC waveform, with some studies reporting an acceleration in the presence of glutamate transporter blockers (Mennerick & Zorumski, 1995) and others no or a small effect (DiGregorio *et al.*, 2002; Overstreet *et al.*, 1999). For instance, at the cerebellar mossy-fibre to granule cell (MF-GC) synapse, there is little effect of glutamate transporter blockers on the shape of the mean EPSC waveform, probably because transporters

are located at a distance from synaptic release sites (Chaudhry *et al.*, 1995; Xu-Friedman & Regehr, 2003). However, multiple stimuli at high frequency can reveal a prolonged current that is reduced by glutamate transporters, indicating that these can influence cleft glutamate over a longer timescale. The contribution of glutamate transporters to the EPSC waveform will be considered in chapter 5.

1.2.4 The timecourse of glutamate release

Miniature EPSCs evoked by spontaneous glutamate release and recorded under favourable voltage-clamp conditions have very rapid rise time, likely close to 100 μs or faster at physiological temperature (Finkel & Redman, 1983; Forti *et al.*, 1997; Geiger *et al.*, 1997; Silver *et al.*, 1992) indicating that glutamate release can be very rapid. In addition, the timecourse of displacement of low-affinity rapidly equilibrating antagonists has indicated that the glutamate concentration rises instantaneously (or faster than the resolution of antagonist displacement) and decays with a dual or multi-exponential timecourse (Clements, 1996; Diamond & Jahr, 1997). The lack of probes to measure glutamate on a rapid timescale has prevented estimates of exactly how fast glutamate could be released into the synaptic cleft. At the neuromuscular junction, one study found that in order to replicate the timecourse of the mEPSC, it was necessary to assume a dilation of the fusion pore at a velocity of at least 25 nm/ms (Stiles *et al.*, 1996), at which rate 90% of vesicular contents are released within 100 μs. However, instantaneous release of acetylcholine was not distinguishably faster in terms of the mEPSC kinetics. There is therefore no lower bound estimate for the duration of vesicle emptying in fast neurotransmission.

Nevertheless, in some cells it has been possible to estimate the timecourse of vesicle emptying. Two techniques have been used to make this measurement:

amperometry, which uses a carbon-fibre electrode as a probe of certain neurotransmitters such as serotonin and dopamine, and capacitance measurement, which measures the cell surface area. The latter technique reports the increase in cell membrane associated with fusion of presynaptic vesicles. These techniques have revealed that in cells that secrete the contents of large dense-core vesicles, release can occur very rapidly (Chow *et al.*, 1994). However, in some release events, opening of the fusion pore can be reversible and in a flickering mode, and release only a small amount of neurotransmitter, which can be determined by the synaptotagmin subunit expressed (Wang *et al.*, 2003). Occasionally, a flickering fusion pore is followed by a large rapid release event (Alvarez de Toledo *et al.*, 1993; Albillos *et al.*, 1997; Ales *et al.*, 1999; Zhou *et al.*, 1996). It has been suggested that the flickering fusion pore is the physiological correlate of the mode of endocytosis Ceccarelli called "kiss-and-run," and the term has since been used to describe both a mode of release and a mode of endocytosis. Here, I will use the term "prolonged release" to denote the possibility of a prolonged, low-amplitude flux of neurotransmitter from a narrow fusion pore.

Amperometry and capacitance measurement is more difficult to apply to central neurons, because the vesicles are smaller and glutamate and GABA cannot be measured with amperometry. Capacitance measurement of small clear vesicles from posterior pituitary nerve terminals has revealed that reversible fusion pores occur in 5% of release events (Klyachko & Jackson, 2002), and that these fusion pores have a low conductance. One study has reported the flickering release of dopamine from ventral midbrain neurons neurons as measured with amperometry (Staal *et al.*, 2004). However, studies addressing the possibility of prolonged release from glutamatergic synapses have relied on indirect methods.

Choi *et al.* (2000) and Renger *et al.* (2001) both recorded slow-rising AMPAR-mediated currents that they attribute to prolonged release of glutamate. Choi

et al. (2000) suggests that a switch from prolonged to rapid release can underlie long-term potentiation (LTP) in the hippocampus, whereas Renger *et al.* (2001) show that the prolonged release is a feature of immature cultured synapses. The former study showed that the glutamate concentration changes after LTP, as assayed with the fractional block by low-affinity NMDA receptor antagonists, whereas the latter relied on monitoring changes in the kinetics of the synaptic current while showing no change in the response of glutamate receptors to exogenously applied glutamate. The possibility of two distinct modes of vesicle fusion has also been investigated with the lipophilic dye FM1-43. Zakharenko *et al.* (2002) showed that following mGluR-mediated long-term depression (LTD) at the hippocampal CA3-CA1 synapse, destaining of FM 1-43 proceeded at a slower rate without a change in release probability, indicating that less dye was able to escape from fused vesicles. Studies of escape of FM 1-43 dye or pH changes associated with fusion of single vesicles (measured with synapto-pHluorin) have concluded that a minor (Zenisek *et al.*, 2002) or a large (Aravanis *et al.*, 2003; Gandhi & Stevens, 2003) proportion of vesicles may undergo kiss-and-run endocytosis. Unfortunately, the timecourse of neurotransmitter release from these release events is unknown, and cannot readily be estimated from the rate of escape of FM1-43 or protons.

1.2.5 Multivesicular release

At active zones of central synapses, EM studies have shown that more than one vesicle is often docked to the presynaptic membrane (Schikorski & Stevens, 1997). However, it is controversial whether in response to a presynaptic action potential, at most one or more than one vesicle can be released at a single active zone. I will call these two possibilities the univesicular and the multivesicular hypothe-

sis, respectively. Most studies investigating this question have examined whether the concentration of glutamate in the synaptic cleft changes with release probability, which is predicted by the multivesicular but not the univesicular hypothesis. Perkel & Nicoll (1993) suggested that if the glutamate concentration changes, the relative contributions of AMPA and NMDA receptors to the postsynaptic current should change, based on the difference in the affinity for glutamate of these two receptor classes. They showed that changing the release probability with activation of presynaptic receptors or with inducement of LTP did not change the ratio of AMPA and NMDA-mediated currents at a hippocampal synapse, suggesting that release is limited to one vesicle per active zone.

It is also possible to assay the concentration of glutamate in the synaptic cleft by examining the block by rapidly equilibrating low-affinity competitive antagonists. Tong & Jahr (1994) found that the fractional block of NMDA currents by teh low-affinity antagonist L-AP5 changed when release probability was manipulated with extracellular calcium or pharmacological agents at a cultured hippocampal synapse. Wadiche & Jahr (2001) also found a large difference in the fractional block by γ-DGG when using short-term synaptic plasticity to change the release probability at the cerebellar climbing fibre to Purkinje cell synapse.

However, it is clear that at other synapses, multivesicular release does not happen. Silver *et al.* (2003) used two methods to investigate the number of released vesicles per active zone at the cortical layer 4-layer 2 synapse. First, they used quantal analysis to determine the number of discrete release sites underlying the synaptic depolarisation, assuming a model of transmitter release where each release site functioned in an all-or-none manner. This number of release sites was found to correspond to the number to active zones detected using EM. Secondly, they found the block of the EPSP by γ-DGG to be independent of the release probability. Taken together, these studies indicate that multivesicular

release can occur at some, but not all synapses. In chapter five, I will investigate whether multivesicular release occurs under physiological conditions at the cerebellar MF-GC synapse, and whether it can occur at high release probability.

1.3 AMPA-sensitive glutamate receptors

Due to their rapid responses to glutamate, AMPARs are better suited to investigating the dynamics of glutamate in the synaptic cleft than other ionotropic glutamate receptors. AMPAR can be expressed natively on the soma (Jonas & Sakmann, 1992; Hausser & Roth, 1997), in the dendrites (Hausser & Roth, 1997), and in the postsynaptic density (PSD; DiGregorio *et al.*, 2002; Nusser, 2000). However, on some cells, such as the cerebellar granule cell, expression can be restricted to the postsynaptic density (DiGregorio *et al.*, 2002). Hausser & Roth (1997) compared the properties of glutamate receptors found on the soma and on the dendrite, and found no difference in their properties. However, there is some evidence that synaptic and extrasynaptic receptors may have different properties in cultured neurons from the CA1 region of the hippocampus. Forti *et al.* (1997) measured a fast decay time constant of synaptic conductances of 0.6 ms, whereas Diamond & Jahr (1997) found a deactivation time constant of 2 ms in patches pulled from the soma in response to a brief impulse of glutamate, recorded at a similar temperature. However, it is possible that differences in culture preparation contribute to thee difference in timecourses. Estimates of the number of AMPARs in a single PSD using non-stationary noise analysis have varied between 30 and 80 (Silver *et al.*, 1996c; Matsuzaki *et al.*, 2001; Momiyama *et al.*, 2003). One study using immunocytochemistry found a range of 3-140 AMPARs per active zone (Nusser *et al.*, 1998), and the number of AMPARs mediating the EPSC may depend on the distance from the soma (Smith *et al.*, 2003).

1.3.1 Single channel properties

The maximal open probability of AMPARs estimated with non-stationary noise analysis, is 0.7-0.8 (Silver *et al.*, 1996c; Momiyama *et al.*, 2003; Hausser & Roth, 1997). Estimates of the open probability following synaptic release of a single quantum are lower than this, with most studies concluding that AMPA receptors are not saturated during the mEPSC (Larkman *et al.*, 1991; Silver *et al.*, 1996c; Ishikawa *et al.*, 2002; McAllister & Stevens, 2000; Liu *et al.*, 1999), but can be, following multivesicular release (Foster *et al.*, 2002; Harrison & Jahr, 2003). AMPAR conductances have shown a large variability between studies (4-50 pS) when investigated with non-stationary noise analysis, and indeed, within a single preparation. Single channel studies of AMPARS activity have shown that a single receptor can have multiple discrete conductance levels, generally three (Rosenmund *et al.*, 1998; Wyllie *et al.*, 1993) but occasionally two to five (Smith *et al.*, 2000). Rosenmund *et al.* (1998) suggested that changing conductance levels reflected the binding and unbinding of agonists from each of four binding sites, and Smith & Howe (2000) showed that the single-channel conductance depends on the concentration of perfused agonist.

Several attempts have been made to model the responses of AMPAR channels with kinetic schemes. Although most of these have included two binding steps, one open state and two or more desensitised states (Jonas *et al.*, 1993; Hausser & Roth, 1997), a model of AMPARs in the chick nucleus magnocellularis synapse has three open states, one fast, one slow, and one associated with desensitised states, all with equal conductances (Raman & Trussell, 1992, 1995). To account for recent single channel recordings, Robert & Howe (2003) proposed a model for AMPARs that includes four independent binding sites and three open states with unequal conductances that each require two, three and four bound glutamate

molecules, respectively. A table with details of the 12 different kinetic AMPAR models used in this thesis is shown in Table 1.1, with the corresponding state diagrams in Figure 1.1.

1.3.2 Modulation of AMPAR properties

The properties of AMPARs can be modified by several mechanisms, including subunit selection, DNA splice variants, RNA editing and phophorylation. A 38 amino acid cassette on the extracellular loop preceding M4 can exist in two splice varieties ('flip' and 'flop') in all four AMPAR subunits. Flip isoforms are expressed both in young and in adult animals, whereas the expression of flop increases with development (Mosbacher *et al.*, 1994). These isoforms influence desensitisation properties. Mosbacher *et al.* (1994) found that for GluR4, the homomeric receptors consisting of the flop isoform desensitised four times faster than the flip isoform in response to a long 1 mM step of glutamate. However, for GluR1, there was no difference in desensitisation time courses in the two isoforms, and in heteromeric channels, a flop isoform in GluR4 but not GluR2 confers rapid desensitisation properties on the channel. Desensitisation in AMPARs can be reduced with the allosteric modulator cyclothiazide. Cyclothiazide sensitivity also appears to be regulated by flip/flop isoforms (Partin *et al.*, 1996). The C-terminus of GluR2 and 4 can also exist in two splice varieties each, with long and short tails. Comparatively less is known about the effects of long/short splice variants, although only short variant receptors are able to interact with the protein PICK1 (Dev *et al.*, 1999), and long variants are preferentially delivered to the PSD following LTP (Kolleker *et al.*, 2003).

AMPAR RNA from all subunits can undergo further editing at at least two sites. In the pore region of M2, a genomically encoded glutamine amino acid can

Scheme	Reference	EC_{50} (mM)	τ_{des} (ms)	τ_{dea} (ms)	Power	Diagram
JMS	Jonas *et al.* (1993), set 1	0.76	3.12	0.90	1.74	A
DJ	Diamond & Jahr (1997)	0.82	3.60	0.59	1.73	A
RH4	Robert & Howe (2003)	2.68	1.23	0.14	1.76	D
RT	Raman & Trussell (1995)	3.93	0.72	0.20	1.38	C
WJ	Wadiche & Jahr (2001)	0.62	2.24	0.76	1.54	B
GN	Krampfl *et al.* (2002)	1.84	0.69	0.27	1.79	A
JMS2	Jonas *et al.* (1993), set 2	0.76	2.69	1.12	1.65	A
KO	Koike *et al.* (2000)	2.36	2.48	0.18	1.93	A
RN	Krampfl *et al.* (2002)	1.29	2.44	0.30	1.82	A
PM	Partin *et al.* (1996)	2.04	0.72	0.30	1.42	A
HR	Hausser & Roth (1997)	0.89	1.92	0.41	1.68	B
RH1	Robert & Howe (2003)	1.11	0.67	0.22	1.42	D

Table 1.1: Kinetic models of AMPARs used in this thesis. The rate constants have been adjusted to 37°C using a Q_{10} of 1.25 for concentration-dependent steps (Nielsen *et al.*, 2004) and 2 for non-concentration-dependent steps (Silver *et al.*, 1996a). **EC_{50}**, calculated from the dose-response curve generated using the average spillover $[glut]_{cleft}$ waveform (Figure 4.7) and fit with the Hill equation (1.4). τ_{des} (desensitisation), determined from a long 1 mM glutamate pulse. τ_{dea} (deactivation), determined from a 20 μs 1 mM glutamate pulse. **Power**, determined from the same dose-response curve as the EC_{50}, fit in the range corresponding to release probability 0-0.5. **Diagram**, State diagram for kinetic scheme (see Figure 1.1).

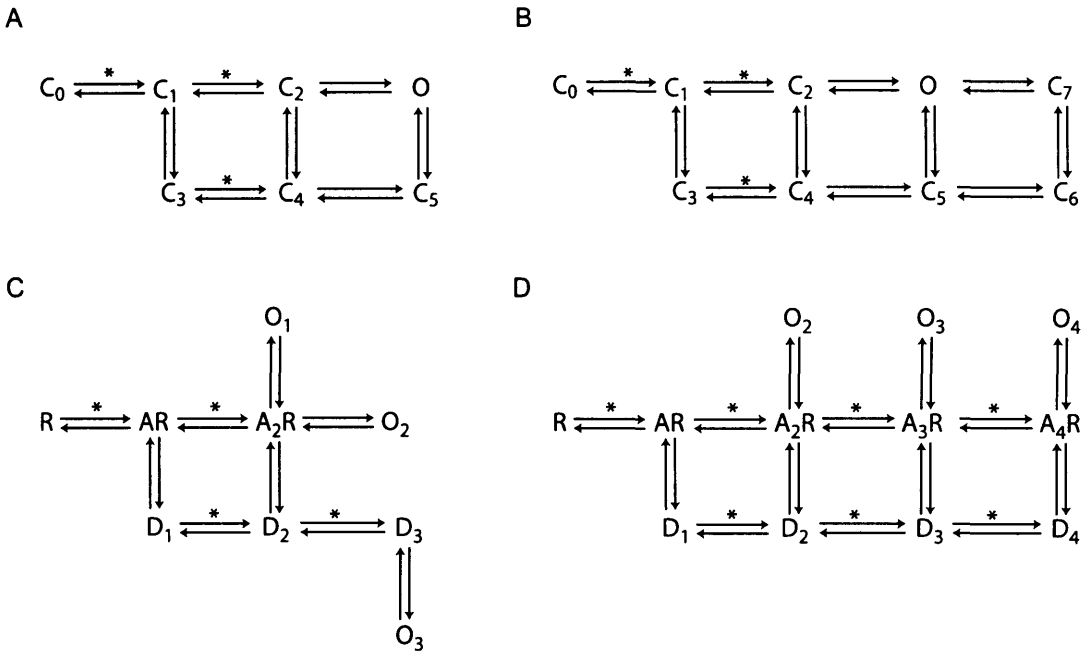

Figure 1.1: State diagrams of AMPAR kinetic schemes. See Table 1.1 for details of the 12 published kinetic schemes for AMPARs used here. $*$ denotes state transition depending on the agonist concentration.

be exchanged for arginine (Q/R site) and immediately preceding the flip/flop cassette, arginine can be edited to glycine (R/G site; Seeburg, 1996). For GluR2, almost all RNA found in the postnatal brain has been edited on the Q/R site to arginine. Interestingly, unedited GluR2 is found in aged human neural tissue (Nutt & Kamboj, 1994) and in patients suffering from amyotrophic lateral sclerosis (Kawahara *et al.*, 2004). As previously mentioned, single channel properties can also be altered by phosphorylation. Editing of the Q/R site in GluR2 in a single subunit dramatically reduces Ca^{2+} permeability of the entire receptor. Since the unedited GluR2 is not expressed in the healthy adult brain, GluR2 expression effectively regulates Ca^{2+} permeability of AMPARs (Jonas *et al.*, 1994; Geiger *et al.*, 1995). Inclusion of a single edited GluR2 subunit also confers a linear current-voltage relationship on the receptor, and a low single-channel conductance. Inward rectification in unedited AMPARs is likely mediated by block of endogenous polyamines (Bowie & Mayer, 1995; Kamboj *et al.*, 1995). Recovery from desensitisation is also affected by R/G editing (Lomeli *et al.*, 1994). Phosphorylation of AMPA receptors (Derkach *et al.*, 1999), which can mediate an increase the single channel conductance (Benke *et al.*, 1998), can enhance the AMPAR-mediated response magnitude on a timescale faster than changes in receptors expression (Shi *et al.*, 2001).

Taken together, these results indicate that cells can determine, and alter on a variety of timescales (from seconds to hours) the diverse kinetics of the fast response to synaptically released glutamate. At some synapses, these kinetics cannot be determined with rapid perfusion techniques, because AMPA receptors are not expressed on the soma (DiGregorio *et al.*, 2002). Photolytic uncaging of glutamate has previously been used to activate synaptic glutamate receptors (Matsuzaki *et al.*, 2001; Pettit *et al.*, 1997; Smith *et al.*, 2003), but not to examine AMPAR kinetics. In chapter six, I will develop a quantitative framework for pre-

dicting the concentration of glutamate and AMPAR response evoked by laser photolysis of chemically caged glutamate.

1.4 Glutamate spillover

1.4.1 Significance of glutamate spillover

Communication between pre- and postsynaptic neurons in a point-to-point manner is a tenet of the classical model of synaptic transmission. However, the possibility that neurotransmitter, and in particular glutamate, released from one synaptic connection can diffuse to receptors at neighbouring active zones has received considerable interest in the last 20 years, since lateral synergism was shown for inhibitory inputs to goldfish Mauthner cell (Faber *et al.*, 1985). This question has been examined from both experimental and theoretical approaches.

One reason for the intense interest in glutamate spillover is the prominence of LTP as a model for information storage in the brain. Spillover between neighbouring synapses occurring to a significant extent will interfere with the independent operation of individual synaptic contacts, and therefore lower the reliability or capacity of stored information in the brain (Barbour & Hausser, 1997). However, it is also possible that spillover could in some circumstances be beneficial for information processing, for instance in synchronising network activity (Schoppa & Westbrook, 2001) or lowering the variability of synaptic transmission by averaging over a large number of release sites (Kullmann *et al.*, 1996; DiGregorio *et al.*, 2002).

Whether or not spillover between neighbouring active zones occur, diffusion out of the active zone is likely to be an important determinant for the activation of receptors that are located at the periphery of the synapse, such as autorecep-

tors (Scanziani *et al.*, 1997) and postsynaptic metabotrobic receptors (Brasnjo & Otis, 2001). Glutamate has also been shown to activate high-affinity metabotropic receptors on neighbouring synapses (Semyanov & Kullmann, 2000; Mitchell & Silver, 2000b). Spillover may also contribute to the waveform of the EPSC (DiGregorio *et al.*, 2002; Otis *et al.*, 1996), which is important for information processing in the brain, because it determines such basic properties as temporal precision and reliability (Cathala *et al.*, 2003; Galarreta & Hestrin, 2001; Harsch & Robinson, 2000) and the gain of rate-coded signals (Mitchell & Silver, 2003). It is therefore important to examine whether spillover contributes to the shape of this waveform, and whether the magnitude of spillover can be actively regulated.

1.4.2 Experimental evidence for glutamate spillover

The first evidence for spillover of glutamate came from recordings from large synapses. Trussell *et al.* (1993) found that in the presence of cyclothiazide, the waveform of the EPSC depends on the release probability, such that at low release probability the decay is faster than at high release probability. In addition, the mEPSC have a faster decay than the evoked EPSC, both with and without cyclothiazide. Although this observation was very similar to that of Hartzell *et al.* (1975) at the neuromuscular junction, Trussell *et al.* (1993) explained this acceleration in terms of diffusion rather than receptor activation. They suggested that the glutamate concentrations following release of a small number of quanta decay more rapidly in the synaptic cleft, because the packet of glutamate is surrounded by a region with a low concentration on all sides, thus leading to faster disspation through a larger concentration gradient. At high release probability, however, glutamate released at the centre of the synapse is surrounded by more glutamate from neighbouring release sites, and only glutamate at the edge of the synapse

sees a large concentration gradient. Silver *et al.* (1996c) gave a similar explanation of the release-probability dependence of the EPSC at the MF-GC, suggesting that at lower release probability, the mean distance between releasing active zones increase, thus increasing the effective distance glutamate would have to travel to activate receptors.

Spillover was proposed as an explanation for the difference in quantal content underlying AMPAR and NMDAR EPSCs and for silent synapses on CA1 cells in the hippocampus by Kullmann *et al.* (1996). Because NMDA receptors have a higher affinity for glutamate than AMPA receptors, it is possible that the stimulation of synapses onto other cells can activate NMDA, but not AMPA, receptors onto the cell recorded from. Kullmann *et al.* (1996) used voltage clamp of a specific cell to prevent induction of potentiation of the AMPA component by tetanic stimulation. However, they showed that the NMDA component to the same cell increased following tetanic stimulation, together with the AMPA field EPSP, which reflects the activity of many cells. These results were interpreted as a potentiation of the release probability onto different cells activating NMDA receptors by spillover. However, Asztely *et al.* (1997) found that the difference in the quantal content between that AMPA and the NMDA component was smaller at physiological temperature than at room temperature, at which previous experiments had been performed. They attributed a large fraction of the discrepancy to the steep temperature dependence of glutamate transporter activation. Diamond (2001) showed that small stimuli could evoke spillover onto CA1 NMDA receptors cells using a combination of low-affinity antagonists, glutamate transporter blockers even at high temperature. However, he showed that spillover is affected to a large degree by postsynaptic glutamate transporters, which depend on the membrane potential. Thus spillover is almost absent in the resting state of the neuron.

In the olfactory bulb, glutamate released from mitral cell dendrites activates NMDA receptors located on the same dendrite. Despite the absence of mitral cell-mitral cell anatomical connections, depolarisation of one mitral cell also leads to activation of NMDA receptors on neighbouring mitral cells (Isaacson, 1999). This current has a rise time of 61 ms compared to the 6.4 ms rise time of synaptically evoked NMDA currents on mitral cells (Isaacson, 1999) and is restricted to sets of mitral cells connected to the same glomerulus in the olfactory bulb (Urban & Sakmann, 2002). Spillover of glutamate in the olfactory glomerulus can drive a 2 Hz synchronised oscillation between mitral cells, which is thought to be important for olfactory coding (Schoppa & Westbrook, 2001).

At the cerebellar parallel fibre to stellate cell synapse, brief high-frequency bursts of high-intensity stimulation can evoke a prolonged EPSC mediated by spillover of glutamate onto AMPA and NMDA receptors (Carter & Regehr, 2000). This EPSC is present at near-physiological temperature, and can be prolonged by block of glutamate transporters. By stimulating an indirect pathway, the authors were able to evoke an isolated spillover AMPAR EPSC with a rise time of 0.5-1 seconds. Marcaggi *et al.* (2003) showed that increasing the stimulus intensity, thus increasing the number of parallel fibres stimulated, prolongs the Purkinje cell non-NMDA EPSC in GLAST knock-out mice, consistent with the recruitment of indirect fibres. Blocking GLT-1 in wildtype mice has the same effect, indicating that both subtypes contribute to the removal of glutamate from the synaptic cleft.

Mitchell & Silver (2000b) showed that stimulation of glutamatergic MFs in the cerebellar granule cell layer leads to decreased release of GABA from Golgi cell axons in the cerebellar glomerulus. This effect is mediated by the activation of mGluRs, which are present on the Golgi cell axon terminal (Ohishi *et al.*, 1994). Since there are no direct MF-Golgi axon synaptic connections, this effect is likely to be mediated by spillover of glutamate. The slow-rising AMPAR EPSC at

the MF-GC synapse, which may be mediated by glutamate spillover (DiGregorio *et al.*, 2002), will be discussed below in detail.

Taken together, these observations indicate that spillover of glutamate alone can activate NMDARs and mGluRs. However, the evidence for AMPAR activation by glutamate spillover is more indirect and it is uncertain to what extent such activation occurs in isolation under physiological conditions, or whether it is an artifact of intensive, synchronised stimulation of multiple fibres. While at large synapses it is clear that spillover may be able to shape the EPSC, it is uncertain whether postsynaptic receptors could be activated alone, and if so to what extent this might occur. Some indications of spillover, such as a dependence of the concentration of glutamate in the synaptic cleft on the release probability, or the presence of slow-rising currents, are also consistent with multivesicular release or prolonged release of glutamate. Indeed, many studies of spillover (DiGregorio *et al.*, 2002), fusion pore modulation (Choi *et al.*, 2000; Renger *et al.*, 2001) and multivesicular release (Wadiche & Jahr, 2001) have found it difficult to experimentally differentiate between these mechanisms (Jahr, 2003). In chapter three I will develop a general method for distinguishing between prolonged release and spillover of glutamate.

1.4.3 Theoretical studies of glutamate spillover

In parallel with experimental studies of glutamate spillover, several investigators have developed detailed models of synaptic function to examine whether spillover is possible on theoretical grounds. The use of these models is partly justified by the difficulty of making direct recordings of cell pairs that are not directly connected but have close synaptic connections, and partly by the variety of alternative hypotheses faced by experimental studies of spillover. However, these

studies have produced inconclusive results due to the many unknown parameters in biophysical models of synaptic function. Whether glutamate spillover is seen in a model depends on the geometry in which diffusion occurs and the distance between release and detectors, the amount of released glutamate per vesicle and the number of released vesicles, the location, concentration and kinetics of glutamate transporters, the kinetics and location of postsynaptic receptors, and the diffusion coefficient of glutamate in the synaptic cleft.

Simulations of large synapses have often approximated the diffusional space as the region bound by two infinite and parallel planes separated by the cleft width (Holmes, 1995; Otis *et al.*, 1996; Xu-Friedman & Regehr, 2003). These studies have concluded that diffusion of glutamate can strongly activate neighbouring synapses, both when the simultaneous release of direct and distant synapses are considered (Otis *et al.*, 1996) or when release of one vesicle at a distance is considered alone (Holmes, 1995; Xu-Friedman & Regehr, 2003). Simulations of geometries pertaining to synapses on spines, such as in the hippocampus or cerebellar molecular layer, are more difficult to implement. In the absence of an accurate reconstruction of high-resolution EM images, abstractions of spiny synapses have been represented explicitly by a three-dimensional city-block architecture (Franks *et al.*, 2003). Alternatively, it is possible to treat the extracellular space as a porous medium, which can be described with the two parameters α (extracellular volume fraction) and λ (tortuosity; Nicholson & Sykova, 1998). $\alpha < 1$ scales up the absolute glutamate concentration by

$$[\text{glutamate}]_{\text{effective}} = \frac{[\text{glutamate}]_{\text{real}}}{\alpha} \tag{1.7}$$

whereas λ lowers the effective diffusion coefficient by

$$D_{effective} = \frac{D_{real}}{\lambda^2} \tag{1.8}$$

Both α and λ can be measured by comparing the diffusion of fluorescent tracers or small inorganic molecules in brain tissue to diffusion in free solution, or from averaged EM images (Rusakov & Kullmann, 1998a). These parameters can be incorporated into an analytical solution for diffusion in three dimensions (Barbour & Hausser, 1997). Simulations of spiny synapses have come to a variety of conclusions about whether ionotropic glutamate receptors can be activated by spillover, with studies predicting negligible (Barbour, 2001; Franks *et al.*, 2003) or measurable (Rusakov & Kullmann, 1998a; Rusakov, 2001) activation. It is at present not clear whether geometrical differences (Barbour, 2001) or the distribution of glutamate transporters (Rusakov, personal communication) contribute to these differences.

1.4.4 The diffusion coefficient of glutamate in the synaptic cleft

These theoretical studies of glutamate diffusion have concluded that the value chosen for the diffusion coefficient of glutamate in the synaptic cleft (D_{glut}) has a large impact on the magnitude of both local and distant receptor activation. The diffusion coefficient of glutamate in free solution is often taken to be equal to that of glutamine, which was measured as 0.76 $\mu m^2/ms$ at 25°C (Longsworth, 1953). Glutamate and glutamine have nearly identical molecular weights (147.1 and 146.15 g/mol, respectively) and very similar chemical structures. However, it has been suggested that the diffusion coefficient of small ions could be different in the synaptic cleft than in free solution. This assumption has been justified on two grounds: buffering by transporters or receptors and viscosity of the extra-

cellular solution. Buffering of glutamate will slow down the diffusion out of the synaptic cleft, and indeed it is possible to calculate an effective D_{glut} based on the concentration and binding site kinetics (Rusakov & Kullmann, 1998b; Trommershauser *et al.*, 1999). However, as (Barbour, 2001) points out, this can be an inaccurate approximation. For instance, lowering D_{glut} will increase the activation of local and distant receptors. In contrast, the introduction of buffers will always decrease receptor activation when modelled explicitly. The explicit modelling of buffers is therefore likely to be the most accurate representation of buffering and is also the most widely used.

There is far more disagreement about the possibility of diffusion in the synaptic cleft being influenced by a viscosity caused by large macromolecules. Rusakov & Kullmann (1998b) suggested that two factors contribute to the total tortuosity: a geometric component due to the synaptic ultrastructure, which would only appear when not explicitly simulating a full reconstruction that could come from electron microscopy; and a residual viscous component due to the presence of macromolecules in the extracellular solution. The experimentally measured tortuosity in the hippocampus is 1.6 (Nicholson & Sykova, 1998), while Kume-Kick *et al.* (2002) were unable to obtain a tortuosity higher than 1.225 in simulations of a variety of abstract geometries. This would imply a slowing of D_{glut} to 50-60% due to viscous tortuosity, although it has been proposed that the introduction of dead-end pores in the theoretical simulations could increase geometric tortuosity (Hrabetova & Nicholson, 2004). The observation that it is possible to slow the diffusion of neurotransmitter by the introduction of inert macromolecules (Min *et al.*, 1998; Perrais & Ropert, 2000) suggests that it is at least physically possible that any endogenous macromolecules present in the synaptic cleft, such as integrins, adhesion molecules and ion channels, slow diffusion compared to free solution (Sykova, 2001).

There is also some circumstantial experimental evidence that the diffusion coefficient of glutamate could be lower in the synaptic cleft than in free solution. The diffusion coefficient is proportional to the resistivity of solution to an ion. Kiessling *et al.* (2000) grew red blood cells on silicon circuitry, and found that the specific resistivity of the space between the circuitry and the cell was four-fold lower than in free solution. However, it is uncertain how applicable this is to the diffusion of glutamate, as the glycohelix of the red blood cell could present charge-specific interactions that do not slow glutamate. Overstreet *et al.* (2002) investigated the GABA concentration profile in the synaptic cleft using a low-affinity antagonist, and found that the slow decay could only be explained by an effective diffusion coefficient more than 20-fold lower than in free solution, although buffering by GABA transporters could have contributed to this decay.

Thus, the theoretical and experimental grounds for supposing a lower diffusion coefficient in the synaptic cleft than in free solution are uncertain, and some investigators have suggested that in the absence of evidence that diffusion is slowed due to factors other than buffering and geometric viscosity, theoretical studies of synaptic function should use the diffusion coefficient from free solution (Barbour, 2001). In chapter four, I will present evidence that diffusion coefficient in the synaptic cleft is three-fold lower than in free diffusion.

1.5 The cerebellar mossy-fibre to granule cell synapse

1.5.1 Anatomy

The cerebellar cortex consists of three layers: the granule cell layer, the Purkinje cell layer and the molecular layer. Glutamatergic mossy fibres, originating from a variety of sources throughout the brain, form synaptic connections in the gran-

ule cell layer onto granule cells and Golgi cells. Of these, the former are small, densely packed cells that make glutamatergic connections onto Golgi cells and Purkinje and interneurons of the molecular layer. Golgi cells are large interneurons that provide inhibitory input to granule cells. The sole output of the cerebellum is the GABAergic projections from Purkinje cells to the deep cerebellar nucleus (Shepherd, 2004). Mossy fibres form synaptic connections to granule cells in large structures known as glomeruli. Each mossy fibre can participate in several different glomeruli, thus forming en-passant synaptic boutons known as mossy fibre rosettes along their axon. One glomerulus can innervate approximately 50 different granule cells in the rat cerebellum, and each granule cell receives innervation from 4-5 different glomeruli (Hamori & Somogyi, 1983). The granule cell sends one dendrite to each glomerulus, but in adult animals, each dendrite forms a different claw-like structure where each digit has a single PSD (Jakab & Hamori, 1988). The whole glomerulus is wrapped in a glial sheath that expresses glutamate transporter GLAST (Chaudhry *et al.*, 1995). The anatomical structure undergoes several changes through development (Hamori & Somogyi, 1983). The mossy fibre surface becomes increasingly invaginated and claws from the same dendrite become increasingly separated in the glomerulus. At the same time, the number of synaptic contacts decreases, which continues months after birth.

The density of synaptic contacts on the mossy fibre surface has previously been inferred indirectly from two-dimensional sections of the glomerulus (Silver *et al.*, 1996c; DiGregorio *et al.*, 2002). However, measurements of the nearest neighbour distances in sections are likely to overestimate the true intersite distance, as closer neighbours in other section may be missed. The most realistic estimate of the density of active zones therefore comes from the only three-dimensional reconstruction to include PSDs, from Xu-Friedman & Regehr (2003).

This analysis revealed that in 18-day old rats there are 2.5 active zones per μm^2 on the mossy fibre surface.

1.5.2 The MF-GC synapse as a model for glutamatergic transmission

Recordings of synaptic currents in granule cells initially attracted attention due to the excellent voltage-clamp conditions that can be imposed on this cell using the patch clamp. Silver *et al.* (1992) reported a mean rise time of 200 μs for mEPSCs and 410 μs for evoked EPSCs, both recorded in APV. Correction for the cell-electrode circuit (see chapter 2) gave an upper limit of 95 μs for the rise time of the conductance underlying the mEPSC. This rise time is faster than that of non-NMDA mEPSCs recorded in other preparations (e.g. Jonas *et al.*, 1993). In addition, without APV and extracellular Mg^{2+}, individual NMDA receptor openings can be resolved in the EPSC. The rise times of these openings are very close to the rise time predicted from the cascaded cell-electrode and apparatus filters, indicating that the cell behaves as a single electrical compartment (Silver *et al.*, 1996b).

A second advantage of the MF-GC synapse as a model synapse is the ability to stimulate a single mossy fibre reliably. Silver *et al.* (1996c) showed that electrical stimulation with a patch pipette in the granule cell layer evoked all-or-none EPSCs in individual voltage-clamped granule cells. While it is impossible to exclude, on the basis of this observation, the possibility that extracellular stimulation can stimulate a fixed set of fibres, quantal analysis has found an agreement in the statistics of neurotransmitter release following all-or-none stimulation of mossy fibres and the average number of PSDs on granule cells (Sargent *et al.*, in preparation). In addition, the sparseness of MFs innervating a single GC in the granule cell layer may act to isolate afferent fibres. In the hippocampus and the

cerebellar molecular layer, it is much more difficult to reliably stimulate a single fibre (McAllister & Stevens, 2000).

A subset of synaptic connections at the MF-GC synapse are mediated by a single release site, both in younger (Silver *et al.*, 1996c) and 25-day old (Sargent *et al.*, in preparation) rats. Such a connection opens the possibility of studying the variability of quantal EPSCs, which can then be contrasted with the variability between release sites. This variability can also be used to predict the occupancy and the single-channel conductance underlying the EPSC (Silver *et al.*, 1996c), and whether the quantal EPSC summate linearly or non-linearly with other current components (Sargent *et al.*, in preparation). It is also possible to use single release sites to distinguish desensitisation from presynaptic depression as contributions to paired-pulse plasticity, although this has not yet been examined.

These advantages combined make the granule cell a very attractive model for studying the mechanisms underlying the waveform of the fast EPSC in the central nervous system. In addition, a considerable amount of existing and emerging knowledge makes it possible to start modelling synaptic processes in detail.

1.5.3 Determinants of the timecourse of the AMPAR EPSC

The MF-GC non-NMDA EPSC, which is entirely mediated by AMPA receptors, has a multi-exponential decay (DiGregorio *et al.*, 2002). A large proportion of this decay is mediated by spillover, which will be discussed below. However, the mEPSC, which is thought to be mediated by direct release of glutamate alone, still has at least a dual-exponential decay (Silver *et al.*, 1996a). The fast decay is slightly slower than the timecourse of deactivation in patches pulled from cultured granule cells, and the slow decay is slower than the timecourse of both deactivation and desensitisation. The evoked waveform is accelerated by Kyn (DiGregorio

et al., 2002). The decay of the mEPSC accelerates in older animals (Wall *et al.*, 2002), which contributes to enhanced temporal precision of the granule cell EPSP (Cathala *et al.*, 2003).

Although recent studies (Sargent *et al.*, in preparation) indicate that the number of release sites mediating the evoke MF-GC EPSC, as measured with quantal analysis, is similar to the number of anatomical release sites, previous results indicate that mEPSCs can be mediated by multiquantal release events. Wall & Usowicz (1998) found that in 39-day old, but not 11-day old, rats, the amplitude distribution showed clearly distinct peaks that might be expected from the release of an integral number of quanta. They also found a positive correlation between amplitude and rise time, as might be expected if large events are mediated by slightly asynchronous multivesicular release. It is unclear if these multivesicular mEPSCs are released at the same or at different release sites. If this release occurs at the same release site, it is possible that AP-evoked release could also lead to multivesicular release. However, different studies have not been able to replicate the peaks in the mEPSC amplitude distribution (Cathala *et al.*, 2003).

1.5.4 Spillover of glutamate and GABA at the MF-GC synapse

Silver *et al.* (1996c) suggested, based on the release-probability dependence of the EPSC decay at multi-site, but not single site, synapses that released glutamate could activate different synaptic contacts onto the same cell (intrasynaptic spillover). It was also suggested that spillover could be responsible for saturation of a subset of the multi-site synapses in 12-day old rats.

Spillover of GABA released from Golgi cells onto high-affinity GABA receptors was proposed to contribute to the inhibitory postsynaptic current (IPSC) in granule cells (Rossi & Hamann, 1998). As well as the decay of the evoked IPSC

being slower than the decay of the spontaneous IPSC, the evoked currents consisted of two distinct classes: a fast rising, fast decaying and large-amplitude class, and a class of IPSCs with slow rise times (10s of milliseconds), slow decays and low amplitudes. This latter class of events were preferentially sensitive to furosemide, an antagonist for the high-affinity GABA subunit $\alpha 6$. Rossi & Hamann (1998) proposed that spillover of GABA onto receptors on the granule cell being recorded from underlies this current.

DiGregorio *et al.* (2002) showed that evoked AMPAR-mediated EPSCs in 25-day old rats fall into two similar classes, although on a faster timescale. Slow-rising AMPAR-mediated events have rise times less than 1 millisecond, but slower than the ~0.2 ms rise time of fast-rising events. Slow-rising events were identified on the basis of their rising phase and averaged, together with failures, to form the 'slow-rising EPSC' that was contrasted with the 'mean EPSC,' which included all events regardless of their rise time. The slow-rising EPSC had a slow decay and peak amplitude smaller than the mean EPSC (the mean amplitude ratio was 0.34), but appears to determine the decay of the mean EPSC, similar to the GABAergic current described by Rossi & Hamann (1998).

DiGregorio *et al.* (2002) showed that both the slow-rising and the mean EPSC were mediated entirely by AMPA receptors and were not influenced by inadequate voltage clamp. The authors proposed that due to the stochastic nature of transmitter release, occasionally all the release sites connected to the granule cell recorded from would fail, which would reveal activation by a slowly rising glutamate concentration originating from neighbouring release sites. Consistent with this spillover hypothesis for the slow-rising current, this component is preferentially blocked by Kyn. Reductions in $[Ca^{2+}]_o$ accelerate the decay of the mean EPSC, as previously described for currents to which spillover contribute. In addition, reductions in $[Ca^{2+}]_o$ decrease the amplitude ratio of the slow-rising to mean

EPSC. Although block of glutamate transporters does have a small influence on the decay of the EPSC, this effect is only apparent 2-3 ms after the beginning of the EPSC and does not change the peak amplitude of the slow-rising EPSC.

As for spillover in the hippocampus (Kullmann *et al.*, 1996), the MF-GC slow-rising current has a lower variability relative to the mean EPSC. Based on the difference in the coefficient of variation early and late in the mean EPSC, DiGregorio *et al.* (2002) estimated that the slow-rising component originates from at least three times as many release sites as the fast-rising component. Due to its slow decay, the slow-rising component also mediates at least half of the total synaptically evoked charge transfer, indicating that it plays a large role in transducing signals from mossy fibres to granule cells.

Nevertheless, it is uncertain how the very large spillover activation of AMPARs following single-fibre activation can be reconciled with the modest activation of AMPARs previously seen experimentally and predicted theoretically in other preparations. Moreover, DiGregorio *et al.* (2002) were unable to exclude the possibility that the slow-rising current was mediated by prolonged release of glutamate rather than spillover. If prolonged release originates from a single vesicle, the fusion pore diameter would have to be sensitive to $[Ca^{2+}]_o$, and the lower variability would be unexplained. However, these difficulties for a prolonged release mechanism could be overcome by supposing that the slow-rising current originates from many vesicles at each active zone, each slowly releasing a small amount of glutamate. If either the number of such partially released vesicles, or the amount they release, is related to the release probability (i.e. the probability of full, rapid fusion), a non-linear activation of postsynaptic receptors could explain the $[Ca^{2+}]_o$ sensitivity of the slow-rising EPSC.

Even if spillover is responsible for the slow-rising EPSC, the observations discussed above do not exclude that multivesicular release, if it occurs at this

synapse, contributes to the acceleration of the EPSC decay in low $[Ca^{2+}]_o$. It is also unknown whether a model based only on spillover and univesicular release could explain quantitatively the non-linearity of the EPSC, as proposed by DiGregorio *et al.* (2002), or whether experimental evidence can be produced for such a hypothesis. However, if the slow-rising EPSC is mediated by diffusion between active zones, it could open up the possibility of using experiments, together with modelling, to constrain some of the unknown parameters in studies of synaptic function.

CHAPTER

TWO

Experimental and Theoretical Procedures

2.1 Dissection

Twenty-five day-old Sprague-Dawley rats were decapitated and the head cooled in ice-cold slicing solution (see below) during removal of the brain. The skull was cut open using a smaller pair of scissors and the brain placed on a petri-dish coated at the bottom with ~3 mm thick layer of hardened Sylgard and filled with slicing solution. Two needles were used to fix the brain to the Sylgard bottom. The meninges were removed with a pair of fine tweezers, and the cerebellum was separated from the cerebrum and the brainstem with a razor blade. Two parasaggital cuts were made to isolate the central (vermal) section of the cerebellum. The vermis was glued to the bottom of a tissue chamber of a vibratome-type slicer (DSK or Leica), and this chamber was filled with ice-cold slicing solution which was changed at regular intervals. 200-250 μm parasaggital cuts were made with a razor blade attached to the vibratome-type slicer. After a slice was cut from the block of tissue, it was transferred to an incubating chamber containing slicing solution at 32 °C. After 45 mins incubation, the slices were transferred to room

temperature and stored until used in slicing or recording solution.

2.2 Solutions

Both recording and slicing solutions were based on the standard extracellular solutions for electrophysiological recordings from brain slices (Sakmann & Stuart, 1995). The slicing solution (table 2.1) contained relatively low concentration of sodium and calcium, in order to limit neural excitability and neurotoxicity (Geiger *et al.*, 2002).

The intracellular solutions used were based on Bean (1992). A caesium-based intracellular solution with methyl sulfate at the main anion was used for some initial experiments, but did not yield recordings with appreciably lower background noise than an equivalent potassium-based solution. To accommodate recent findings that intracellular $[Ca^{2+}]$ regulates AMPAR mobility (Borgdorff & Choquet, 2002), the amount of $CaCl_2$ added to the internal solution "K-internal 1" was calculated to yield a final free $[Ca^{2+}]$ of 60 nM, corresponding to the measured resting $[Ca^{2+}]$ in granule cells (Kirischuk *et al.*, 1996), using the program MaxChelator (http://www.stanford.edu/~cpatton/maxc.html).

All recordings were made in the presence of (concentration in μM): APV (10), 7-chlorokynurenic acid (20), strychnine (0.5), SR-95531 (Gabazine; 10). The following agents were used as pharmacological manipulations: Kynurenic acid (1000), TBOA (200), E4CPG (20), CPPG (20), CGP 52432 (2) and LY 341495 (2). Dextran 43 kDa was added in a concentration of 5% w/v (~1 mM). Kyn, strychnine and dextran were obtained from Sigma, and all other pharmacological agents from Tocris.

Compound	Concentration (mM)	
	Recording solution	Slicing solution
NaCl	125	85
KCl	2.5	2.5
NaH_2PO_4	1.25	1.25
$NaHCO_3$	26	25
$CaCl_2$	2	0.5
$MgCl_2$	1	4
Glucose	25	25
Sucrose	-	63
pH	7.3	7.3
Osmolality	315	315

	K-internal 1	K-internal 2	Cs-internal
$KMeSO_4$	110	110	-
$CsMeSO_4$	-	-	110
HEPES	40	40	40
NaCl	4	4	4
EGTA	5	0.5	0.5
$CaCl_2$	1.78	-	-
KCl	-	1	1
NaGTP	0.3	0.3	0.3
MgATP	4	4	4
pH	7.3	7.3	7.3
Osmolality	285	285	285

Table 2.1: Intracellular and extracellular solutions used in electrophysiological experiments.

2.3 Slice visualisation

Slices were placed under an Olympus upright microscope during experiments. Each individual slice was placed in the recording chamber on a stainless steel washer covered with thin nylon threads to form a net (the "trampoline"). A "harp", that is a square U-shaped flattened platinum wire with nylon strings attached, was placed on top of the slice, such that the latter was immobilised between the harp and trampoline. Recording solution was perfused at a rate of 1.5-2 mL/sec, and was heated to ~45 °C. The temperature in the bath was monitored and was between 35 and 38 °C in all recordings.

The Olympus microscope was initially set up for Kohler illumination, and the slice was visualised through a 60x objective. An infra-red long-pass filter was inserted in between the slice and the light source, and the differential interference contrast components of the microscope were adjusted to give granule cells an artificial three-dimensional appearance for maximal contrast. The image was captured with a video-rate CCD camera (Hamamatsu). Contrast was further enhanced using an electronic contrast enhancement box (Hamamatsu).

Under the microscope, different regions of the cerebellar cortex of the cerebellum can clearly be distinguished. The granule cell layer is positioned between the Purkinje cell layer and the white matter, and contain densely packed granule cells. Healthy granule cells have a smooth appearance and an irregular shape, unlike dead granule cells, which look granulated and round.

2.4 Patch-clamp recordings

Borosilicate glass pipette were pulled in a vertical (Narashige) or horizontal (Sutter) multistage pipette puller, and the tip was firepolished. When filled with

intracellular solution, a 5 mV voltage step applied between the inside of the electrode and the bath solution passed a 0.5-0.8 nA current, indicating that the electrodes had resistances of 6-10 MΩ. The pipette was controlled electrically by an Axoclamp 200B patch clamp amplifier and mechanically by Luigs & Neumann micromanipulators. Upon immersion in the bath, a positive pressure was applied to the pipette to avoid contamination of the tip. This pressure was maintained as the pipette was lowered into the slice and advanced towards a healthy-looking granule cell to clean the surface of the cell membrane (Sakmann & Stuart, 1995). When the pipette tip is very close to the cell surface, a "dimple" appears in the cell membrane. At this point the pressure is changed to a small negative pressure to establish a seal with the cell membrane on the order of 1 GΩ (Hamill *et al.*, 1981). Electrical access to the interior of the cell is provided by short, sharp suction to establish the whole-cell configuration.

The passive electrical properties of neurons can be idealised as a capacitor, representing the cell membrane, in parallel with conductances with various reversal potentials (Figure 2.1). A "simple" neuron could for instance have a leak conductance, which is independent of the membrane potential, active conductances for generating the action potential, and synaptic inputs for which the conductance input depends on the concentration of neurotransmitter in a complex manner (see below). For glutamate-activated non-NMDA receptors, the reversal potential is close to 0 mV (Colquhoun *et al.*, 1992).

If the membrane potential is set at a fixed value ("voltage clamp") below the threshold for activation of voltage-gated conductances, the capacitative current is zero at steady-state, synaptic conductances can be measured in isolation when the synapse is stimulated. The ideal voltage clamp is a pure voltage source in series with an ammeter and the cell-equivalent circuit. The synaptic current can be directly read from the ammeter when the synapse is stimulated. In practice,

the real voltage clamp circuit deviates from the ideal case (Figure 2.1), and this can introduce artifacts in the measurement of membrane currents. Most importantly, electrical access to the internal cell compartment is often limited, which introduces a resistor in series with the voltage source. If glass electrodes are used to make the recording, a capacitative current can arise between the electrode and the extracellular solution. Moreover, a leak current can arise at the interface between the glass electrode and the cell membrane. On modern amplifiers, it is possible to compensate for the capacitative current of the electrode without introducing additional noise.

A large leak current associated with intracellular recordings is problematic because it introduces noise in the recordings, and puts considerable stress on the cell's mechanisms for ionic regulation. However, recordings with very low leak current can be established with the patch clamp technique, where the electrode tightly seals to the cell membrane before the membrane inside the pipette is ruptured. Thus, the cell membrane outside the pipette opening is left intact.

Therefore, the most important deviation from the ideal case for the purpose of recording EPSCs from granule cells is the error introduced by the series resistance. This will introduce three types of error in voltage clamp recordings (Johnston *et al.*, 1994):

1. When imposing a step-like voltage change on the cell, the actual membrane potential will be filtered with a corner frequency of $(2\pi R_s C_m)^{-1}$. However, since recording the EPSC often does not involve changing the command voltage, this error can be ignored.

2. There is a voltage drop over the series resistance, which can be calculated by Ohm's law, and changes the holding potential and therefore the driving force of AMPA receptors. In the worst case the EPSC at the MF-GC synapse

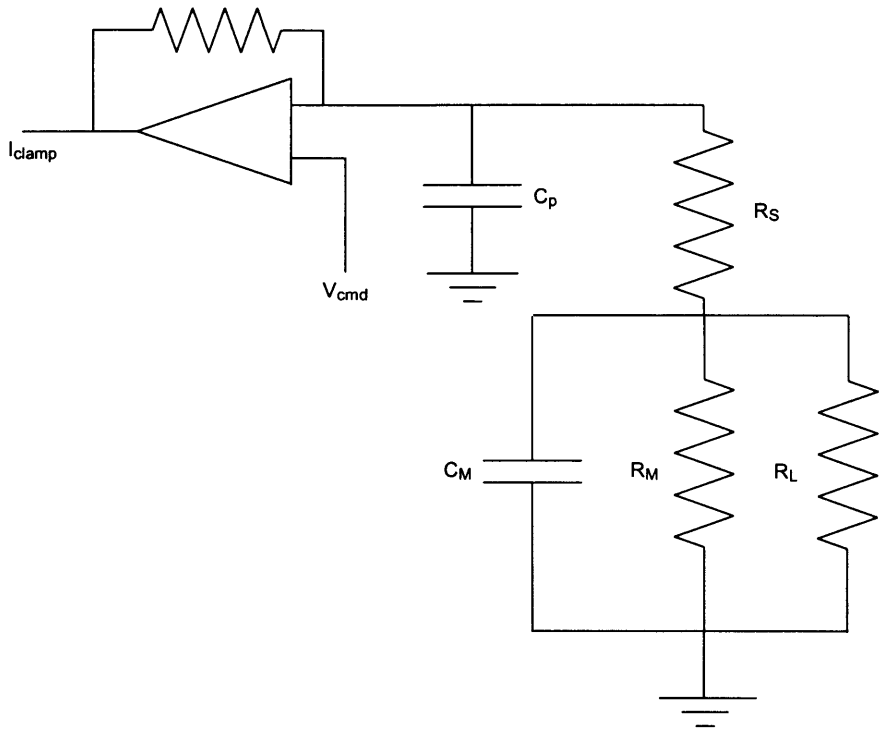

Figure 2.1: The realistic voltage clamp circuit uses an operational amplifier with a feedback resistor as a voltage source. The recorded membrane current (I_{clamp}) can be distorted by uncompensated pipette capacitance (C_p), the series resistance (R_s) and a leak resistance (R_L).

is 200 pA (DiGregorio *et al.*, 2002). For a 35 MΩ series resistance, this will give a change in the holding potential of 7 mV, a 10% error. This is therefore only likely to influence recordings of large currents from cells with large series resistances.

3. Recorded currents will be low-pass filtered by the RC filter comprising the series resistence and the cell membrane capacitance, again giving a corner frequency of $(2\pi R_s C_m)^{-1}$. Again, for a 35 MΩ series resistance and a 4 pF cell, this will give a filter frequency of 1.1 kHz, for which the step response has a rise time of 272 μs. This can introduce a very significant error in recording events with fast rise times, even in recordings from cells as small as the granule cell.

The calculated errors all assume that the input conductance is negligible compared to the series conductance. Series resistance errors can be corrected for, during or after recordings, but not without introducing noise (Traynelis, 1998). It is therefore desirable to make recordings with as low and stable series resistances as possible. Junction potentials, which arise from a difference in the mobility of the ions in the intracellular and extracellular solutions, were not corrected for (Neher, 1992).

2.5 MF stimulations

Mossy fibres were stimulated with an electrode with a tip size slightly larger than the patch electrodes, filled with extracellular solution. A voltage step of amplitude 5-80V and at least 40 μs durations was applied between the stimulating electrode and a stimulus ground wire, made of platinum and located in the bath opposite the patch clamp ground electrode. Once a whole-cell configura-

tion on a granule cell had been established, the stimulating electrode was moved around in the granule cell layer until a single mossy fibre input was found. The stimulation voltage and duration was lowered as far as possible, and the location optimised, to minimise the changes of stimulating multiple fibres and minimising the stimulation artifact. For recording EPSCs, mossy fibres were stimulated at 0.5-5 Hz with single or double pulses.

2.6 Diffraction-limited uncaging of glutamate

For the preliminary results from glutamate uncaging described in chapter 6 (recorded in collaboration with D.A. DiGregorio), the patch pipette contained 10-20 μM Alexa 488 or 594. Isolated claws of granule cell dendrites were illuminated with a mercury lamp and fluorescence was captured with a cooled CCD camera (Hamamatsu).

A second pipette with an opening ~10 times larger than the patch pipette was used to perfuse the granule cell dendrite with MNI-glutamate. A positive pressure of 5-15 mBar was applied to the back of this pipette, which contained recording solution but with (in mM) NaCl 110, $NaHCO_3$ 2, HEPES 40, 4-methoxy-7-nitroindolinyl–glutamate (MNI-glutamate) 10 and 0.01 APV. MNI-glutamate is a caged glutamate compound that is cleaved by the absorption of a photon of UV light (photolysis). MNI-Glutamate has a fast rate of photolysis and does not interact with glutamate receptors in its caged form (Canepari *et al.*, 2001). Occasionally, the perfusion included Alexa 488 or 594 to trace the extent of local perfusion.

A continuous-mode Argon laser (Innova I328; Coherent) with a wavelength of 351 nm was gated by both a mechanical shutter and an acousto-optical tunable filter (AOTF). A single-mode fibre (Oz Optics) connected the laser with the

microscope, where it was adjusted to overfill the back aperture of a 100x objective (1.0NA; Olympus). The location of the spot was adjusted with motors, which were calibrated with respect to the CCD image by capturing fluorescence resulting from laser illumination of bath-applied fluorescein.

2.7 Data acquisition

Synaptic currents recorded with the Axoclamp 200B amplifier were filtered to 10 kHz with the built-in four-pole Bessel filter, and further filtered by a custom-made 10 kHz eight-pole Bessel filter, to give a total filter frequency of 7.1 kHz. This signal was digitised at 100 kHz by a 18-bit ITC18 (Instrutech) or a 16-bit NIDAQ 6052 analogue to digital converter. Data acquisition was controlled by Axograph 4 software on a Apple computer, or Nclamp (an acquisition program written in Igor Pro) on a PC.

2.8 Data analysis

Synaptic currents were analysed using Neuromatic or Synaptix, both running in Igor Pro on PCs. EPSCs were aligned on the artifact, and baselined using a 3 ms window immediately preceding the artifact. Analysis was restricted to time-stable events, as assayed with a Spearman rank-order correlation test (Silver *et al.*, 1996c) on the current averaged over a 100 μs window centred on the peak of the mean EPSC.

In some experiments, 500 traces of the stimulus artifact below the threshold for synaptic stimulation was recorded from each cell before the beginning of the experiment. Occasionally, the stimulation artifact distorted a recording to such an extent that there was no period of zero-level current before the rise of the EPSC.

In that case, a recorded subthreshold artifact could be scaled to match the time-course of the pre-EPSC current due to stimulation artifact and then be subtracted from the entire trace. Alternatively, in cells in which a subthreshold artifact was not available, a single or double exponential function could be fit to the pre-EPSC artifact. An extrapolation of the fit into the time of the EPSC could then be subtracted from the entire recording.

Events were separated into failures and successes. For this purpose, two 1 ms windows were defined (Figure 2.2). One ("EPSC window") was placed so as to include the peak of the EPSC in its first half. The second window ("background window") was placed before the artifact, such that its midpoint was defined by the reflection of the midpoint of the first window in the midpoint of the window used for baselining. If there are low-frequency components in the noise, this procedure ensures that the contribution of background variance to these two windows are similar. Successes were identified by the average current during the EPSC window being at least 3 standard deviations of the background window below zero. Occasionally, a stricter criterion of 5 standard deviations was used to isolate successes in low $[Ca^{2+}]_o$.

EPSCs were then separated into slow-rising and fast-rising based on a method described by DiGregorio *et al.* (2002). The successes were separated into fast-rising and slow-rising events by a two-step process. First, a Gaussian function was fitted to a histogram of the measured 10-90% or 20-80% rise times of all successes. Events with rise times longer than five standard deviations above the mean (of the parameters of the gaussian fit) were considered putative slow-rising currents. Of these, some had long rise times because of asynchrony in release rather than having a smooth slow rising phase. The former were excluded from the slow-rising group by measuring the peak derivative in the rising phase, and passing events with peaks less than -60 to -100 pA/ms to the fast-rising group.

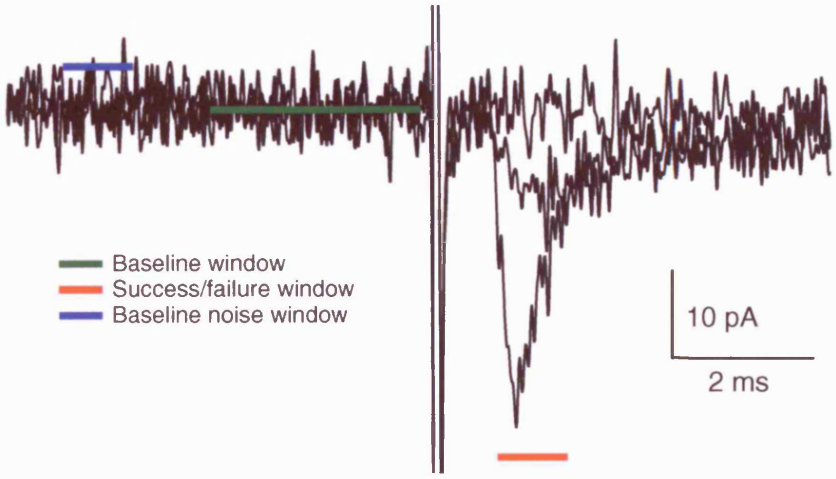

Figure 2.2: Windows for subtracting the baseline current, estimating the baseline noise, and separating failures from successes, displayed with a fast-rising success, a slow-rising success, and a failure trace.

In addition, all failures were considered slow-rising. Rise times and derivatives were measured after digital filtering with the 25 passes of the binomial algorithm (Marchand & Marmet, 1983), corresponding to a final corner frequency of 2.5 kHz (including the 7.1 kHz pre-acquisition filtering but not considering the cell-electrode circuit.)

The mean EPSC is defined as the average of all stimuli, and the slow-rising EPSC as the average of slow-rising currents including failures. We also defined the fast-rising EPSC as the mean EPSC minus the slow-rising EPSC. The failure probability of the fast-rising component is defined as the ratio of slow-rising events to the overall number of stimuli. To improve the estimate of the time-to-peak and amplitude of slow-rising currents, we fitted them with the following equation (derived from Bekkers & Stevens, 1996):

$$A_1\left(1-\exp\left(-\frac{t-t_0}{\tau_{rise}}\right)\right)^n\left(A_2\exp\left(-\frac{t-t_0}{\tau_1}\right)+(1-A_2)\exp\left(-\frac{t-t_0}{\tau_2}\right)\right) \tag{2.1}$$

The time-to-peak of the slow-rising current was measured as the time from the 20% rise time of the mean EPSC to the peak of the fitted slow-rising EPSC. Values are states as mean ± standard error of the mean, and statistical tests were done with Student's paired two-tailed t-test unless stated otherwise.

2.9 Brownian motion and Fick's laws

Diffusion is a process that redistributes uneven concentrations (the "diffusant") in a volume of gas or aqueous solution (the "solvent"). Eventually, in the case of simple diffusion, the diffusant will be evenly distributed throughout the entire volume. Diffusion was first studied quantitatively as a macroscopic property by

Thomas Graham, who discovered that the transfer of diffusant during a fixed time interval is proportional to the initial mass. Fick proposed in 1855, based on Graham's studies, a law of diffusion analogous to the laws of conduction of heat and electrical charge, namely that the transfer of mass by diffusion between two volume elements is proportional to the concentration difference and inversely proportional to the separation of the elements (Weiss, 1996). This law is written as:

$$J = -D\frac{\partial C}{\partial x} \tag{2.2}$$

where J is the flux of particles in the x-direction, C is the concentration, and D is a constant of proportionality know as the diffusivity, diffusion constant or (throughout this thesis) the diffusion coefficient. If flux is defined as the transfer of mass, concentration or number of particles per unit time through a unit area, D will have units of length^2/time. When applying diffusion to fast synaptic transmission at a single contact, it is often convenient to use units of μm^2/ms.

Robert Brown unwittingly stumbled across the microscopic properties of diffusion in an experiment in 1827. He dissolved some pollen seeds in water and peered down at the solution in a microscope. Inside the pollen seeds he observed small particles exhibiting erratic motion. Brown's experiments showed that the movement was unrelated to vitality of pollen grain, but did not elucidate its physical basis.

Albert Einstein concluded based on theoretical considerations that individual molecules would show thermal agitation. Temperature above absolute zero confers a positive kinetic energy and thus motion on molecules suspended in solution or gases. Einstein predicted that in a solution, the solute particles would collide randomly with solvent molecules, causing an apparently erratic motion.

It should be noted that Einstein did not present his work as a theoretical foundation of Brown's observations, and it is still controversial whether the movement of particles within the pollen was due to thermal agitation. In modern terms, "Brownian motion" refers to the motion predicted by Einstein rather than that observed by Brown.

Einstein proved furthermore that Fick's laws can be derived from Brownian motion, thus unifying the microscopic and macroscopic notions of diffusion. He used the following argument (Berg, 1992; Koch, 1998): say particles can only be in discrete locations separated by dx. We choose a time interval dt such that a molecule in x at t moves to the voxel $x - dx$ with probability 50%, and to the voxel $x + dx$ with probability 50% at $t + dt$. At time t, all the molecules in x must equal the sum of half the molecules in adjacent voxels at previous timesteps. For two locations separated by dx:

$$N(x,t) = N(x - dx, t - dt)/2 + N(x + dx, t - dt)/2 \tag{2.3}$$

Thus, the net transfer of particles across the boundary at $x + \frac{dx}{2}$ will equal

$$\frac{N(x,t)}{2} - \frac{N(x + dx, t)}{2} \tag{2.4}$$

If this boundary has area A, the flux across this boundary is

$$J_{x+\frac{dx}{2}} = -\frac{N(x + dx, t) - N(x,t)}{2Adt} = -\frac{dx}{2dt}\left(\frac{N(x + dx, t)}{Adx} - \frac{N(x,t)}{Adx}\right) \tag{2.5}$$

If we define $D = \frac{dx^2}{dt}$ and take $\frac{N(x)}{Adx}$ to be $C(x)$,

$$J_{x+\frac{dx}{2}} = -D\frac{C(x + dx, t) - C(x,t)}{dx} = -D\frac{\partial C}{\partial x} \tag{2.6}$$

for a small dx.

Fick's second law, or the diffusion equation, can be derived from the first law. In a row of rectangular volumes separated by dx, the net influx of particles into a voxel with a centroid at $x + \frac{dx}{2}$ during the time interval dt is the difference between the flux into the voxel at the interface at x and the flux out of the voxel at the interface to the next voxel at $x + dx$:

$$\Delta n = (J(x,t) - J(x+dx))dx^2dt \tag{2.7}$$

Similarly, this net change in the number of molecules can be expressed as a concentration difference:

$$\Delta n = (C(x+dx/2, t+dt) - C(x+dx/2, t))dx^3 \tag{2.8}$$

If the total number of molecules is preserved, we can equate these two expressions to find

$$\begin{aligned} \frac{C(x+dx/2,t+dt) - C(x+dx/2,t)}{dt} &= \frac{J(x,t) - J(x+dx,t)}{dx} \\ &= -\frac{J(x+dx,t) - J(x,t)}{dx} \end{aligned} \tag{2.9}$$

When dt and dx are small,

$$\frac{\partial C}{\partial t} = -\frac{\partial J}{\partial x} \tag{2.10}$$

If we differentiate Fick's first law with respect to distance, assuming that D is constant

$$\frac{\partial J}{\partial x} = -\frac{\partial}{\partial x}\left(D\frac{\partial C}{\partial x}\right) = -D\frac{\partial^2 C}{\partial x^2} \tag{2.11}$$

and combining this with (2.10) yields Fick's second law, or the diffusion equation:

$$\frac{\partial C}{\partial t} = D\frac{\partial^2 C}{\partial x^2} \tag{2.12}$$

which can be used to predict the concentration time-course.

2.10 Analytical solutions to the diffusion equation.

Before the advent of the digital computer, the only feasible way of calculating concentration timecourse ($C(t)$) shaped by diffusion was by an analytical solution to the diffusion equation. The disadvantage of using this approach is that a new solution has to be derived for each particular geometry. However, if this obstacle can be overcome, an analytical solution provides a (usually) computationally efficient and accurate solution. Moreover, an analytical solution can give insights into the influence of individual parameters which do not easily follow from alternative methods for solving the diffusion equation. I will illustrate this point with a simple model of neurotransmitter diffusion (similar to an argument in Xu-Friedman & Regehr, 2003).

In the brainstem, several synapses consist of a large presynaptic bouton activating a single postsynaptic cell (Forsythe & Barnes-Davies, 1993; Trussell *et al.*, 1993). It is not unreasonable, to a first approximation, to assume that an amount of neurotransmitter released at the centre of this synapse, would behave as if it was freely diffusing in a region bound by two parallel and impermeable planes separated by a short distance. If we make the further assumptions that the distance between these planes is short, compared to the mean displacement of neurotransmitter on the timescale we are interested in and that the release of neurotransmitter is fast, we can ignore the transsynaptic dimension and treat this

problem as diffusion in a single plane following instantaneous release at a point. In this case the diffusion equation has the following solution (Crank, 1975):

$$C(r,t) = \frac{Q}{4\pi Dt} \exp -\frac{r^2}{4Dt} \tag{2.13}$$

where r is the distance from the location of release and Q is the total amount released. If we are interested in the relationship between the peak of the neurotransmitter concentration and, for instance, D or r, we begin by deriving an expression for $\frac{\partial C}{\partial t}$ at a fixed r:

$$\frac{\partial C}{\partial t} = \frac{Q(r^2 - 4Dt)\exp\frac{-r^2}{4Dt}}{16D^2\pi t^3} \tag{2.14}$$

At the concentration peak, $\frac{\partial C}{\partial t} = 0$ which simplifies to

$$t_{peak} = \frac{r^2}{4D} \tag{2.15}$$

We may also be interested in $C(r, t_{peak})$ which is simply obtained by combining (2.13) and (2.15)

$$C(r, t_{peak}) = \frac{Q}{4\pi D\frac{r^2}{4D}} \exp -\frac{r^2}{4D\frac{r^2}{4D}} = \frac{Q}{\pi r^2 e} \tag{2.16}$$

This derivation reveals that the peak concentration at any distance r is independent of the diffusion coefficient, which is perhaps intuitively surprising.

2.11 Finite difference solutions

The difficulty associated with solving the diffusion equation in complex, three-dimensional geometries make the application of analytical solutions to synaptic transmission challenging. Indeed, an analytical solution may not exist at all. In contrast, the appearance of the digital computer made solutions based on numerical integration feasible. Most often, these approaches are based on dividing both space and time into discrete units (voxels and time steps, respectively), where the concentration associated with a voxel represents the concentration at the centre of the voxel. At each time step the concentration at each voxel is then calculated based on previously made calculations. In the simplest case, space is divided up in to square (2D) or cube (3D) voxels arranged in a regular grid, and a invariant time step is adopted, which is often dictated by the numerical solution algorithm. The simplest such algorithm is the explicit finite-difference, which is simply the application of Euler's method for numerical integration to the diffusion equation. For an ordinary differential equation,

$$\frac{df}{dt} = F(f,t) \tag{2.17}$$

Euler's rule states that

$$f(t+dt) = f(t) + dt \cdot F(f(t),t) \tag{2.18}$$

I will derive the explicit finite-difference scheme for two dimensions from Fick's first law. The derivation extends trivially to three dimensions. A derivation based on the second law is given by Crank (1975) and leads to the same result.

The two-dimensional plane has been divided into square voxels of side length dx and the (infinite) matrix of concentrations $C(i,j)$ is known at t. The flux

subsequent timesteps, it is necessary that the stability factor

$$\begin{array}{ll} \frac{2 \cdot D \cdot dt}{dx^2} & \text{(two dimensions)} \\ \frac{3 \cdot D \cdot dt}{dx^2} & \text{(three dimensions)} \end{array} \qquad \begin{array}{l} \\ \text{(two dimensions)} \end{array} \tag{2.23}$$

be less than 0.5 (Crank, 1975). On the other hand, if dt is small, more computations are performed, which will make the overall integration time consuming. In addition, since computers are able to store and calculate with real numbers to only a finite accuracy, each computation introduces a round-off error. The total error, being the sum of the round-off and truncation errors, as a function of dt, can therefore take a U shaped curve (Boyce & DiPrima, 2000). This shape was found in the concentration amplitude at late times (Figure 2.3A) when the numerical integration routine was written in Fortran 95 using the REAL*8 representation of floating-point numbers and the Salford FTN95 compiler (Salford Software). However, for numerical integration using the Intel C Compiler and double-precision arithmetic, there was no evidence of a large dependence on the stability factor of the concentration either at the peak or at late times (Figure 2.3B). All diffusion simulations presented in this thesis were performed using the Intel C Compiler and double-precision arithmetic, and a stability factor of 0.4. It is possible to improve on the accuracy and speed of the explicit scheme. Many of these improved solutions involve writing expressions in which $C(t + dt)$ appear on both sides of the equation and cannot be isolated. In this case these equations must be written out for all voxels and then solved iteratively using methods from linear algebra. This is straightforward for one-dimensional diffusion, which yields the Crank-Nicholson form (Crank, 1975) but more difficult in two and three dimensions. The benefit is usually that the scheme is unconditionally stable, i.e. there are no restrictions on dt similar to (2.23).

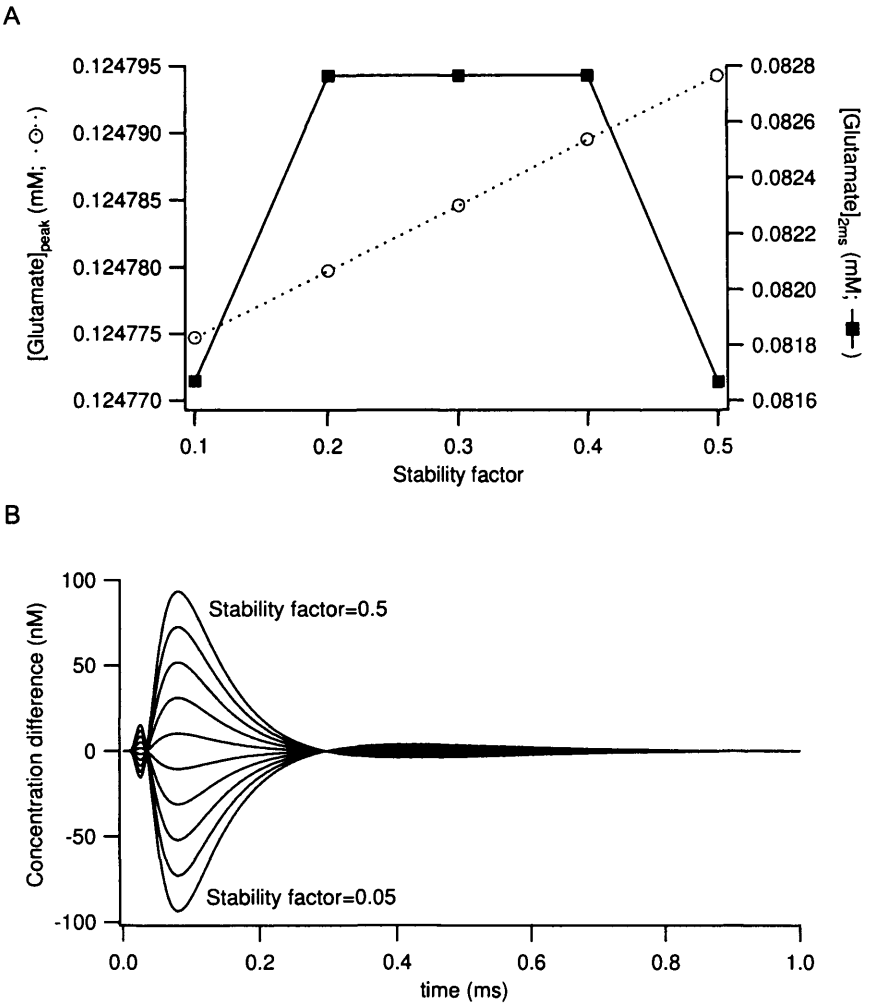

Figure 2.3: Influence of stability factor on calculated glutamate concentration waveforms. **A**, Glutamate concentration at the time of the peak (left axis, dotted line) and after 2 ms (right axis, solid line), for different values (0.1-0.5) of the stability factor, using the Salford FTN95 compiler and the REAL*8 data type. **B**, Average spillover $[glut]_{cleft}$ calculated with the Intel C Compiler and double-precision arithmetic with stability factors of 0.05-0.5. The average of the concentration waveforms were subtracted from each waveform.

2.12 Boundary conditions

The previous analysis assumed an unbounded geometry. It is not clear from this analysis how an algorithm, which can feasibly be implemented in a computer program, would handle the concentrations at the edge of the necessarily finite geometry. Two possible solutions to this problem are to assume that the boundary absorbs the diffusant, or that it forms an impermeable boundary. Both of these solutions involve defining a row of fictitious voxels beyond the boundary of the solvent (Crank, 1975).

An absorbent boundary can be combined with the explicit finite-difference scheme if edge voxels are set to a fixed value. Thus, one would calculate the concentrations for the voxels neighbouring the fictitious row of edge voxels using (2.22), but assume that the edge voxels have a constant concentration, typically zero or a chosen resting concentration. A disadvantage of this method is that the total concentration of diffusant is not constant (concentration is lost at the edges) and so it becomes difficult to verify that there are no unintended losses of diffusant elsewhere in the model.

Reflective (impermeable) boundaries require that there be no flux across the boundary, i.e. $J = 0$ at the edge. According to (2.19), if $D > 0$, this will only happen if $C_{edge} = C_{neighbour}$. Practically, this can be done with a fictitious row of voxels beyond the edge. These voxels are, again, not updated for each timestep using (2.22). Rather, at the end of each timestep, the voxels with the fictitious edge concentrations are set equal to the concentrations of their respective neighbours, such that for the next timestep, when the neighbour is updated for the next timestep, the flux between it and the fictitious voxel is zero (Figure 2.4A). However, this "trick" will only work for concave corners. If the geometry contains an internal impermeable obstacle, there will be some fictitious voxels inside

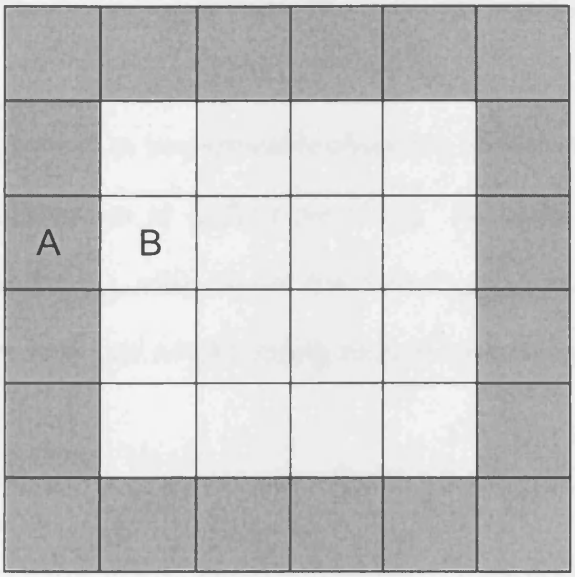

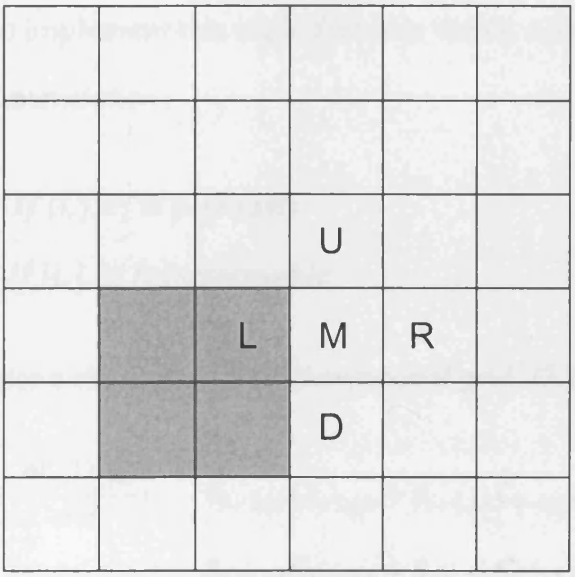

Figure 2.4: Different types of boundaries in finite-difference simulations. **A**, edge bounaries give only concave corners **B**, a geometry with an internal obstacle giving convex corners.

this obstacle which will form convex corners (Figure 2.4B), i.e. have more than one non-fictitious neighbour. If these (permeable) neighbours are not equal in concentration, it is not clear what value the fictitious voxel should adopt after each timestep.

For a general approach to impermeable obstacles, including edge boundaries, we return to the derivation of (2.22) from (2.19). As above, $J_{A->B}$=0 implies C_A=C_B. If we cancel C_{edge} with one of the four $C_{neighbour}$'s at the end, in the case of 2D diffusion with one neighbouring impermeable voxel L:

$$C_M(t+dt) = C_M(t) + \frac{dt \cdot D}{dx^2}(C_U(t) + C_D(t) + C_R(t) - 3C_M(t)) \tag{2.24}$$

This argument is similar if M has more than one impermeable neighbour. We simply drop concentration terms from these neighbours, and set the factor of C_M(t) to the number of permeable neighbours.

A simple way to implement this algorithm is to define a binary matrix S, here defined for three dimensions:

$$S_{i,j,k} = \begin{cases} 1 & if\ (i,j,k)\ is\ permeable \\ 0 & if\ (i,j,k)\ is\ impermeable \end{cases} \tag{2.25}$$

where (i,j,k) identifies a voxel in a three-dimensional grid. (2.22) then becomes:

$$\begin{aligned} C'_{i,j,k} = C_{i,j,k} + \frac{dt \cdot D_{glut}}{dx^2}(\quad & S_{i+1,j,k}C_{i+1,j,k} + S_{i-1,j,k}C_{i-1,j,k} + \\ & S_{i,j+1,k}C_{i,j+1,k} + S_{i,j-1,k}C_{i,j-1,k} + \\ & S_{i,j,k+1}C_{i,j,k+1} + S_{i,j,k-1}C_{i,j,k-1} - \mathbf{S}C_{i,j,k}) \end{aligned} \tag{2.26}$$

where

$$\mathbf{S} = S_{i+1,j,k} + S_{i-1,j,k} + S_{i,j+1,k} + S_{i,j-1,k} + S_{i,j,k+1} + S_{i,j,k-1} \tag{2.27}$$

This method can also be used to implement edge boundaries if we define a row of $S_{i,j,k}$=0 at the edge. The stability criterion is the same as for (2.23).

2.13 Chemical reaction kinetics

In classical thermodynamics, the Gibbs free energy of a molecule determines the reactions in which the molecule can participate. In a typical reaction, for instance,

$$2H_2 + O_2 \rightarrow 2H_2O \tag{2.28}$$

one can calculate the Gibbs energy of the left hand side, and the right hand side. Only if the Gibbs energy of the products is less than that of the reactants can the reaction occur at all. For a reversible reaction, such as

$$2H_20 \rightleftharpoons H_3O^+ + OH^- \tag{2.29}$$

the Gibbs energy can furthermore predict the equilibrium concentrations of the reactants and the products, in that the equilibrium constant K is equal to the ratio of Gibbs energies of the left and right hand sides of the equation. Nevertheless, the Gibbs energy cannot predict how long one must wait for such a system to reach equilibrium. The rate of reaction is instead related to the activation energy, which is the energy barrier that must be exceeded for the reaction to occur. Empirically, the reaction rate k is often found to be determined by the Arrhenius equa-

tion:

$$k = A \exp \frac{-E_a}{RT} \tag{2.30}$$

where E_a is the activation energy, R the gas constant and T the temperature.

A central assumption of classical chemical kinetics is that individual molecules can exist in a finite number of discrete states, and that transitions can occur between at least some of these states (Colquhoun & Hawkes, 1995). Patch-clamp recordings have confirmed that for ion channels, there are at least two discrete states, namely closed or open (Neher & Sakmann, 1976). Although some individual ion channels can open in some states with sub-maximal conductance, these conductance levels themselves appear as discrete states rather a continuum between closed and open (e.g. Rosenmund *et al.*, 1998; Wyllie *et al.*, 1993), thus reinforcing the validity of the classical kinetic view. In this view, reaction kinetics is concerned with the speed (or, in the case where it is possible to observe a single molecule, the probability) of rate transitions. It is a further assumption that the transition rate depends on the identity of the currently inhabited and future state, and perhaps the current state of the environment, such as for instance the presence of a ligand, but not the history of past rate transitions.

The law of mass action states that the rate at which a chemical reaction or a rate transition proceeds is proportional to the product of the reactants. The constant of proportionality is known as the rate constant. For instance, agonist binding to a receptor can be formulated as follows, following Del Castillo & Katz (1957):

$$\mathrm{A} + \mathrm{R} \rightleftharpoons \mathrm{AR} \tag{2.31}$$

Thus, by the law of mass action,

$$\frac{dR}{dt} = -\mathrm{k}'[\mathrm{A}][\mathrm{R}] + \mathrm{k}''[\mathrm{AR}] \tag{2.32}$$

and

$$\frac{dAR}{dt} = \mathrm{k}'[\mathrm{A}][\mathrm{R}] - \mathrm{k}''[\mathrm{AR}] \tag{2.33}$$

Where k′ and k″ are the forward and backward rate constants, respectively. Instead of evaluating the concentration of free and bound receptors, it is often convenient to consider the proportion of the total amount of receptors which are bound and free (p_R and p_{AR} where p_R+p_{AR}=1). We can therefore write

$$\begin{aligned} \frac{dp_{AR}}{dt} &= \mathrm{k}'[\mathrm{A}]p_R - \mathrm{k}''p_{AR} = \mathrm{k}'[\mathrm{A}](1 - p_{AR}) - \mathrm{k}''p_{AR} \\ &= -p_{AR}(\mathrm{k}'[\mathrm{A}] + \mathrm{k}'') + \mathrm{k}'[\mathrm{A}] \end{aligned} \tag{2.34}$$

This differential equation is straightforward if [A] is constant, but if it is a time-variant function [A](t) shaped by diffusion, it is much more difficult to solve. It is therefore more convenient to turn to numerical solutions developed for ordinary differential equations.

As for the diffusion equation, the simplest solutions are based on a regular discretisation of time and the application of Euler's rule. Thus (2.34) becomes:

$$p_{AR}(t + dt) = p_{AR}(t) + dt \cdot (-p_{AR}(t)(\mathrm{k}'[\mathrm{A}](t) + \mathrm{k}'') + \mathrm{k}'[\mathrm{A}](t)) \tag{2.35}$$

A more efficient method of solving ordinary differential equations is the Runge-Kutta family of solutions. These rely on a series of intermediate evaluations within each timestep. As such, there is more work done for each timestep, but

timesteps can be much bigger without compromising accuracy. For the second order Runge-Kutta method and the ordinary differential equation (2.17),

$$\begin{aligned} k_1 &= dt \cdot F(f(t), t) \\ k_2 &= dt \cdot F(f(t) + \tfrac{k_1}{2}, t + \tfrac{dt}{2}) \\ f(t + dt) &= f(t) + k_2 \end{aligned} \tag{2.36}$$

and the fourth-order Runge-Kutta scheme:

$$\begin{aligned} k_1 &= dt \cdot F(f(t), t) \\ k_2 &= dt \cdot F(f(t) + \tfrac{k_1}{2}, t + \tfrac{dt}{2}) \\ k_3 &= dt \cdot F(f(t) + \tfrac{k_2}{2}, t + \tfrac{dt}{2}) \\ k_4 &= dt \cdot F(f(t) + k_3, t + dt) \\ f(t + dt) &= f(t) + \tfrac{k_1}{6} + \tfrac{k_2}{3} + \tfrac{k_3}{3} + \tfrac{k_4}{6} \end{aligned} \tag{2.37}$$

Although this requires four evaluations of F(f(t),t) per timestep rather than one, twenty-fold larger timesteps can be taken to achieve the same accuracy as with the Euler method.

For kinetic schemes that are more complex than (2.31), such as those that have been proposed for AMPARs (see Figure 1.1), the law of mass action must be evaluated once for each reaction leading away from each state for each time step. It is convenient to store the rate constants in a matrix, such as the Q-matrix described by Colquhoun & Hawkes (1995):

$$Q_{ij} = \mathrm{k_{ij}} \tag{2.38}$$

where $\mathrm{k_{ij}}$ is the rate constant for transition from state i to j. Colquhoun & Hawkes (1995) found it convenient to set Q_{ii} such that the sums of the rows are zero, but this is not necessary for the finite-difference solution outlined here. For each

timestep, for state i, which has non-zero transitions with, for instance states j and m, we can then use Euler's rule to calculate

$$p_i(t+dt) = p_i(t) - dt \cdot Q_{ij}p_i + dt \cdot Q_{ji}p_j - dt \cdot Q_{im}p_i + dt \cdot Q_{mi}p_k \qquad (2.39)$$

or the Runga-Kutta equivalent. In addition, in a complex kinetic scheme, some rate constants have to be multiplied by the concentration of agonist (similarly to k' in 2.32).

It is possible to use the trial-to-trial variability of the postsynaptic response to deduce the number of channels and their open probability (Sigworth, 1980). In the general case where N identical channels each have k open states with single channel conductance $i_1,...,i_k$, and at time t these open states are occupied with probabilities $p_1(t),...,p_k(t)$, the current and variance at time t are given by:

$$\begin{aligned} I(t) &= N\sum_k p_k(t)i_k \\ \sigma^2(t) &= N\left(\sum_k p_k(t)i_k^2 - \left(\sum_k p_k(t)i_k\right)^2\right) \end{aligned} \qquad (2.40)$$

(Sigworth, 1980). It is therefore possible to predict the theoretical variance-mean relationship using finite-difference modelling (Figure 2.5A).

However, if we want to simulate the effect of cell-electrode filtering on the mean-variance relationship, it is necessary to resort to stochastic modelling of individual ion channels, because filtering depends not just on the P_{open}, but also on the mean open length. This is illustrated in Figure 2.5B, which shows the mean-variance relationship predicted from finite-difference modelling, the filtered relationship, and the mean-variance relationship predicted by stochastic simulations with filtering of individual traces corresponding to a typical MF-GC cell-electrode circuit. The variance-mean traces are similar without filtering, but

differ when filtering is added.

In a Monte-Carlo simulation, individual channels are assumed to be in one of the possible discrete states in the kinetic scheme. As in the finite-difference simulations, time is divided into discrete time steps, and in each time step the probability of transition into neighbouring states is calculated. The probability of a transition from state i to state j occurring in the time interval dt is approximately equal to $k_{ij}dt$ (Colquhoun & Hawkes, 1995). But if k_{ji} is large, in theory the channel could make the transition back to i in the same time interval. It is therefore necessary to keep dt sufficiently small, which can be verified by testing the predicted current against the finite-difference prediction.

2.14 Optical Point Spread Function

In order to model concentration changes following uncaging of glutamate, we are interested in the intensity of illumination $I(x, y, z)$ in the diffraction-limited microscope when the light is focused at (x_0, y_0) and the focal plane is at z_0. We define a normalised optical coordinate system (u, v) by

$$v = \frac{2\pi}{\lambda} r \sin\alpha \tag{2.41}$$

and

$$u = \frac{8\pi}{\lambda}(z - z_0)\sin^2(\alpha/2) \tag{2.42}$$

where r is the distance from (x, y) to (x_0, y_0), λ is the wavelength, and α is the maximal angle of light emitted through the lens (Wilson, 1990). For an evenly

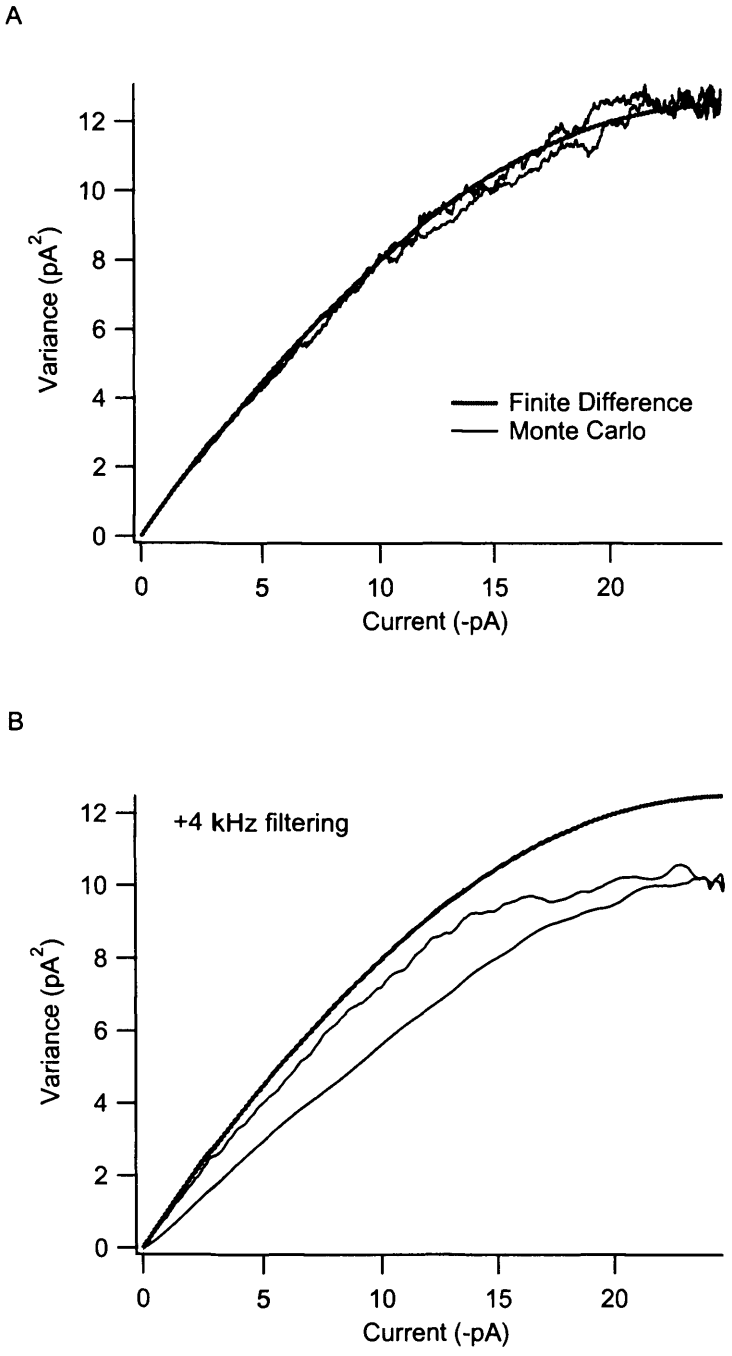

Figure 2.5: Effect of filtering on the predicted variance-mean relationship. **A**, variance-mean relationship predicted for a 1 ms 1mM concentration step and the WJ kinetic scheme, at 37°C. The grey line indicates the relationship predicted for finite-difference simulations, and the black line that predicted for Monte Carlo simulations. **B**, as for A but including a 4 kHz filter, corresponding to a 2 pF cell with 20 MΩ access resistance.

illuminated circular aperture of radius a, we additionally define

$$P(\rho) = \begin{cases} 1 & \rho < 1 \\ 0 & \rho > 1 \end{cases} \tag{2.43}$$

where $\rho = d/a$ and d is the distance from the centre of the aperture.

In that case,

$$I(u,v) = |h(u,v)|^2 \tag{2.44}$$

and

$$h(u,v) = 2\int_0^1 P(\rho)\exp(\frac{iu\rho^2}{2})J_0(v\rho)\rho d\rho \tag{2.45}$$

where J_0 is the Bessel function of the First Kind (Wilson, 1990). The integral can be numerically integrated using the trapezoidal rule.

2.15 Reaction-diffusion modelling

The numerical integration of the diffusion equation is very time-consuming. For calculating the average response from several stochastic release sites, it is not feasible to calculate the cleft glutamate concentration ($[glut]_{cleft}$) from the diffusion equation for every trial. It is therefore desirable to simply these simulations.

Under conditions of linear diffusion, the concentration response to multiple sources will equal the linear sum of the concentration responses to the individual sources alone. Linearity holds for simple diffusion, i.e. that described by the diffusion equation in any environment in the absence of buffering, with any waveform of release from sources with fixed locations and where the amount of

diffusant released is independent of the amount of diffusant present in the environment. Thus, for simulations of $[glut]_{cleft}$ arising from multiple stochastic and asynchronous release sites, it is possible to calculate the $[glut]_{cleft}$ arising from each release site alone, and then to add these up for releasing sites to give a total $[glut]_{cleft}$ for a given trial, shifting $[glut]_{cleft}$ from individual sites in time to simulate release latency. The AMPAR response to the total $[glut]_{cleft}$ for that trial can then be calculated as described above. This simulation ignores the effect of buffering of glutamate by AMPARs (see chapter 3 and 4).

Linear diffusion does not always hold, for instance when taking into account buffering (chapter 4) or glutamate uncaging (chapter 6). For the correct simulation of buffering, the amount of diffusant that binds to the buffer must not be able to diffuse into different compartments until it is released from the buffer again. For correct simulations of uncaging, it is important to track depletion of the caged compound. Concentration fluctuations due to chemical reactions are incorporated in finite-difference solutions of the diffusion equation by calculating the net transfer of concentrations using a finite-difference equivalent of the law of mass action at each timestep and for each compartment. In the case of uncaging, this net transfer is then added to the concentration of free glutamate and subtracted from the concentration of free cage. In the case of buffering, two mass action calculations are made per time step, one for the on rate, and one for the off rate. The difference of the amounts transferred from these two calculations gives the net transfer which is added to the concentration of bound buffer and subtracted from both the concentration of free buffer and the free glutamate concentration.

2.16 Optimisation

Optimisation is the problem of finding a set of parameters $(p_1, \ldots, p_n)$ such that the function $f(p_1, \ldots, p_n)$ known as the fitness is minimised. Optimisation is applied to two problems in this thesis: In chapter 3, the $[glut]_{cleft}$ that mediates a $P_{open}(t)$ is calculated, given an AMPAR kinetic scheme. In chapter 6, I fit an AMPAR kinetic scheme to recorded $P_{open}(t)$, given calculated $[glut]_{cleft}$ waveforms. In order to convert the $P_{open}(t)$ waveform(s) to a scalar fitness, I calculated the squared sum of differences between the fitted and expected values.

The $[glut]_{cleft}$ waveform was optimised by changing the amplitudes of 100 equally spaced points over 10 ms using the Levenberg-Marquardt algorithm (Press *et al.*, 1993) in Igor Pro (WaveMetrics). AMPAR kinetic rate constants were optimised using a stochastic search algorithm (Vanier & Bower, 1999), with a Gauss-Newton (Mardis & Sibert, 1998) step every 20^{th} trial.

The principle behind these algorithms are similar: the current guess for an optimal set of parameters $(p_1, \ldots, p_n)_i$ are associated with a fitness $f(p_1, \ldots, p_n)_i = f_i$. Based on the fitness and $(p_1, \ldots, p_n)_i$ a new set of parameters $(p_1, \ldots, p_n)'$ are produced and the corresponding f' is evaluated. If $f' < f_i$, $(p_1, \ldots, p_n)_{i+1}$ are set to $(p_1, \ldots, p_n)'$ and the procedure is repeated. The Levenberg-Marquardt and Gauss-Newton algorithms calculate $(p_1, \ldots, p_n)'$ from $\frac{\partial f}{\partial p}$ and $\frac{\partial^2 f}{\partial p^2}$. Because these algorithms are deterministic, $f' \geq f_i$ indicates the presence of a minimum, and the iterations end. These algorithms can therefore "get stuck" in local minima. This problem can be circumvented by using the stochastic search algorithm, which determines the next guess $(p_1, \ldots, p_n)'$ by adding a vector of gaussian noise with mean 0 and a given standard deviation (here set such that the coefficient of variation is 0.05-0.4). If $f' \geq f_i$, $(p_1, \ldots, p_n)_i$ are therefore merely retained as the next guess and the iterations continue. The stochastic

algorithm continues until a sufficient number of iterations have been performed or until a set threshold for f has been reached. This algorithm does not necessarily become trapped in local minima. In addition, since adding gaussian noise to $(p_1, \ldots, p_n)_i$ is much less time consuming than evaluating $\frac{\partial f}{\partial p}$ and $\frac{\partial^2 f}{\partial p^2}$. A much larger number of iterations can therefore be achieved with the stochastic search algorithm compared to the Levenberg-Marquardt or Gauss-Newton algorithms.

CHAPTER

THREE

Predictions of the effect of slowing diffusion on synaptic currents at the MF-GC synapse

3.1 Introduction

At central glutamatergic synapses the rapid rise time of AMPAR-mediated synaptic currents (Finkel & Redman, 1983; Forti *et al.*, 1997; Geiger *et al.*, 1997; Silver *et al.*, 1992) and time course of displacement of competitive antagonists (Clements, 1996; Diamond & Jahr, 1997) suggest that glutamate release can occur on a rapid timescale. However, AMPAR-mediated conductances with slow rise times (Choi *et al.*, 2000; Renger *et al.*, 2001; Carter & Regehr, 2000; DiGregorio *et al.*, 2002; Schoppa & Westbrook, 2001) indicate the presence of prolonged low concentrations of glutamate in the synaptic cleft.

At least two mechanisms could produce prolonged low concentrations of neurotransmitter: prolonged local release (PLR) via a narrow fusion pore, also known as 'slow kiss-and-run,' and diffusion of neurotransmitter from distant sites ('spillover'). However, previous studies have not been able to experimentally differentiate between these two mechanisms (Choi *et al.*, 2000; DiGrego-

rio *et al.*, 2002; Renger *et al.*, 2001). Studies reporting altered modes of vesicle recycling in glutamatergic synapses have also not been able to measure the time course of glutamate release. Therefore, glutamate release through a narrow fusion pore could, at least in principle, give rise to a cleft concentration ($[glut]_{cleft}$) similar to one that might be expected from spillover of glutamate, and thus it is not possible to distinguish between these two mechanisms based on the kinetics of the postsynaptic response or manipulations of receptor function. Here I demonstrate with simulations that lowering the diffusion coefficient in the synaptic cleft (D_{glut}) has different effect on currents generated by spillover and PLR, and can therefore be used as a general method to distinguish the mechanism underlying slow-rising currents.

3.2 Results

I first examined whether PLR and spillover of glutamate are physically plausible as mechanisms for slow-rising AMPAR-mediated currents using simulations of glutamate release, diffusion and receptor activation at the MF-GC synapse.

3.2.1 Geometry of the diffusional space at the MF-GC synapse

Cerebellar MF terminals are large with hundreds of active zones (Jakab, 1989; Jakab & Hamori, 1988; Xu-Friedman & Regehr, 2003) contacting approximately 50 different GCs. The 3-5 claw-like structures at the end of a GC dendrite each receive one synaptic contact. To develop a realistic model of glutamate diffusion within the MF-GC cleft, I constructed a simplified three-dimensional diffusional space that captured the essential anatomical features of this synaptic connection including the diffusional sink of the extracellular space between claws. Figure 3.1Ai shows a schematic representation of part of the diffusional space where

long rectangular columns represent dendritic claws, the grey surface represents the MF terminal membrane, and the spheres indicate locations of release sites. The dimensions are illustrated in Figure 3.1Aii, which shows a cross-section of part of the model geometry. the model contained a regular array of 49 release sites with a synaptic cleft width of 20 nm (Xu-Friedman & Regehr, 2003). The distance between a PSD and its nearest neighbouring PSD has previously been measured as 0.46 μm in the serial EM sections of the 18-day old rat glomerulus. However, the mean intersite distance is likely to be larger than the distance between nearest sites. I therefore calculated the intersite distance from the PSD density (2.5 sites/μm^2; Xu-Friedman & Regehr, 2003), which gave an estimate of 0.64 μm.

An assumption of linear diffusion in the synaptic cleft in the model is justified by several strands of evidence. Block of glutamate transporters does not affect the mean EPSC waveform at early times or the amplitude of slow-rising currents relative to the mean EPSC at the MF-GC synapse (DiGregorio *et al.*, 2002). Moreover, glutamate transporters are located on glial cells (Chaudhry *et al.*, 1995), which are distant from MF release sites (DiGregorio *et al.*, 2002; Xu-Friedman & Regehr, 2003), and buffering by the glutamate binding sites on AMPARs is thought to make negligible contributions to postsynaptic currents (Barbour, 2001). Rapid local release (RLR) of a vesicle at an individual release site was simulated by releasing 4000 glutamate molecules (Riveros *et al.*, 1986) instantaneously into a single voxel.

3.2.2 Simulations of EPSCs arising from distant release sites

To examine whether measured slow-rising currents could arise from glutamate spillover, I modelled rapid release from many spatially distributed release sites

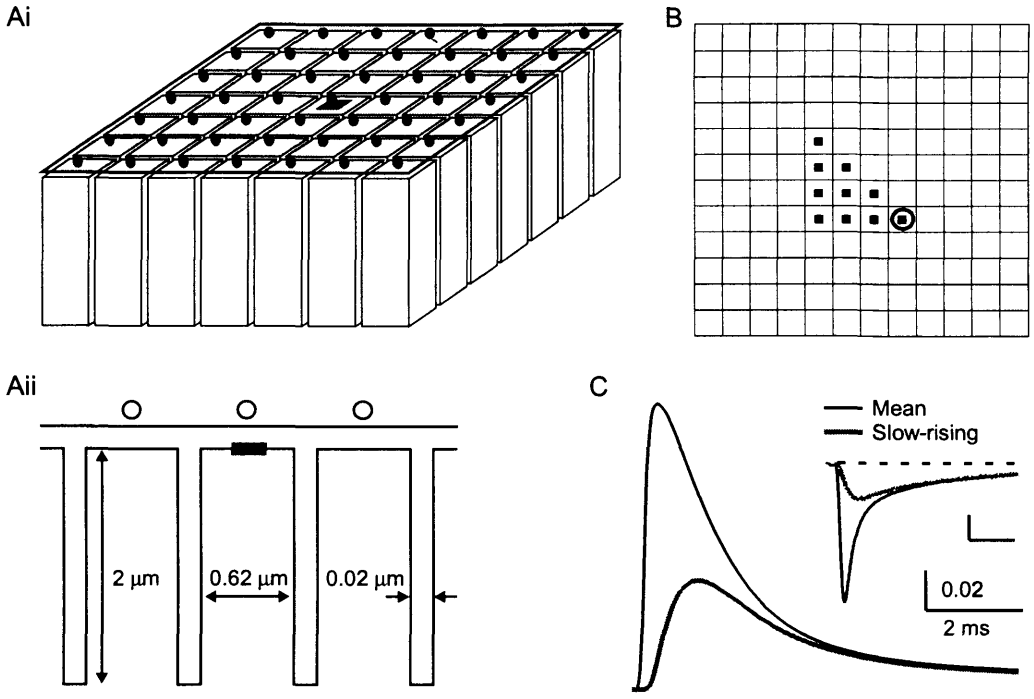

Figure 3.1: Simulation of glutamate diffusion and receptor activation for rapid local and distant release at the MF-GC synapse. **Ai**, Schematic representation of part of the 3D geometry used for simulation of glutamate diffusion. Spheres denote presynaptic release sites, grey shading indicates presynaptic membrane and columns represent dendritic claws. Glutamate was detected over the central postsynaptic density (dark grey square). **Aii**, Cross-section of the 3D geometry illustrating the sinks created by the space between dendritic claws. **B**, Top view of the actual diffusional space (12x12 claws) showing the location of the glutamate source (circle) and multiple detection sites (filled squares) used to calculate concentration transients from each site. I calculated the $[glut]_{cleft}$ waveform arising from multiple sites by summating the individual waveforms detected from each of the 10 different release site to central PSD distances (squares) in our diffusional geometry. **C**, Simulated mean and slow-rising responses expressed as AMPAR open probability for the geometry in A. Responses were calculated with the WJ scheme and a D_{glut}=0.5 $\mu m^2/ms$. Inset, population mean EPSC and slow-rising current recorded from granule cells at 37°C from DiGregorio *et al.* (2002). Scale bar 10 pA and 2 ms.

(Figure 3.1Ai, spheres) and detected glutamate at a single PSD (Figure 3.1Ai, square). It was possible to simplify the computation of the glutamate concentrations, since several sites had the same distance to the PSD (Figure 3.1B). This was achieved by calculating the contribution to $[glut]_{cleft}$ from release at each site by sampling a single release event at multiple different synaptic locations (Figure 3.1B). For these initial simulations I used a value of D_{glut} of 0.5 $\mu m^2/ms$ (half the diffusion coefficient of glutamine in aqueous solution at 37°C; calculated from Longsworth, 1953). To simulate vesicular release following an action potential, each release site was modelled stochastically using the measured release probability and latency distribution for vesicular release (0.46 and 54 μs, respectively; Sargent *et al.*, in preparation). For each trial, the $[glut]_{cleft}$ waveform was calculated by summing the glutamate concentrations arising from all sites that released on that trial. Since the kinetic properties of GC AMPARs are largely unknown, as they are absent from the soma (Silver *et al.*, 1996a) and non-synaptic regions of the dendrites (DiGregorio *et al.*, 2002), I used an AMPAR model from cerebellar Purkinje cells (Wadiche & Jahr, 2001, adjusted from 33°C to 37°C) to calculate the channel response from the $[glut]_{cleft}$. AMPAR activation is expressed as an open probability waveform ($P_{open}(t)$), since this does not require assumptions about the single-channel conductance or the number of receptors in a PSD. Simulations exhibited a rapidly rising $P_{open}(t)$ when release occurred from the site opposite the central PSD, and a slow-rising $P_{open}(t)$ when this local release site failed (Figure 3.1C). The slow-rising $P_{open}(t)$ simulated under these conditions had a 10-90% rise time (0.58 ms) and an amplitude, relative to the mean $P_{open}(t)$ (0.41), comparable to measured slow-rising and mean EPSC averaged across the population (Figure 3.1C, inset; from DiGregorio *et al.*, 2002). It is clear from these simulations that a spillover mechanism based on rapid release from distant sites can, in principle, generate the slow-rising AMPAR-mediated EPSC observed at the MF-GC

synapse.

3.2.3 Simulations of EPSCs arising from prolonged local release

Constructing a model of synaptic transmission mediated by PLR of glutamate requires a time course of release from single vesicles that could mediate slow-rising currents. Since there are no measurements of this time course for glutamatergic synapses, I estimated the $[glut]_{cleft}$ waveform from the measured slow-rising EPSC, and used this waveform to derive a neurotransmitter release time course. To accomplish this, the recorded population average slow-rising EPSC (DiGregorio *et al.*, 2002, Figure 3.2C inset) was first expressed as $P_{open}(t)$ (Figure 3.2Ai). The P_{open} at the peak of the slow-rising EPSC was calculated by

$$P_{open}(t_2) = \frac{P_r P_Q L_Q EPSC_{slow}(t_2)}{EPSC_{fast}(t_1)}$$

where P_r is the release probability, L_Q is the ratio of stimulus-aligned and rise-aligned quantal currents (0.84; Sargent *et al.*, in preparation) and P_Q is the estimated P_{open} of the quantal event (0.45 ; Silver *et al.*, 1996c), t_1 and t_2 refer to the time of the peaks of the fast-rising ($EPSC_{fast}$) and slow-rising ($EPSC_{slow}$) EPSCs (DiGregorio *et al.*, 2002). $P_r P_Q L_Q$ thus gives average P_{open} underlying the fast-rising component, taking release probability into account. This gave a peak P_{open} of 0.05 for the slow-rising EPSC.

I then used a least squares optimisation algorithm to search for the $[glut]_{cleft}$ waveforms for which the AMPAR $P_{open}(t)$ response was most similar to that underlying the measured slow-rising current (Figure 3.2Ai; see chapter 2). Since the properties of the AMPARs are likely to influence the estimate of the underlying glutamate waveform, I used temperature adjusted native AMPAR models from brain regions where they have been studied in detail: cerebellar Purkinje

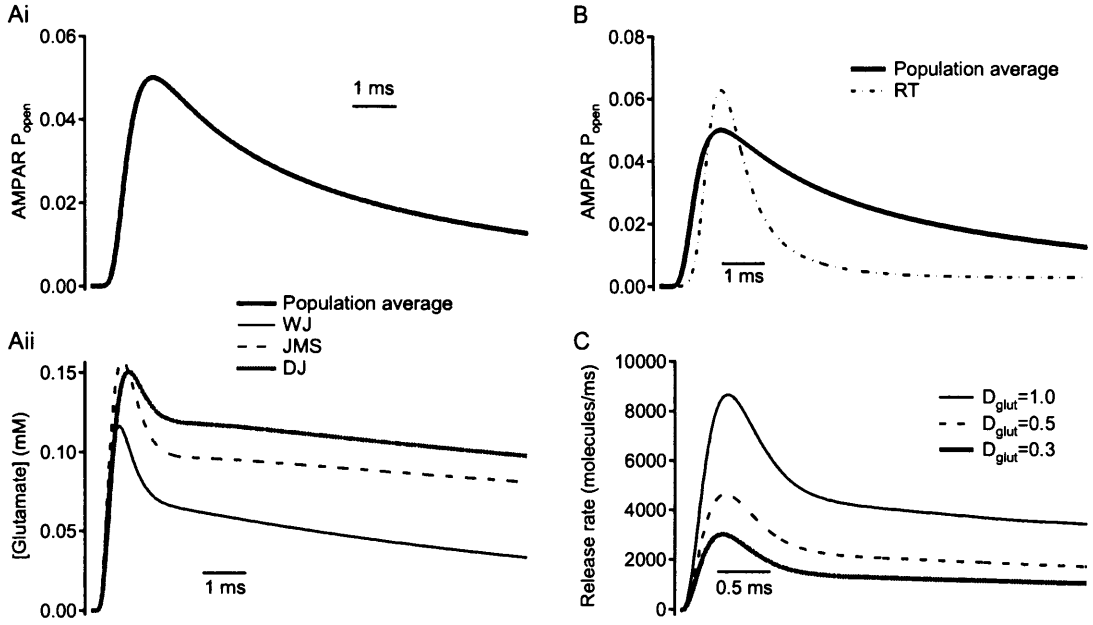

Figure 3.2: Estimation of cleft glutamate concentration and prolonged local release time course from slow-rising EPSCs. **Ai**, Measured slow-rising current, expressed as AMPAR open probability ($P_{open}(t)$) together with optimised $P_{open}(t)$ waveforms for the WJ, JMS and DJ kinetic schemes. All waveforms overlie. **Aii**, Concentration waveforms underlying optimal $P_{open}(t)$ waveforms in i. **B**, Measured slow-rising $P_{open}(t)$ and optimised $P_{open}(t)$ waveform for the RT scheme. **C**, Local glutamate release time course calculated by deconvolving the concentration waveform derived using the WJ scheme with the impulse response function for local release calculated from the 3D geometry in Figure 3.1A for different values for D_{glut} (units of $\mu m^2/ms$).

cells (Wadiche & Jahr, 2001, WJ), CA1 cultures (Diamond & Jahr, 1997, DJ), CA3 pyramidal neurons in hippocampal slices (Jonas *et al.*, 1993, Set 1; JMS) and auditory brainstem (Raman & Trussell, 1995, RT). The AMPARs underlying the RT scheme include GluR4$_{flop}$ (Ravindranathan *et al.*, 2000), which are thought to be expressed in GCs (Mosbacher *et al.*, 1994). These models covered the wide range of desensitisation characteristics across cell types (Raman et al., 1994) and had a 4-fold range of EC_{50} (Table 1.1). Figure 3.2Ai shows the best fits to the $P_{open}(t)$ of the slow-rising EPSCs using the WJ, JMS, and DJ AMPAR kinetic models (traces overlie). The $[glut]_{cleft}$ concentration derived from the three models had rapid rise times (10-90%, 0.27-0.38 ms) and all had a similar shape and peak (116-157 μM, Figure 3.2Aii), with a decay that could be fit with dual exponentials with τ_1= 0.28-0.32 ms and τ_2=12-45 ms. In contrast, the $P_{open}(t)$s generated with the rapidly desensitising RT kinetic scheme was unable to reproduce the slow-rising EPSCs from the MF-GC synapse (Figure 3.2B), and thus the RT scheme was not used for further simulations of PLR.

In the absence of buffering and uptake, removal of glutamate from the synaptic cleft is determined by diffusion alone. The $[glut]_{cleft}$ waveform thus equals the convolution of the timecourse of release and the impulse response function of glutamate decay. It is therefore possible to calculate the glutamate release time course by deconvolving (Press *et al.*, 1993) the $[glut]_{cleft}$ waveform underlying the slow-rising EPSC with the $[glut]_{cleft}$ waveform following instantaneous local release in the MF-GC synaptic geometry (Figure 3.1A). Figure 3.2C shows the deconvolved local release time courses, derived from the $[glut]_{cleft}$ waveform for the WJ kinetic scheme for three values of D_{glut}. The decay for each waveform was initially rapid (τ_1=0.32-0.35 ms) with a slower prolonged tail (τ_2=18-21 ms). These release time courses are within the range of calculated durations of emptying of small clear vesicle through a narrow fusion pore (Klyachko & Jackson,

2002). Depending on the initial value of D_{glut}, the integral of the glutamate release rate corresponds to 2.6-8.4 vesicles per EPSC (over 10 ms; WJ scheme), consistent with the observed lower relative variability of the slow-rising EPSC than the fast-rising component (DiGregorio *et al.*, 2002). These models of PLR and spillover demonstrate that both are physically plausible mechanisms for the slow-rising current at the MF-GC synapse.

3.2.4 Simulating the effects of slowing diffusion on spillover

Since one of the key differences between currents produced by transmitter spillover and PLR is the distance over which glutamate diffuses, it is possible that changing the mobility of glutamate could be used to distinguish between these mechanisms. Figure 3.3A shows a simulation of the effect of slowing diffusion on spillover-mediated $[glut]_{cleft}$. Lowering D_{glut} from 1.0 (the value in free solution) to 0.5-0.1 $\mu m^2/ms$ had no effect on the peak glutamate concentration (130 μM), but slowed the time-to-peak of the $[glut]_{cleft}$ waveform by up to 997 μs (Figure 3.3A). The AMPAR-mediated $P_{open}(t)$ responses to these concentration waveforms (WJ kinetic scheme) are shown in Figure 3.3B. Lowering D_{glut} to 0.1 $\mu m^2/ms$ increased the peak P_{open} by 124% and delayed the current onset, increasing the time-to-peak of spillover-mediated currents by 110%. Figure 3.3C shows the time-to-peak of the spillover $P_{open}(t)$ for different kinetic schemes as a function of D_{glut}. Changes in D_{glut} in the mid-to-high range led to small changes, while in the lower range, even small reductions in D_{glut} caused substantial increases in the time–to-peak. The peak amplitude of the spillover-mediated $P_{open}(t)$, shown in Figure 3.3D, increased monotonically over the entire range of simulated D_{glut}. The slowing in the time-to-peak of spillover-mediated P_{open} was also observed over a wide range of molecules per vesicle (2000-6000; see Figure

3.4).

$P_{open}(t)$ mediated by RLR also increased in amplitude when diffusion is slowed (Figure 3.5A) as previously predicted (Rusakov & Kullmann, 1998a) and observed (Min *et al.*, 1998). Changes in the peak AMPAR P_{open} mediated by RLR were more pronounced than the increase in spillover-mediated P_{open}, increasing more steeply over the full range of D_{glut} (Figure 3.5B). These simulations suggest that lowering D_{glut} will increase the time-to-peak and increase the amplitude of slow-rising currents mediated by spillover.

3.2.5 Simulating the effects of slowing diffusion on prolonged local release

Figure 3.6A shows the effect of slowing diffusion on a $[glut]_{cleft}$ mediated by PLR. Lowering D_{glut} from 1.0 to 0.5-0.1 $\mu m^2/ms$ markedly increased the amplitude of the $[glut]_{cleft}$ transients (derived with the WJ kinetic scheme) from 116 to up to 811 μM by retarding diffusion out of the cleft. However, the shape of concentration transients arising from PLR was relatively insensitive to lowering D_{glut}, with the peak slowing by only 154 μs. Figure 3.6B shows that the large amplitude increases are also preserved in the AMPAR responses, with the peak amplitude increasing by up to 707%. In contrast to spillover, the time-to-peak of the $P_{open}(t)$ *decreased* by 39% when D_{glut} was lowered, due to the concentration-dependence of the AMPAR response rise time. This decrease in the time-to-peak (Figure 3.6C) and the increase in the peak P_{open} (Figure 3.6D) were observed consistently when lowering D_{glut} from 1.0 $\mu m^2/ms$. Since our estimate of the release time course depends on the initial D_{glut}, these simulations were repeated with initial D_{glut} values of 0.2, 0.3 (Figure 3.6CD, open symbols) and 0.5 $\mu m^2/ms$. In general, these simulations showed that the time-to-peak decreased and the amplitude increased

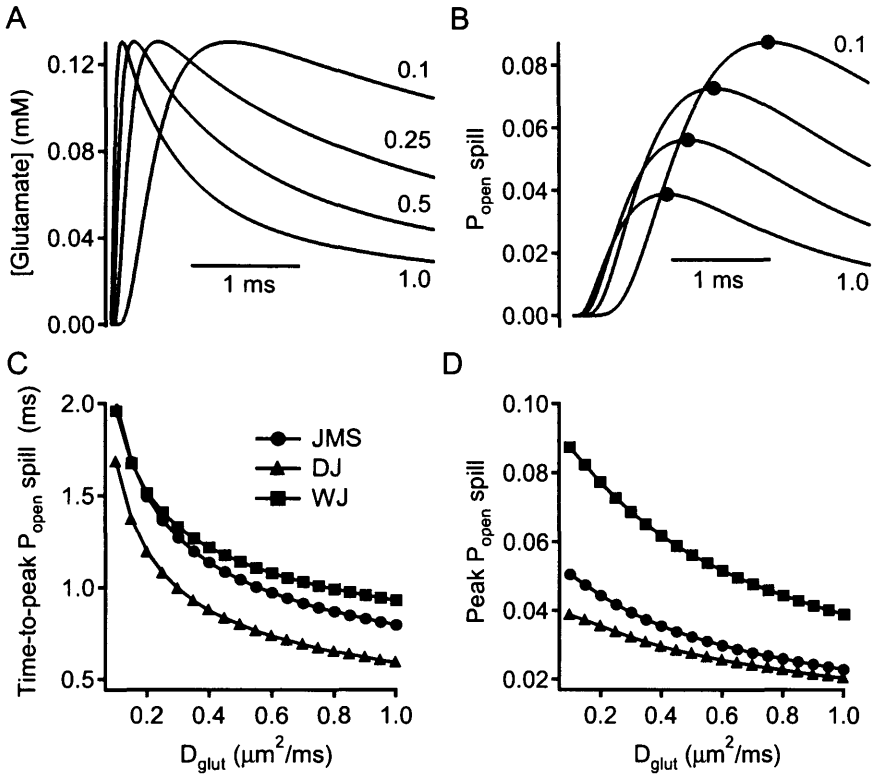

Figure 3.3: The effect of slowing diffusion on simulated spillover. **A,** Simulated average glutamate concentration and **B,** AMPAR open probability ($P_{open}(t)$) for spillover using D_{glut} of 1.0, 0.5, 0.25 and 0.1 $\mu m^2/ms$ and the WJ kinetic scheme. These spillover concentrations and P_{open} waveforms were calculated without release latency or stochasticity. Filled circles indicate the peak. Transients had times-to-peak of 0.93, 1.14, 1.41, 1.96 ms, respectively. **C,** Time-to-peak and **D,** peak amplitude of simulated slow-rising $P_{open}(t)$ mediated by spillover as a function of D_{glut}, for the three different kinetic schemes.

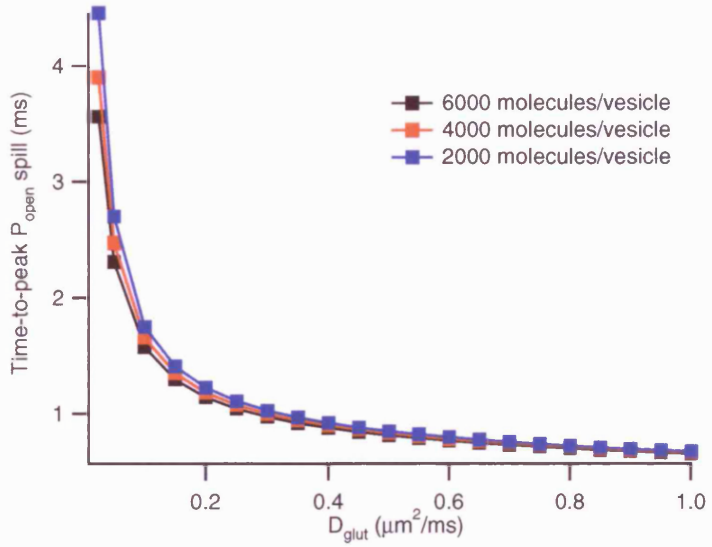

Figure 3.4: The slowing in the time-to-peak does not depend on vesicular content. Time-to-peak of simulated slow-rising $P_{open}(t)$ mediated by spillover as a function of D_{glut}, for the WJ kinetic scheme, for 2000, 4000 and 6000 molecules per vesicle.

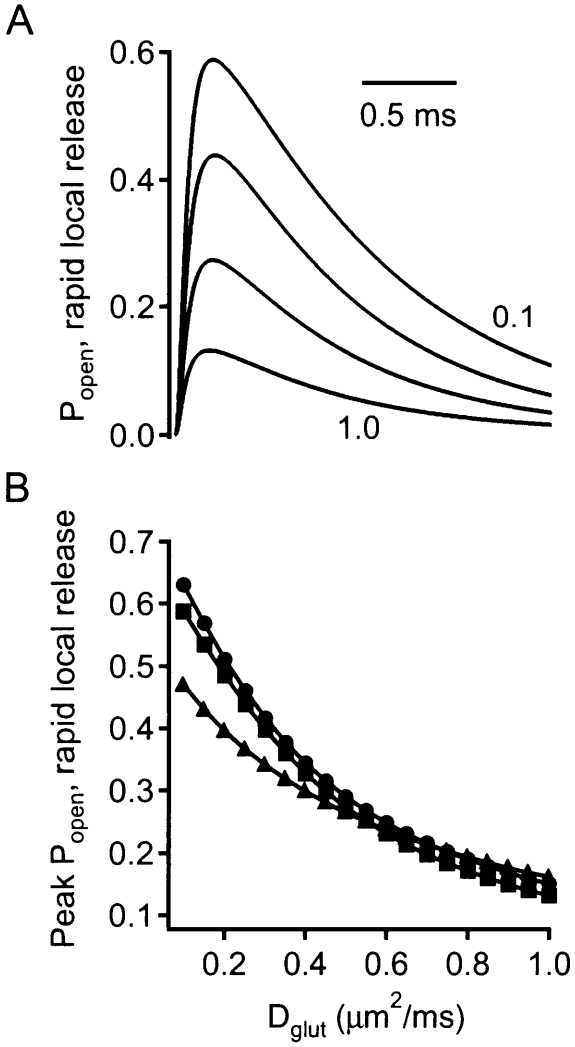

Figure 3.5: The effect of slowing diffusion on simulated RLR. **A**, Simulated $P_{open}(t)$ for rapid local release (RLR) of 4000 molecules for the WJ scheme and a D_{glut} of 1.0, 0.5, 0.25 and 0.1 $\mu m^2/ms$. **B**, Peak amplitude of $P_{open}(t)$ mediated by RLR as a function of D_{glut}, symbols as for 3.3D.

as above. However, some simulations with an initial D_{glut} of 0.2 or 0.3 $\mu m^2/ms$ exhibited a small increase in the time-to-peak (<5%). Under these low initial D_{glut} conditions, amplitude increases were still 100-200% for a 50% reduction in D_{glut}. These simulations suggest that in contrast to spillover, lowering D_{glut} will generally decrease the time-to-peak of slow-rising currents mediated by PLR. However, in those cases where the time-to-peak is slightly increased by lowering D_{glut}, the peak amplitude of these currents will be increased dramatically.

To test a wider range of conditions, I examined the effect of lowering D_{glut} on release waveforms of different durations and amplitudes. Figure 3.7A shows a 3D plot of the relationship between the change in the time-to-peak of $P_{open}(t)$ generated with step-shaped release events of different duration (0.1-10 ms) and release rate (10^2-10^4 molecules/ms) for the WJ model. These simulations covered a wide range of peak P_{open} values (10^{-6}-0.34). As for the simulations above, the time-to-peak of currents mediated by PLR usually remained the same or decreased on lowering D_{glut} from 0.5 to 0.25 $\mu m^2/ms$. As the release time course becomes brief (<1 ms), the time-to-peak began to increase when lowering D_{glut}. In those cases where the time-to-peak increased more than 5%, large increases (>100%) in the peak amplitude were again observed (Figure 3.7B). Moreover, their initial time-to-peak is rapid (>2-fold faster than slow-rising currents in the GC). I also verified that calculating $P_{open}(t)$ in the model by averaging $[glut]_{cleft}$ over the PSD did not mask an increase in the time to peak, by examining currents generated by discrete annular receptor distributions in the PSD following PLR.

3.3 Discussion

These simulations of spillover and prolonged release show that lowering D_{glut} has different effects on the time-to-peak and amplitude of slow-rising EPSCs aris-

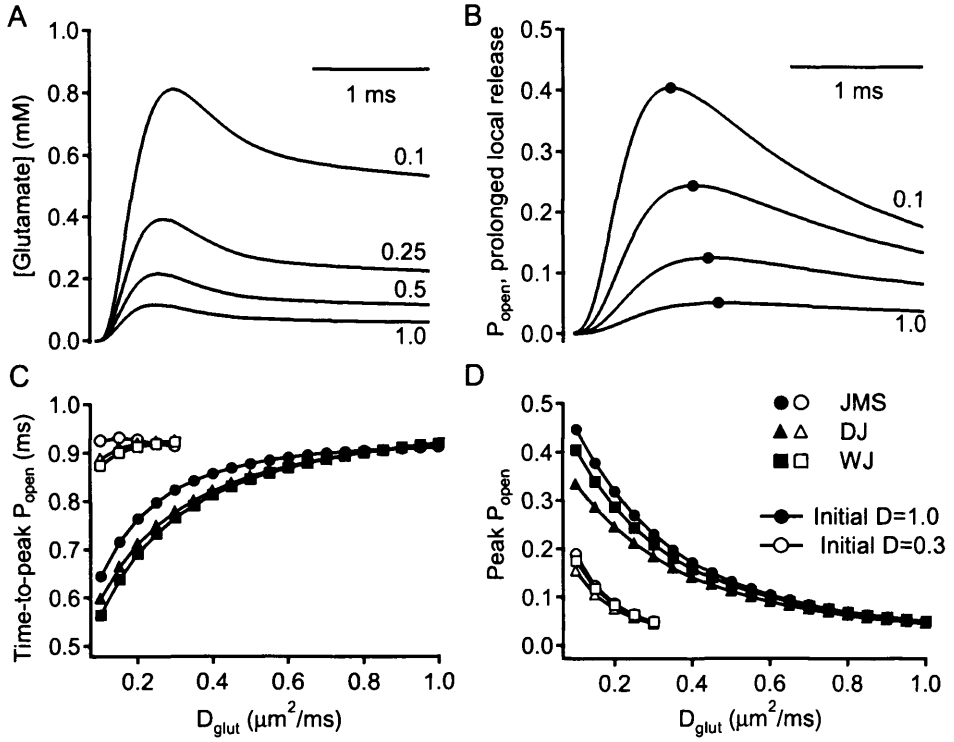

Figure 3.6: The effect of slowing diffusion on simulated prolonged local release. **A**, Simulated concentration waveforms resulting from prolonged local release (PLR) for D_{glut} of 1.0, 0.5, 0.25 and 0.1 μm^2/ms. The release time course in this panel was determined from the measured slow-rising EPSC, for an initial D_{glut} of 1.0 μm^2/ms and the WJ kinetic scheme. **B**, Open probability responses to the concentration waveforms in A for PLR, using the WJ kinetic scheme. Filled circles indicate peaks, with times-to-peak of 0.92, 0.85 0.73 and 0.57 ms, respectively. **C**, Time-to-peak and **D** peak amplitude of simulated slow-rising $P_{open}(t)$ mediated by PLR as a function of D_{glut}, for the three different kinetic schemes. The release time courses were determined with an initial D_{glut} of 1.0 μm^2/ms (filled symbols) and 0.3 μm^2/ms (open symbols).

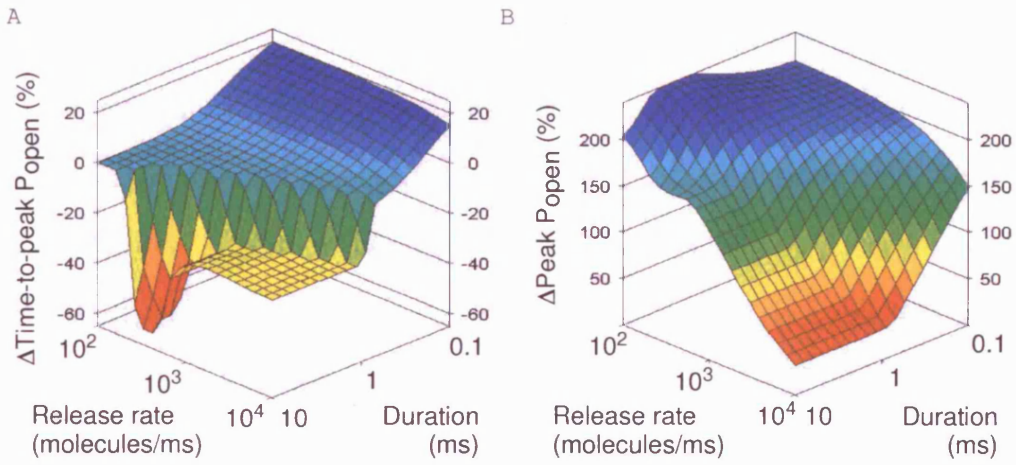

Figure 3.7: The effect of slowing diffusion on simulated prolonged local release with a range of rates and amplitudes. **A**, Relative change in the time-to-peak of the $P_{open}(t)$ when lowering D_{glut} from 0.5 to 0.25 $\mu m^2/ms$ for the WJ scheme. The release time courses were step-shaped of duration 0.1 to 10 ms and amplitude 10^2-10^4 molecules/ms. The times-to-peak in this panel were measured from the beginning of glutamate release. **B**, Relative change in peak amplitude of $P_{open}(t)$ mediated by different time courses of local release, as in A.

ing from these two mechanisms. Agents that lower glutamate mobility can therefore be used to determine whether spillover or PLR underlie slow-rising currents under a wide range of physiologically plausible initial conditions.

This approach for separating local release from distant release relies on slowing glutamate diffusion in the synaptic cleft. A reduction in D_{glut} slows the $[glut]_{cleft}$ waveform arising from distant sites and the time-to-peak of $P_{open}(t)$ mediated by spillover but has little effect on the time-to-peak of $P_{open}(t)$ generated by PLR because of the short distances over which glutamate diffuses within the active zone. Slowing D_{glut} does, however, substantially enhance the accumulation of locally released glutamate by slowing diffusion out of the cleft, leading to a substantial enhancement of the peak $[glut]_{cleft}$. Changing D_{glut} has little effect on the shape of the $[glut]_{cleft}$ waveform mediated by PLR, because it is dominated by the release time course. In contrast, the peak $[glut]_{cleft}$ resulting from spillover is independent of D_{glut}. The modest increases in the predicted peak P_{open} of spillover responses on lowering D_{glut} result from the slower $[glut]_{cleft}$ waveform, which enhances receptor activation. It should be noted that at short intersite distances, the dextran-induced slowing will be small, and may be comparable to the speeding due to channel kinetics and therefore would be difficult to distinguish spillover from PLR.

CHAPTER

FOUR

Modulation of glutamate mobility reveals the mechanism underlying the slow-rising EPSCs and the rate of diffusion

4.1 Introduction

Having established a general method for distinguishing between prolonged local release and spillover as mechanisms for slow-rising currents, I proceeded to apply this method to experimental recordings from granule cells in acute slices. The method is based on lowering D_{glut}, and its practical applicability is thus contingent on the availability of a suitable agent that can modulate diffusion.

Large macromolecules present in the cytoplasm are known to slow diffusion compared to free solution (Ellis, 2001). Macromolecules consisting of glucose chains of various lengths, called dextrans, are used by single-celled organisms to store energy and constitute an ingredient in processed food. Inclusion of 5% dextran 40 kDa increases the viscosity of ACSF from 1.05 to 2.45 mPa·s (Min *et al.*, 1998). Perfusion of this solution enhances synaptic responses mediated by acti-

vation of local and distant receptors (Min *et al.*, 1998) as expected for a reduction in the diffusion coefficient.

According to the Stokes-Einstein relationship, the diffusion coefficient is inversely related to viscosity (Weiss, 1996), but an assumption of this law is that the diffusant is much larger than the solvent. The opposite holds for glutamate diffusion in the presence of dextran, so the Stokes-Einstein relationship cannot predict the change in D_{glut} from the impact of dextran on the viscosity.

Although it may be possible to calculate the change in mobility from the volume fraction occupied by dextran (Rusakov & Kullmann, 1998b), it is unclear how to apply such a calculation to changes in D_{glut} in the synaptic cleft induced by dextran. The concentration of, and volume occupied by, endogenous macromolecules and thus the mobility of glutamate in the synaptic cleft under initial conditions are unknown. Furthermore, it is uncertain if the restriction in diffusion imposed by endogenous macromolecules would add linearly to further restrictions in diffusion imposed by dextran. Thus, both the initial value of D_{glut} and the change imposed by dextran are difficult to predict based on the existing literature. Here, I demonstrate that the change in the amplitude of the local rapid components, and in the time-to-peak of the spillover component can together be used to calculate both the initial value, and the change in dextran, of D_{glut}.

4.2 Results

4.2.1 Slowing diffusion at the mossy fiber-granule cell synapse with dextran

To examine the mechanism underlying slow-rising currents at the MF-GC synapse, I slowed glutamate diffusion by adding 1mM (5% w/v) of the macro-

molecule dextran (43 kDa) to the extracellular medium while recording evoked EPSCs from GCs. Slow-rising AMPAR EPSC were separated from fast-rising currents on the basis of rise time and fitted slow-rising currents with equation (2.1) to determine the amplitude and time-to-peak. The mean and isolated slow-rising EPSCs before and during dextran perfusion are shown in Figure 4.1A for a representative cell. Perfusion of dextran resulted in an increase in the time-to-peak of the isolated slow-rising EPSC (25% for this cell), with an average increase of 17.6±7.1% (time-to-peak 1.35±0.14 ms in control, 1.56±0.17 ms in dextran; p=0.04, n=9; Figures 4.1A,B). The time-to-peak of the mean EPSC, which is dominated by the fast-rising component (DiGregorio *et al.*, 2002), did not slow significantly (0.34±0.04 ms in control, 0.35±0.05 ms in dextran; p=0.56, n=9; Figure 4.1C). The absence of a change in time-to-peak of the mean EPSC excludes the possibility that the effect of dextran on slow-rising currents was caused by changes in filtering properties of the cell-electrode circuit or a change in the properties of the postsynaptic receptors.

In contrast to model predictions for RLR (Figure 3.5), the amplitude of the fast-rising EPSC was unaltered in the presence of dextran (-34.3±9.3 pA in control, -32.1±11.1 pA in dextran; p=0.34, n=9; Figure 4.1D). The failure rate of the fast-rising component (12.9±1.3% in control, 25.0±2.3% in dextran; p=0.04, n=9; Figure 4.1E) also increased, indicating a decrease in release probability in the presence of dextran. I therefore tested whether dextran-induced slowing of the slow-rising EPSCs could be accounted for by lowering the release probability. Figure 4.1F shows slow-rising EPSCs recorded in 2 and 1.5 mM $[Ca^{2+}]_o$ normalised to their peak amplitude. The mean EPSC peak amplitude recorded under these conditions decreased from -49.3 pA to -20.7 pA, respectively ($p<0.001$; Figure 4.1F, inset). However, there was no change in the time-to-peak of slow-rising EPSC (1.32±0.10 ms in 2 mM, 1.43±0.19 in 1.5 mM $[Ca^{2+}]_o$; p=0.42, n=8) demonstrat-

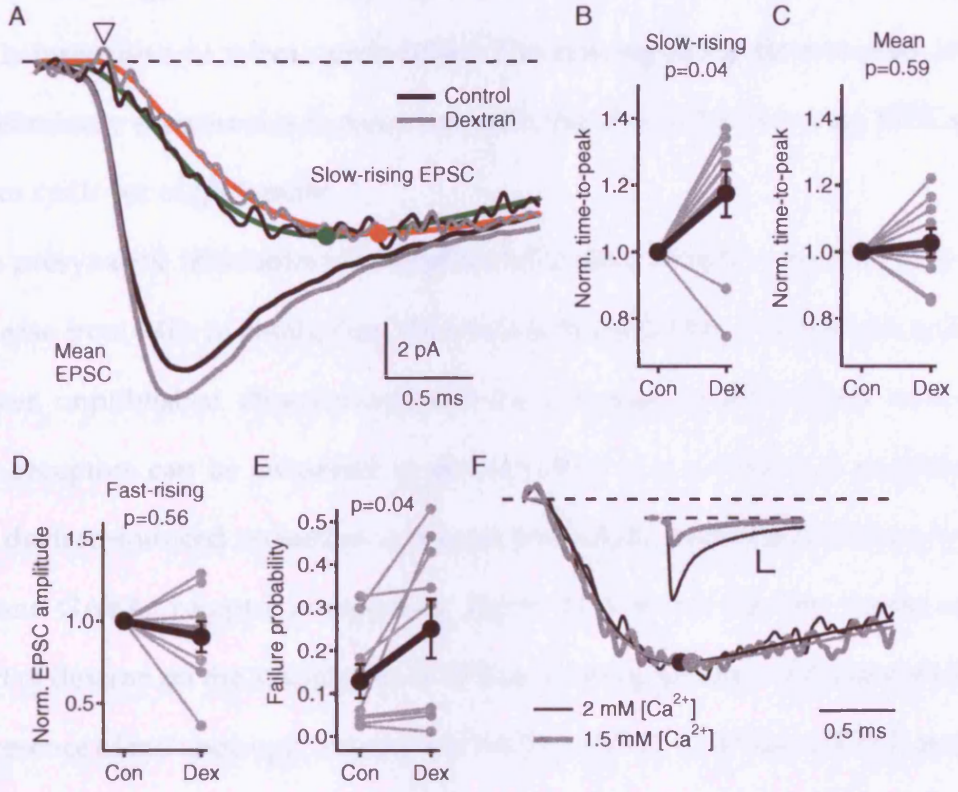

Figure 4.1: Dextran application increases the time-to-peak of slow-rising EPSCs at the MF-GC synapse. **A**, Mean AMPAR EPSC and slow-rising EPSCs recorded in control solution (black trace) and in the presence of dextran (grey trace). The traces were aligned on the 20% rise time of the mean EPSCs (open triangle). The slow-rising current was fitted with equation 1 in control (green) and in dextran (red). Filled circles indicate the peak. **B**, Summary plot of the change in time-to-peak of the slow-rising EPSC in dextran. **B-E**, individual cells indicated in grey, average measurement in black. **C**, Summary plot of the change in time-to-peak of the mean EPSC in dextran relative to control. **D**, Summary plot showing effect of dextran on the amplitude of the fast-rising EPSC. **E**, Summary plot showing effect of dextran on the failure probability of the fast-rising component. **F**, Normalised slow-rising EPSCs recorded in 2 and 1.5 mM $[Ca^{2+}]_o$, aligned on the 20% rise point of the mean EPSC, together with fits. Filled circles indicate peaks. Inset, mean EPSCs recorded in 2 and 1.5 mM $[Ca^{2+}]_o$; calibration bar: 10 pA, 1 ms.

ing that the slowing of the time-to-peak of slow-rising EPSCs in the presence of dextran is insensitive to release probability. The slowing of the time-to-peak in these preliminary experiments is consistent with the idea that slow-rising EPSCs arise from spillover of glutamate.

Since presynaptic metabotropic receptors have been shown to reduce glutamate release from MFs in cerebellum (Mitchell & Silver, 2000a, T.A. Nielsen and R.A. Silver, unpublished observations) and the activation of presynaptic metabotropic receptors can be enhanced in dextran (Min *et al.*, 1998), it is possible that the dextran-induced reduction in release probability could be abolished by mGluR and $GABA_B$ receptor antagonists. Figure 4.2A shows the time course of the effect of dextran on the amplitudes of EPSCs (running average of 20) recorded in the presence of metabotropic antagonists E4CPG, CPPG, CGP 52432 (CPG) and LY 341495 (LY). Figure 4.2B and C show that in the presence of dextran, both the amplitude of the mean EPSC and the time-to-peak of the slow-rising EPSC increased by 26% in this cell and this effect was reversible. Across all cells, the amplitude of the fast-rising EPSC increased significantly with dextran in the presence of metabotropic antagonists (Figure 4.2D, 14±4%; $p<0.01$, n=9). Although the amplitude of the slow-rising current tended to increase, this was not significant (Figure 4.2E, 24±11%; p=0.06, n=9). Moreover, the failure rate of fast-rising events was unaffected by dextran in the presence of metabotropic antagonists (p=0.12, n=9; Figure 4.2F) consistent with the idea that transmitter retention in the presence of dextran reduced release probability by activating presynaptic receptors. On average the time-to-peak of the slow-rising current was slowed by 22±7% (p=0.014, n=9; Figure 4.2G), not significantly different from the slowing observed in the absence of metabotropic antagonists (p=0.65, unpaired t-test). In 6 cells where recordings lasted after returning to control solution, the peak amplitude of the fast-rising EPSC returned to 91% of control, significantly differ-

ent from in dextran (p=0.02). In 3 of 4 cells where long recordings were made and dextran slowed currents by more than 5%, the time-to-peak returned to at least within 5% of the control value; with an average washout of 73% for all 4 cells.

4.2.2 Effect of dextran on quantal EPSCs

To examine the effect of dextran on local release in the absence of slow-rising currents, quantal successes were isolated under low release probability conditions (1 mM $[Ca^{2+}]_o$) when the chances of releasing multiple quanta per trial are small (<5%; Silver, 2003) and slow-rising currents are minimal. The recordings were made in the absence of metabotropic receptor antagonists. Figure 4.3Ai and ii shows isolated, aligned successes recorded in 1 mM $[Ca^{2+}]_o$ control solution and in dextran, respectively. Dextran increased the quantal amplitude by 27±8% (p=0.02, n=6; Figure 4.3B) from a control value of 22.0±2.9 pA and there was no change in the failure rate (90±2% in control, 93±2% in dextran; p=0.17, n=6). The time-to-peak of quantal EPSCs did not change in dextran (191±15 μs and 196±19 μs, respectively; p=0.63, n=6). The potentiation was no different from that observed for the fast-rising EPSC in the presence of metabotropic blockers (p=0.12; unpaired *t*-test). Since the fast-rising EPSC is defined as the difference between the mean EPSC and the slow-rising EPSC, the similar increase in the amplitude of fast-rising and quantal EPSCs indicates that the fast-rising and slow-rising current components sum linearly at the peak of the mean EPSC. τ_w of the quantal EPSCs did not change significantly in dextran, although there was a trend towards acceleration (0.98 ±0.07 ms in control, 0.73 ±0.18 ms in dextran; p=0.08, n=7). The present results, which show that slow-rising currents slow by 20% in the presence of dextran indicate that they arise from glutamate spillover from distant sites, rather than PLR of glutamate, which would predict at most a

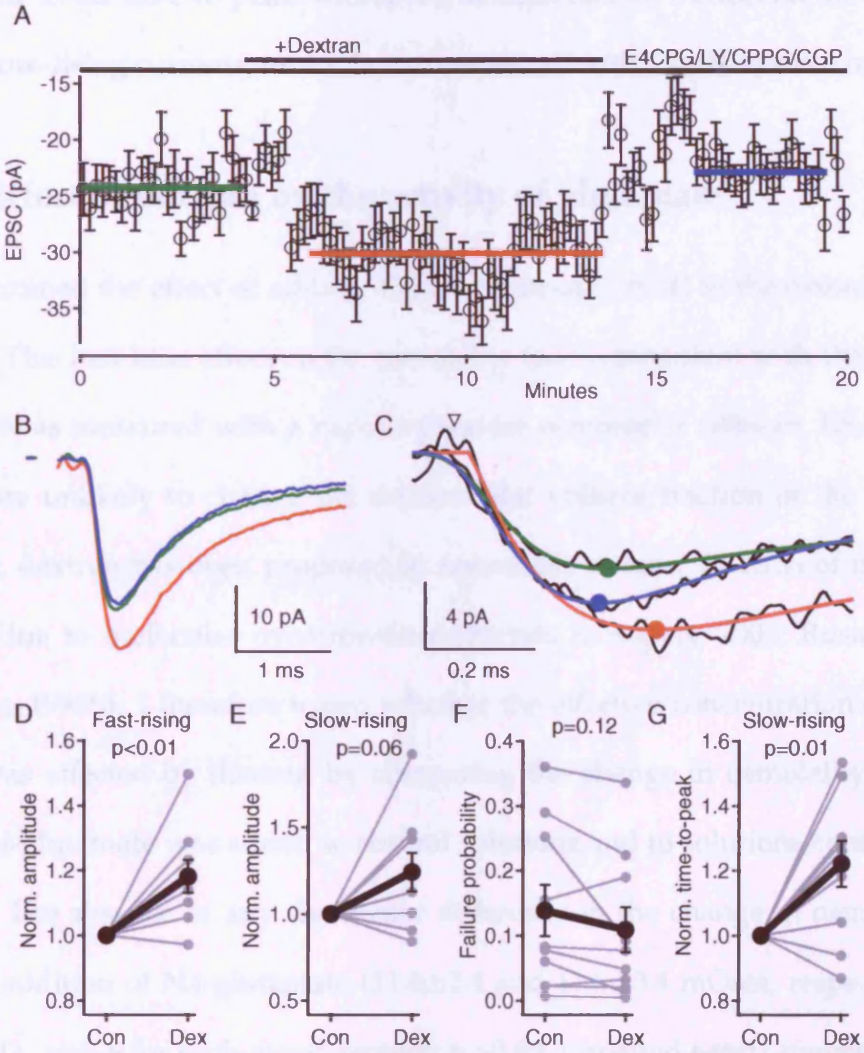

Figure 4.2: The effect of dextran on EPSCs in the presence of metabotropic receptor antagonists. **A**, Running average (n=20) of the EPSC amplitude during wash-in and wash-out of dextran for an individual cell. **B**, Mean EPSC traces before (green), during (red) and after (blue) dextran perfusion measured for periods indicated in A. **C**, Slow-rising EPSCs measured before, during and after dextran perfusion for same cell, fitted with eqn (2.1). Colors as for B, filled circles indicate the peak. The traces were aligned on the 20% rise point of the mean EPSC (open triangle). **D**, Summary plot of the relative change in fast-rising EPSC amplitude during dextran. **E**, Summary plot of the relative change in the amplitude of slow-rising currents in dextran. **F**, Summary plot of the failure probability in control and dextran. **G**, Summary plot of the relative change in the time-to-peak of slow-rising EPSCs in dextran.

5% increase in the time-to-peak. Moreover, dextran had little effect on the amplitude of slow-rising currents, which is also consistent with a spillover mechanism.

4.2.3 Effect of dextran on the activity of glutamate

I also examined the effect of adding 43 kDa Dextran (1 mM) to the extracellular solution. This had little effect on the osmolality (1.1%; consistent with Parsegian *et al.*, 1995) as measured with a vapour pressure osmometer (Wescor, USA) and is therefore unlikely to change the extracellular volume fraction of the tissue. However, dextran has been proposed to reduce the volume fraction of the free solution due to molecular overcrowding (Perrais & Ropert, 2000; Rusakov & Kullmann, 1998b). I therefore tested whether the effective concentration of glutamate was affected by dextran by comparing the change in osmolality when 10mM Na-glutamate was added to control solutions and to solutions containing dextran. The absence of any significant difference in the change in osmolality with the addition of Na-glutamate (11.6±2.4 and 11.6±3.4 mOsm, respectively, mean±S.D., n=5-8 for each measurement; $p>0.95$, unpaired *t*-test) suggests that the activity of glutamate is unaffected by dextran.

4.2.4 Estimation of D_{glut} under control conditions and in dextran

Having established that spillover underlies slow-rising EPSCs I then explored the properties of glutamate diffusion at the MF-GC synapse. Since the simulations in chapter 3 indicate that lowering D_{glut} affects the time-to-peak of the slow-rising current and the amplitude of the RLR component differentially (Figure 4.4A), it was possible to make an estimate of D_{glut} under control conditions and in the presence of dextran from our experimental observations. For each initial value of D_{glut} between 0.1 and 1.0 $\mu m^2/ms$ I calculated the values of D_{glut} in dextran

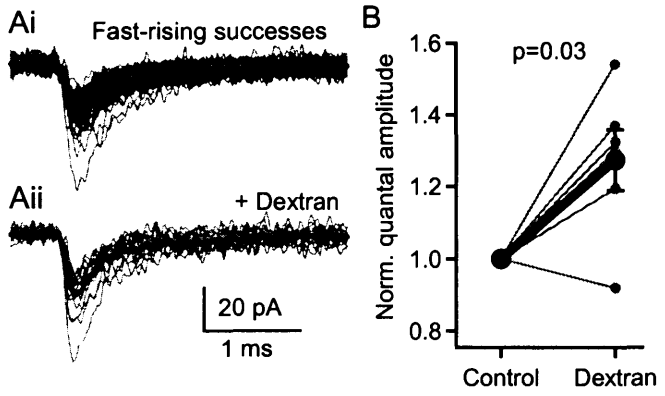

Figure 4.3: Dextran increases quantal current amplitude. **A**, Fast-rising EPSC successes recorded in low $[Ca^{2+}]_o$ in control (**i**) and dextran (**ii**), with individual currents aligned on their 10% rise time. The fraction of failures for this cell was >82% under the two conditions. **A-B**, individual cells indicated in grey, average measurement in black. **B**, Summary plot of the change in the mean quantal amplitude in the presence of dextran across cells.

that reproduced the experimentally observed change in time-to-peak of the slow-rising EPSC (19.9%, p=0.001, n=18 pooled from experiments with and without metabotropic blockers) and increases in the fast-rising EPSC amplitude (19.2%, p=0.0005; n=15 pooled from recordings of normal and low $[Ca^{2+}]_o$; Figure 4.4A). Figure 4.4B shows the relationship between the initial D_{glut} and the D_{glut} in dextran derived from the change in the time-to-peak of the spillover current and the change in amplitude of the RLR component for the WJ scheme. The intersection of these curves represents a unique pair of values for D_{glut} in control and dextran where the experimentally observed changes in time-to-peak and quantal amplitude in dextran were both observed. This approach gave values of D_{glut} in control solution of 0.23, 0.36 and 0.22 $\mu m^2/ms$ for the JMS, DJ and WJ kinetic schemes. The retardation of D_{glut} in dextran was 35-40%. These results suggest that D_{glut} is substantially lower than in free solution.

I attempted to narrow the range of the D_{glut} estimates by taking into account the fact that some kinetic schemes better matched the measured properties of the MF-GC EPSC. To include as many properties of AMPARs as possible, D_{glut} was predicted, as described above, for 12 published kinetic schemes based on fast agonist application experiments (see Table 1.1). For each scheme, I then compared the following characteristics of simulations to experimental data: the decay time course of the local component (Figure 4.5A, weighted over 3 ms), the time-to-peak and peak amplitude of the spillover $P_{open}(t)$ (Figure 4.5BC), and the amplitude ratio of RLR to spillover components (Figure 4.5C). Simulations were carried out for each channel, at the D_{glut} estimated with that scheme, and the goodness-of-fit was assessed from the χ^2 value (Figure 4.5D). The mean value of D_{glut} obtained across the 12 channel models, weighted by $1/\chi^2$, gave a value for D_{glut} of 0.33 $\mu m^2/ms$ and a slowing of diffusion in dextran by 36%. This approach provides an estimate of D_{glut} that is weighted by its ability to predict the experimentally

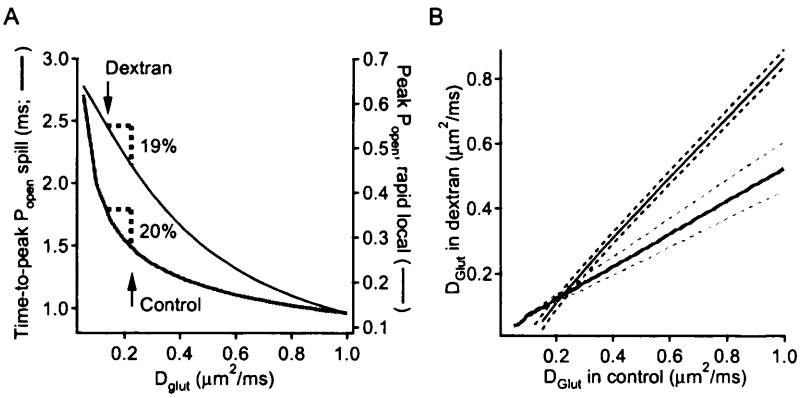

Figure 4.4: Estimation of the diffusion coefficient of glutamate in the synaptic cleft. **A**, Simulated time-to-peak of spillover (grey) and the peak amplitude of the rapid local release component (black) as a function of D_{glut} for the WJ kinetic scheme. Dotted lines indicate the locations on the curves where both the experimentally observed changes in these parameters occur for the same change in D_{glut} (arrows). **B**, Plot showing relationship between the initial D_{glut} and the value D_{glut} in dextran required to replicate our experimental findings of 20% slowing in the time-to-peak of the slow-rising EPSC (grey) and the 19% increase in the quantal amplitude of the fast-rising EPSC (black), for the WJ kinetic scheme. Dashed lines show relationships for the experimental values ± SEM.

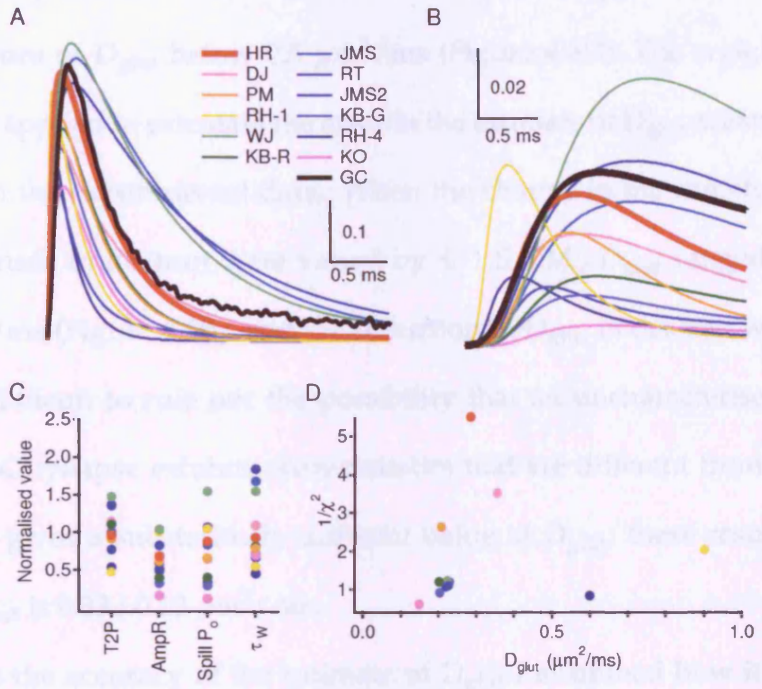

Figure 4.5: Estimation of the diffusion coefficient of glutamate in the synaptic cleft with different AMPAR kinetic schemes **A**, Simulated responses to rapid local release, using the D_{glut} predicted as in (B) for each of 12 different temperature compensated kinetic schemes. Mean quantal waveform under control conditions, expressed as $P_{open}(t)$ (black trace). **B**, Simulated spillover $P_{open}(t)$, as (C), together with fit of measured population slow-rising EPSC expressed as $P_{open}(t)$ (using equation 1; black trace). **C**, Time-to-peak (T2P), ratio of rapid local to spillover peak P_{open} amplitudes (AmpR), peak spillover P_{open} (Spill P_o), weighted decay of rapid local $P_{open}(t)$ (τ_w; over 3 ms) of simulated $P_{open}(t)$ using D_{glut} estimated for each kinetic scheme, normalised to the experimentally observed value. **D**, Goodness-of-fit of T2P, AmpR, Spill P_o, and τ_w, expressed as $1/\chi^2$, for each kinetic scheme plotted against estimated D_{glut}.

measured properties of local and spillover currents at the MF-GC synapse. Of all AMPAR schemes tested the HR had the lowest χ^2 (Figure 4.5D) and gave a value of D_{glut} of 0.29 $\mu m^2/ms$. Ten of the 12 schemes, including those with the lowest χ^2, gave values of D_{glut} below 0.5 $\mu m^2/ms$ (Figure 4.5D). The weighted mean method was applied to calculate the error in the estimate of D_{glut} arising from the variability in the experimental data. When the change in the time-to-peak and EPSC amplitude in dextran were varied by ± 1 S.E.M., D_{glut} ranged from 0.24 to 0.46 $\mu m^2/ms$ (Figure 4.4B), and the reduction in D_{glut} in dextran was 30-42%. While it is difficult to rule out the possibility that an uncharacterised AMPAR at the MF-GC synapse exhibits characteristics that are different from published models and gives a substantially different value of D_{glut}, these results suggest that that D_{glut} is 0.33±0.13 $\mu m^2/ms$.

To assess the accuracy of the estimate of D_{glut} I examined how it was influenced by model parameters that are not well defined for the MF-GC synapse in P25 rats. I report both the weighted mean measure of D_{glut}, since it takes into account the possibility that the best fitting channel is different under different model conditions, and the HR scheme, which had the lowest χ^2. First, the influence of a range of synaptic vesicle glutamate concentrations centred on that estimated in cortex (200±100 mM; Burger *et al.*, 1989; Riveros *et al.*, 1986; Xu-Friedman & Regehr, 2003) was examined. This value corresponds to 4000±2000 molecules in a 48 nm MF vesicle (Palay & Chan-Palay, 1974; Xu-Friedman & Regehr, 2003). D_{glut} was 0.20 $\mu m^2/ms$ and 0.44 $\mu m^2/ms$, for 2000 and 6000 molecules, respectively, for the weighted approach and 0.16 $\mu m^2/ms$ and 0.41 $\mu m^2/ms$ for the HR kinetic scheme. When using an upper bound for the duration of acetylcholine release estimated by Stiles *et al.* (1996) rather than instantaneous release, the estimates of D_{glut} were 3% lower and 0.2% higher, respectively. $P_{open}(t)$ responses following RLR and spillover, both taking into account

the release probability and the latency distribution, with instantaneously released glutamate and with the slower release timecourse, for D_{glut}=0.35 $\mu m^2/ms$ and the HR scheme, are shown in Figure 4.6A. I also examined the sensitivity of D_{glut} to the estimate of release probability, since it influences both the peak concentration of glutamate arising from spillover and the estimate of the peak slow-rising P_{open}. Reducing or increasing the release probability by 50% had little effect on the estimate of D_{glut}, changing it by only 6% and 4%, respectively. To account for potential changes in the intersite distance between P18 and P25 (Hamori & Somogyi, 1983) I increased the intersite distance to 0.80 μm (calculated from the change in number of synapses per MF profile). This increased D_{glut} by 18% and 14% (see Figure 4.6B for spillover and RLR $P_{open}(t)$). Electron micrographs suggest the distance between membranes in the regions between active zones is either approximately equal (Jakab & Hamori, 1988; Palay & Chan-Palay, 1974) or less (Xu-Friedman & Regehr, 2003), which may be due to fixation. I therefore simulated diffusion in a geometry where the cleft width was halved outside the active zone (to 10 nm; Figure 4.6C). With this geometry the weighted mean D_{glut} increased to 0.43 and 0.50 $\mu m^2/ms$. Finally, adding 200 glutamate binding sites (Robert & Howe, 2003) per active zone to mimic glutamate buffering by AMPARs had little effect on the estimated D_{glut}, giving an 1.7% and 0.2% increase for the weighted mean and HR model, respectively. Figure 4.6D shows the small change in $P_{open}(t)$ introduced by adding buffers to the model. These simulations of uncertainties in model parameters suggest that D_{glut} is between 2 and 5-fold lower than free solution.

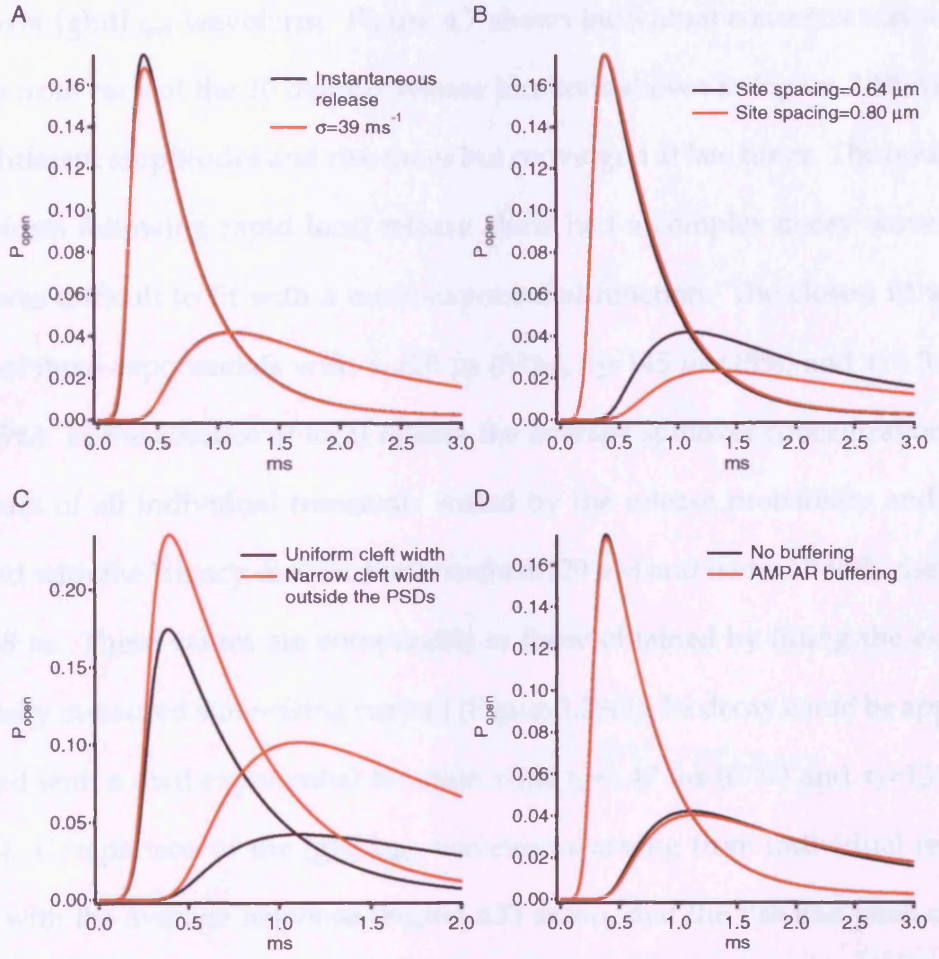

Figure 4.6: Simulated fast-rising and spillover P_{open} under different manipulations used to test robustness of estimate of D_{glut}. **A**, Simulated fast-rising and spillover P_{open} with instantaneous release (black), and the release timecourse estimated by Stiles *et al.* (1996) at the NMJ (red). **B**, Fast-rising and spillover P_{open} with the intersite distance at 0.64 (black) and 0.80 (red) μm. **C**, Fast-rising and spillover P_{open} with uniform cleft width (black) and a cleft width of 10 nm outside the PSD (red). **D**, Fast-rising and spillover P_{open} with (red) and without (black) buffering by 200 AMPAR-like (Robert & Howe, 2003) binding sites per PSD.

4.2.5 The concentration of glutamate in the synaptic cleft

Having estimated D_{glut}, I calculated the components underlying the mean spillover $[glut]_{cleft}$ waveform. Figure 4.7 shows individual concentration waveforms from each of the 10 distinct release locations shown in Figure 3.1B, which had different amplitudes and rise times but converged at late times. The $[glut]_{cleft}$ waveform following rapid local release alone had a complex decay waveform that was difficult to fit with a multi-exponential function. The closest fit was a sum of three exponentials with τ_1=20 μs (84%), τ_2=145 μs (15%) and τ_3= 3.6 ms (0.005%). In the absence of local release the average spillover concentration (i.e. the sum of all individual transients scaled by the release probability and convolved with the latency distribution) reached 129 μM and had a 10-90% rise time of 198 μs. These values are comparable to those obtained by fitting the experimentally measured slow-rising current (Figure 3.2Aii). Its decay could be approximated with a dual exponential function with τ_1=1.47 ms (67%) and τ_2=13.3 ms (33%). Comparison of the $[glut]_{cleft}$ waveforms arising from individual release sites with the average response (Figure 4.7) shows that the rise and peak of the spillover waveform is determined predominantly by a few close sites. In contrast, the slow decay of the $[glut]_{cleft}$ waveform is determined by the summation of glutamate from many, more remote sites. The prediction of $[glut]_{cleft}$ arising from spillover will be least accurate at late times because glutamate uptake (DiGregorio *et al.*, 2002) and sites more remote than those we have simulated may contribute to the waveform.

4.3 Discussion

I have used the macromolecule dextran to slow diffusion in cerebellar slices and examined changes in EPSCs. These results indicate that transmitter spillover,

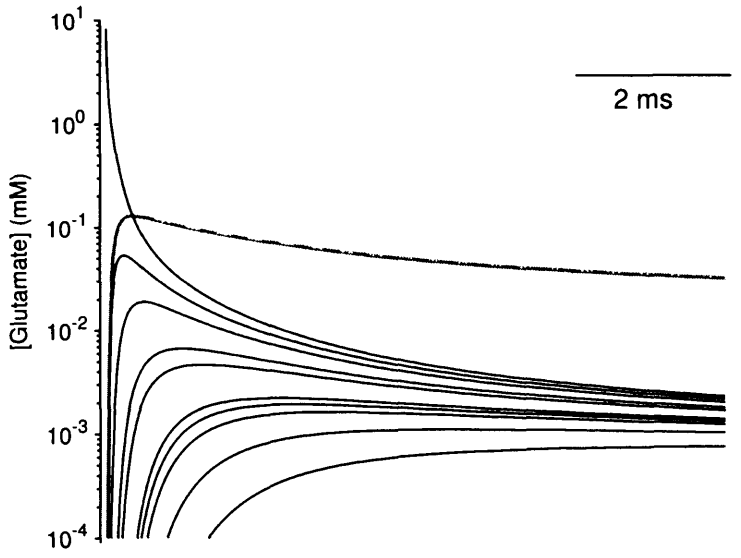

Figure 4.7: Simulated $[glut]_{cleft}$ from each of the 10 distinct release locations (Figure 1B) in our simulations with the weighted D_{glut} of 0.33 $\mu m^2/ms$ (black lines). Thick grey line shows average $[glut]_{cleft}$produced by spillover.

rather than PLR underlies the slow-rising AMPA EPSC at the MF-GC synapse. Moreover, the present results provide the first experimental estimate of the diffusion coefficient of glutamate in the synaptic cleft and suggest that it is approximately one third of the value in free solution at physiological temperature.

4.3.1 Limitations in estimating D_{glut}

This approach for estimating D_{glut}, which involves a perturbation of glutamate diffusion in the cleft, relies on quantification of both the synaptic currents and the anatomy of the MF-GC synapse. Uncertainties in the estimate of D_{glut} arise largely from the AMPAR model, the number of molecules per vesicle, the intersite distance and the experimental error. These parameters affect the estimate of D_{glut} because they alter the sensitivity of either the occupancy of the RLR response or the time-to-peak of spillover $P_{open}(t)$, to changes in D_{glut}. The $[glut]_{cleft}$ arising from RLR is governed by diffusion out of the active zone, while spillover is determined predominantly by diffusion between active zones. The estimation of D_{glut} in the synaptic cleft therefore assumes that the diffusion coefficient in these two regions is similar. Since it is unknown whether this assumption is accurate, I examined how differences in D_{glut} inside and outside the active zone affected the estimate of D_{glut}. Simulations of nonuniform glutamate diffusion where D_{glut} in the active zone was set to between 75% and 25% of the D_{glut} in regions between active zones show that diffusion in the perisynaptic region must be less than free solution in order to explain experimental results. For simulations where D_{glut} was four-fold lower inside the PSD than outside, the weighted D_{glut} was estimated as 0.49 $\mu m^2/ms$ outside the PSD and 0.12 $\mu m^2/ms$ inside the PSD. Moreover, these simulations suggest that estimates made assuming a uniform D_{glut} provide a value of D_{glut} that is approximately midway between the D_{glut} values within

and between active zones, when these are assumed to be different.

The approach to estimating D_{glut} assumes that dextran does not slow the rate of diffusion within the fusion pore as this would increase the time-to-peak of the postsynaptic current. This is unlikely given dextran is an inert macromolecule and that its hydrodynamic radius (7.3 nm; Nicholson & Tao, 1993) is much larger than the estimated fusion pore radius for microvesicles in kiss-and-run release mode (0.3 nm; Klyachko & Jackson, 2002). It is possible that dextran could interact with pores with larger diameters. However, the fact that there was no slowing of quantal currents argues against this possibility. Our method also assumes that dextran does not affect the volume of the extracellular space. If, as a result of dextran perfusion, the distance between pre-and postsynaptic membranes decreased, the amplitude of the RLR response should increase as observed experimentally. However, simulations show that halving the distance between pre- and postsynaptic membranes outside the active zone *decreased* the time-to peak of the slow-rising current by 4% and thus cannot account for the experimental results.

CHAPTER

FIVE

Nonlinear activation of AMPARs determines the EPSC time course

5.1 Introduction

At synapses with independent stochastic release sites such as the snake NMJ (Hartzell *et al.*, 1975) the synaptic current waveform is the arithmetic sum of the currents induced at individual active zones. Changing the release probability will therefore not change the shape of the synaptic current waveform. However, at several glutamatergic synapses in the central nervous system, the shape of the EPSC does depend on the release probability. In the auditory brainstem (Trussell *et al.*, 1993; Neher & Sakaba, 2001), in cultured hippocampal neurons (Mennerick & Zorumski, 1995), at the cerebellar climbing fibre to Purkinje cell synapse (Takahashi *et al.*, 1995; Silver *et al.*, 1998; Wadiche & Jahr, 2001) and at the cerebellar MF-GC synapse (Silver *et al.*, 1996c; Wall *et al.*, 2002; DiGregorio *et al.*, 2002) the EPSC decay accelerates at low release probability.

A number of possible mechanisms have been proposed that could mediate this waveform change. Firstly, the effect could be mediated by the differ-

ent behaviour of the presynaptic terminal in different calcium concentrations, such that either the timecourse of glutamate release from a single vesicle, or the latency distribution of vesicular release changed with $[Ca^{2+}]_o$. Secondly, glutamate buffering by transporters or receptors can change the shape of the concentration waveform depending on the absolute level of glutamate in the synaptic cleft (Takahashi *et al.*, 1995). Thirdly, it has been proposed that high occupancy of receptors following multivesicular release can produce non-linearities in the EPSC waveform (Wadiche & Jahr, 2001). It has also been suggested that lowering release probability can change the shape of the average glutamate concentration waveform following stochastic release from multiple sites, either by increasing the effective distance between releasing sites (Silver *et al.*, 1996c) or by increasing glutamate concentration gradients in the synaptic cleft causing faster glutamate dissipation (Trussell *et al.*, 1993). Lastly, spillover of glutamate could activate receptors at neighbouring synapses in the supralinear part of their dose-response curve (Hartzell *et al.*, 1975).

Here, I used recordings of EPSCs at different levels of $[Ca^{2+}]_o$ and pharmacological manipulations to distinguish between these possible mechanisms, and present a quantitative interpretation of the dependence of the waveform shape on the release probability, which can be replicated in a model based on simple diffusion and receptor activation.

5.2 Results

5.2.1 Mean and spillover EPSC waveform at reduced release probability

Currents were recorded from granule cells voltage clamped with the whole-cell configuration of the patch clamp. Mossy fibres were stimulated extracellularly in ACSF solutions containing between 2 and 1 mM $[Ca^{2+}]_o$ and antagonists for NMDA, GABA and glycine receptors, perfused at 36-37 ° C. Reductions in extracellular calcium decreased the mean and spillover EPSC amplitudes (Figure 5.1AC) as expected for a decrease in release probability (Katz, 1969).

DiGregorio *et al.* (2002) reported that in this preparation, lowering the extracellular calcium concentration accelerates the decay and preferentially decreases amplitude of isolated spillover currents. In order to elucidate the mechanism underlying this effect, I recorded synaptic currents from granule cells in 2, 1.5, 1.25 and 1 mM $[Ca^{2+}]_o$ (4 concentrations, n=12, 3 concentrations, n=1). Figure 5.1A shows the overall mean EPSC recorded from a representative cell in all four levels of $[Ca^{2+}]_o$. When these EPSC waveforms are normalised to the peak value (Figure 5.1B), the acceleration of the decay in low $[Ca^{2+}]_o$ becomes clear. In this cell, isolated spillover currents (Figure 5.1C) were also preferentially reduced with lower release probability, compared with Figure 5.1A. The EPSC decay can be quantified by the normalised integral, which equals the weighted time constant (τ_w) of a multiexponential function. A plot of the normalised integral against the EPSC amplitude recorded for each $[Ca^{2+}]_o$, pooled across all cells, show that for most cells, the EPSC decay accelerates in low $[Ca^{2+}]_o$. On average, τ_w decreased 4±6%, 10±7% and 19±9% in 1.5, 1.25 and 1 mM $[Ca^{2+}]_o$ relative to 2 mM $[Ca^{2+}]_o$ (One-way analysis-of-variance, $p<0.05$). However, two cells showed

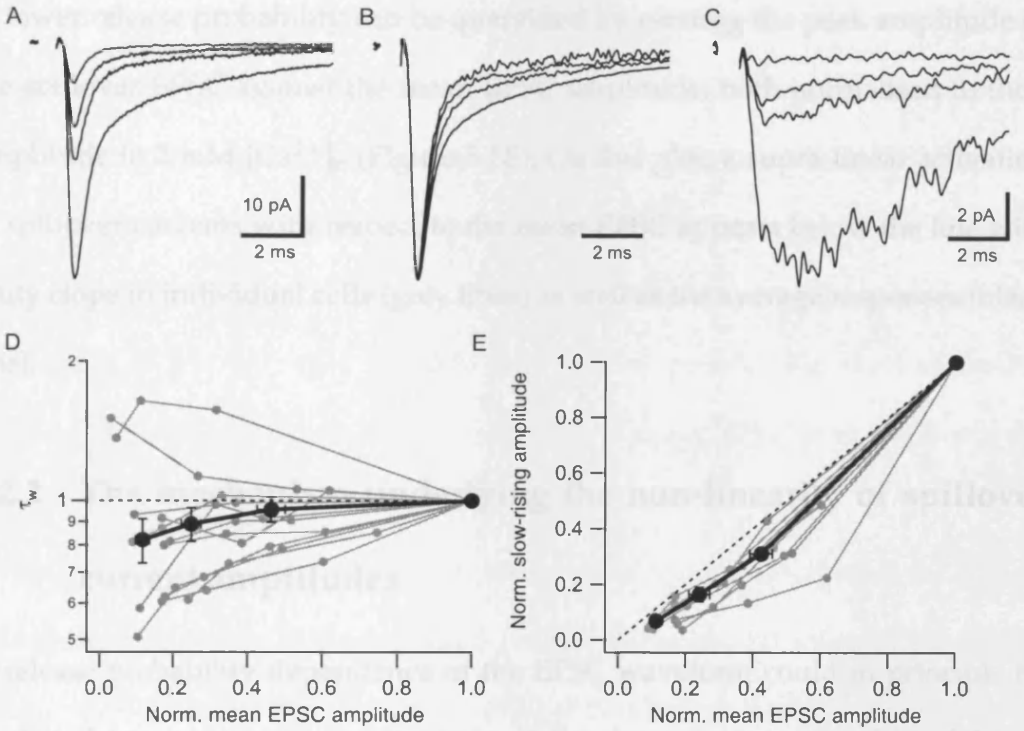

Figure 5.1: Release probability dependence of the mean EPSC waveform and the relative amplitude of slow-rising currents. **A**, mean EPSC waveforms recorded from a representative cell in 2, 1.5, 1.25 and 1 mM $[Ca^{2+}]_o$. **B**, as A but normalised to the peak amplitude. **C**, slow-rising currents isolated from the same recordings as A. **D**, weighted decay in each conditions from all (n=13) cells, plotted against the peak amplitude normalised to the value in 2 mM $[Ca^{2+}]_o$. **E**, isolated slow-rising currents plotted against the peak amplitude of the mean EPSC for each condition in each cell, each normalised to the value in 2 mM $[Ca^{2+}]_o$. Thick black line, averages for 2, 1.5, 1.25, 1 mM $[Ca^{2+}]_o$ across cells

slower decays in lower release probability. These two cells, and three other cells that accelerated in low $[Ca^{2+}]_o$, did not have isolated slow-rising currents, and therefore could not be included in the subsequent analysis.

The preferential reduction in spillover-mediated currents over the mean EPSC at lower release probability can be quantified by plotting the peak amplitude of the spillover EPSC against the mean EPSC amplitude, both normalised to their amplitude in 2 mM $[Ca^{2+}]_o$ (Figure 5.1E). On this plot, a supra-linear activation of spillover currents with respect to the mean EPSC appears below the line with unity slope in individual cells (grey lines) as well as the average responses (black line).

5.2.2 The mechanism underlying the non-linearity of spillover current amplitudes

A release probability dependence of the EPSC waveform could in principle be mediated by presynaptic mechanisms, if the decay is determined by delayed release of glutamate. "Delayed release" could in this context mean either full release of quanta, such that the latency distribution has a prolonged timecourse, or prolonged release through a narrow fusion pore. If either of these processes are sensitive to changes in the release probability, they could influence the shape of the mean EPSC waveform. I have shown in chapter 4 that the slow-rising current is not mediated by prolonged local release. Although it is possible that an unidentified mechanism could regulate the concentration of glutamate spillover, for instance a release probability-dependent buffer, such a mechanism is unlikely (buffering by glutamate transporters will be discussed below). The latency distribution of vesicular release can also influence the EPSC waveform (Atluri & Regehr, 1998). Two observations argue against the possibility: recordings from

synaptic contacts with single release sites in younger rats found no change in the width of the latency distribution in low $[Ca^{2+}]_o$ and these distributions did not contain prolonged extensions (Silver *et al.*, 1996c). In the present recordings, there is no significant difference in the 10-90% rise time (which is determined by the latency distribution and the quantal EPSC rise time) of the mean EPSCs recorded in 2 and 1.25 mM $[Ca^{2+}]_o$ (0.20±0.01 and 0.21±0.01 ms, respectively; p=0.44, n=9). Moreover, the non-linear reduction in the slow-rising EPSC in low $[Ca^{2+}]_o$ is likely to explain the change in the mean EPSC waveform, since it determines the EPSC decay (DiGregorio *et al.*, 2002). Since I have shown in chapter four that spillover underlies the slow-rising EPSC, presynaptic mechanisms are unlikely to mediate the non-linearity of the slow-rising EPSC with respect to the mean EPSC.

DiGregorio *et al.* (2002) previously showed that there is no significant effect of glutamate transporter blockers on the ratio of spillover and mean EPSC amplitudes, which indicates that glutamate transporters have a limited role in the preferential reduction of spillover EPSCs at low release probability. However, glutamate transport blockers do have a significant effect on the weighted decay of the EPSC. In addition, if the glutamate transporters are saturated and have a limited capacity, the proportional effect of transporters on the spillover EPSC could be minimal at high release probability, but increase at lower release probabilities.

To examine the role of glutamate transporters in the acceleration of the EPSC at low release probability, I recorded synaptic currents in the presence of the non-specific competitive glutamate transporter blocker DL-threo-β-benzyloxyaspartate (TBOA; 200 μM). If glutamate transporters contribute to the acceleration of the EPSC decay in low $[Ca^{2+}]_o$, this acceleration should disappear or be less prominent in TBOA. However, in the presence of TBOA, the weighted decay accelerated by 19.3%±7.1% (p=0.02; n=12; Figure 5.2ABC) when lowering

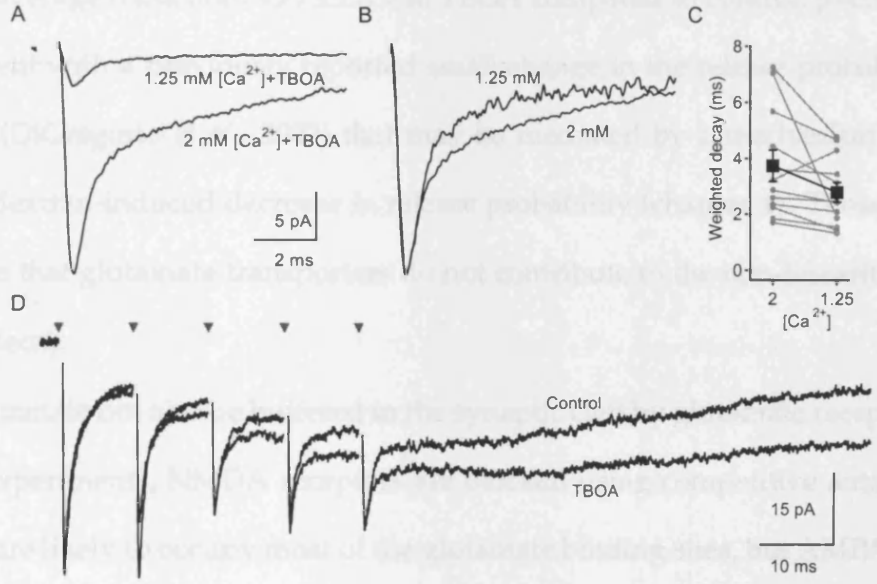

Figure 5.2: Effect of glutamate transporter blockers on the release-probability dependence of the EPSC waveform. **A**, mean EPSCs recorded in 2 and 1.25 mM $[Ca^{2+}]_o$, both in the presence of glutamate transporter blocker TBOA. **B**, as A but normalised to the peak amplitude. **C**, summary plot of weighted decays in 2 and 1.25 mM $[Ca^{2+}]_o$, both in the presence of TBOA. **D**, TBOA enhances a prolonged current evoked with 5 pulses at 100 hz.

$[Ca^{2+}]_o$ from 2 to 1.25 mM. This acceleration was not significantly different from that observed without TBOA (p=0.37). I repeated the positive control for TBOA action described in DiGregorio *et al.* (2002) by comparing the response to five pulses at 100 Hz in 2 mM $[Ca^{2+}]_o$ with and without TBOA. The normalised integral over 60 ms increased significantly in TBOA (p=0.05, n=7; Figure 5.2D). There was a trend towards a reduction in the amplitude of the EPSC evoked by the first pulse (average reduction, 93.7±2.8% in TBOA compared to control; p=0.07, n=7) consistent with a previously reported small change in the release probability in TBOA (DiGregorio *et al.*, 2002) that may be mediated by a mechanism similar to the dextran-induced decrease in release probability (chapter 4). These results indicate that glutamate transporters do not contribute to the non-linearity of the EPSC decay.

Glutamate can also be buffered in the synaptic cleft by glutamate receptors. In these experiments, NMDA receptors are blocked using competitive antagonists which are likely to occupy most of the glutamate binding sites, but AMPARs and mGluRs are unblocked. However, block of 50% of the AMPAR-mediated current with GYKI 53655 (DiGregorio *et al.*, 2002), and full block of mGluRs (unpublished observations, T.A. Nielsen & R.A. Silver) do not alter the EPSC waveform, arguing that buffering by these receptors is minimal. In addition, modelling predicts that AMPAR buffering has a minimal effect on receptor activation (chapter 4). Taken together, these observations indicate that glutamate buffering is unlikely to mediate the non-linearity of the slow-rising EPSC.

Studies of different central glutamatergic synapses indicate that in response to a presynaptic action potential, a release site can release at most one (Silver *et al.*, 2003; Perkel & Nicoll, 1993) or multiple (Wadiche & Jahr, 2001; Oertner *et al.*, 2002) quanta of neurotransmitter. At a synapse of the latter ("multivesicular") type, if the response of postsynaptic receptors is non-linear, the EPSC waveform

resulting from a small number of released quanta may have a different shape than that resulting from a larger number of quanta. This possibility had previously been proposed (Wadiche & Jahr, 2001) to account for the release probability-dependence of the climbing fibre to purkinje cell EPSC shape. One possible mechanism for the change in waveform is that at high release probability, the receptors are saturated during the EPSC peak and thus unable to follow linearly the $[glut]_{cleft}$ (Foster *et al.*, 2002). To test whether multivesicular release occurs at the MF-GC synapse, I recorded EPSCs in 2 and 1.25 mM calcium with and without kynurenic acid (Kyn) from 7 cells. This reduction in $[Ca^{2+}]_o$ caused the mean EPSC amplitude to decrease from -43.9 ±13.4 to -15.7 ±4.2 pA (p=0.03, n=7; Figure 5.3AB). In these cells, the fractional block of Kyn was no different in the two different levels of $[Ca^{2+}]_o$ (54.1±5.4% and 53.7±3.3%, respectively; p=0.94, n=7; Figure 5.3ABC). These data show that the glutamate concentration mediating the peak EPSC is independent of the release probability, which is inconsistent with the multivesicular model of glutamate release at this synapse. Since the change in EPSC amplitude in different release probabilities is larger than that used by Wadiche & Jahr (2001), and the fractional block of the low-affinity antagonist is similar, it is unlikely that the present experiment failed to detect multivesicular release due to insensitivity. It is therefore unlikely that multivesicular release contributes to the release probability dependence of the EPSC waveform at 2 mM $[Ca^{2+}]_o$ and below.

It is possible that multivesicular release could occur at higher release probabilities. To investigate the mechanism underlying univesicular release at 2 mM $[Ca^{2+}]_o$, I compared the effect of Kyn in physiological and high release probability evoked with stimulation in 8 mM $[Ca^{2+}]_o$ (Figure 5.4AB). Increasing the $[Ca^{2+}]_o$ from 2 to 8 mM increased the mean EPSC amplitude from -39.1±15.5 pA to -67.5±22.6 pA (p=0.003, n=7). Under these conditions, there was again no sig-

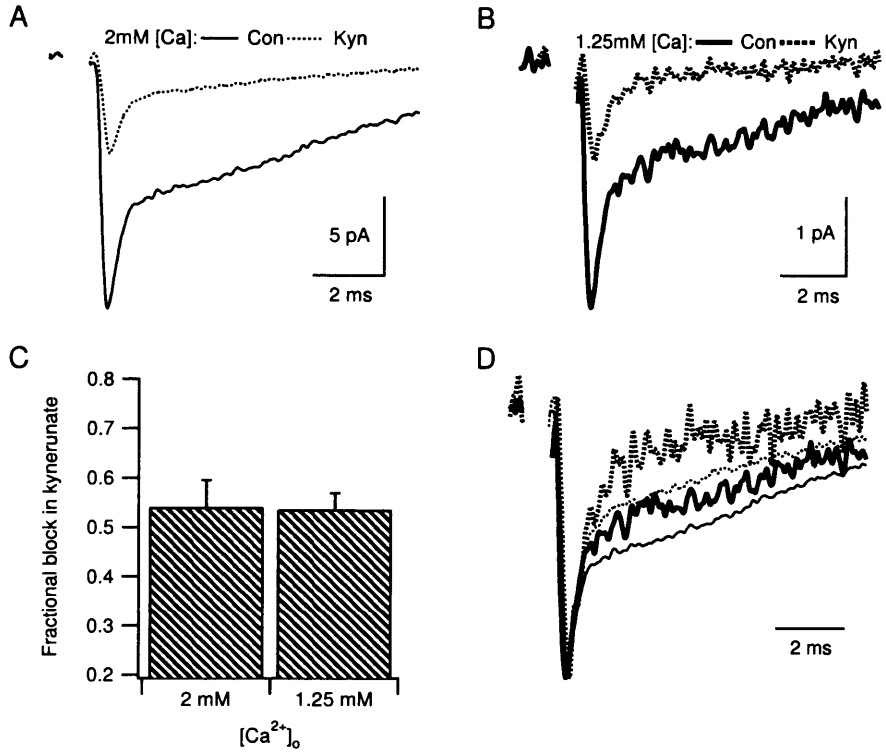

Figure 5.3: Fractional block of kynurenic acid in different release probabilities. **A**, mean EPSCs recorded in 2 mM $[Ca^{2+}]_o$ with (Kyn) and without (Con) kynurenic acid. **B**, as A, but in 1.25 mM $[Ca^{2+}]_o$. **C**, fractional block induced by kynurenic acid in 2 and 1.25 mM $[Ca^{2+}]_o$. **D**, mean EPSCs recorded in 2 and 1.25 mM $[Ca^{2+}]_o$ with and without kynurenic acid, all normalised to the peak EPSC amplitude.

nificant difference in the fractional block of Kyn at the two different release probabilities (62.6±4.1% and 53.7±5.2%, in 2 and 8 mM $[Ca^{2+}]_o$, respectively; p=0.22, n=7; Figure 5.4C). This finding indicates that even at high release probability, release is restricted to a single quantum per active zone, and is consistent with the recent demonstration of univesicular release at a high-probability synapse (Silver *et al.*, 2003).

5.2.3 Non-linear receptor activation in a model based on simple diffusion

The results from experiments with low-affinity competitive antagonists and glutamate transporter blockers allowed me to construct a model of synaptic transmission based on univesicular release from local and distant release sites. In the absence of buffers, the diffusion equation predicts linear summation of responses to release of neurotransmitter. As an illustration of this principle, Figure 5.5A shows the average glutamate concentration at different release probabilities predicted from a diffusion model that includes release latency and an abstraction of the MF-GC synaptic geometry (see chapter 3.) The concentrations waveforms from multiple release probabilities are shown on a logarithmic scale. On this plot, a vertical shift indicates that the amplitude, but not the shape, of the waveform changes with lower release probability.

In order to examine whether a simulation of synaptic currents would predict the acceleration of the mean EPSC decay shown in figure 5.1B, I simulated the response of an AMPAR kinetic scheme to many trials with stochastic, asynchronous release (Figure 5.5B). The normalised mean P_{open} responses show an acceleration from τ_w=1.71 at a release probability (P_r) of 0.46 to τ_w=1.39 at P_r=0.12 (normalised integral over 4 ms). Simulated spillover currents also show a prefer-

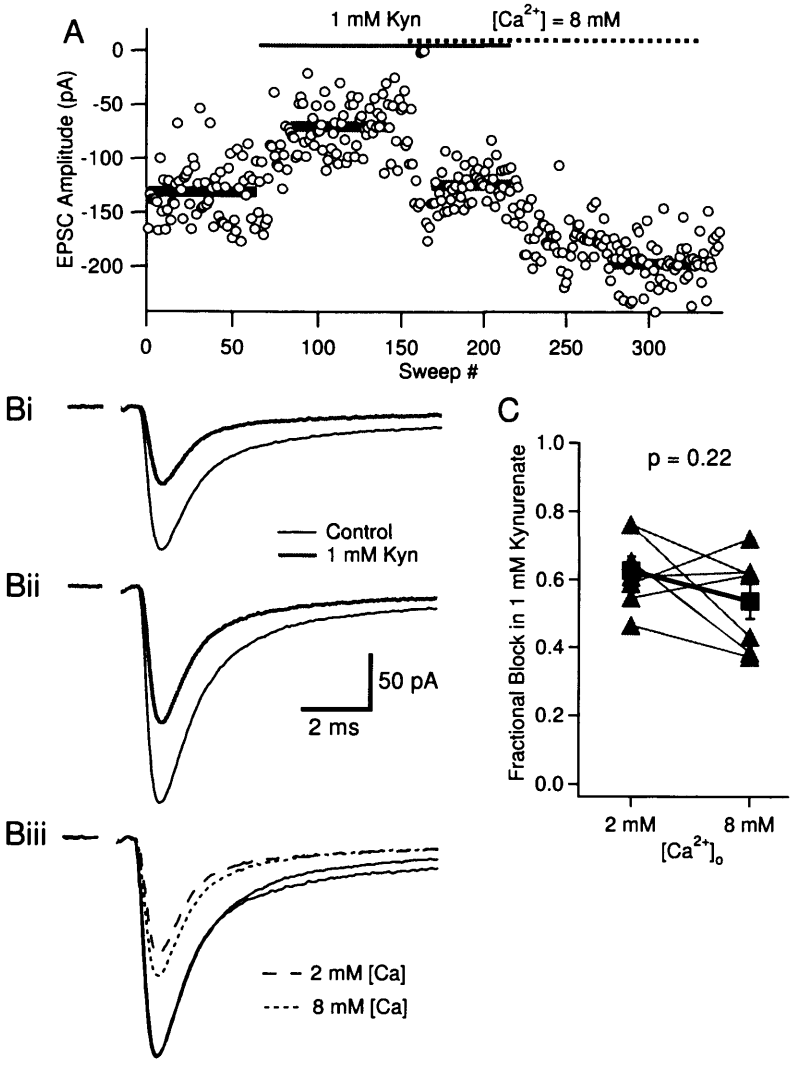

Figure 5.4: Fractional block of kynurenic acid at near-physiological and high probabilities. **A**, EPSC amplitude during wash-in and out of Kyn and 8 mM $[Ca^{2+}]_o$. **Bi**, mean EPSCs recorded in 2 mM $[Ca^{2+}]_o$ with (Kyn) and without (Con) kynurenic acid. **Bii**, as Bi, but in 8 mM $[Ca^{2+}]_o$. **Biii**, mean EPSCs recorded in 2 and 8 mM $[Ca^{2+}]_o$ with and without kynurenic acid, normalised to the peak EPSC amplitude recorded in control (without Kyn). **C**, fractional block induced by kynurenic acid in 2 and 8 mM $[Ca^{2+}]_o$.

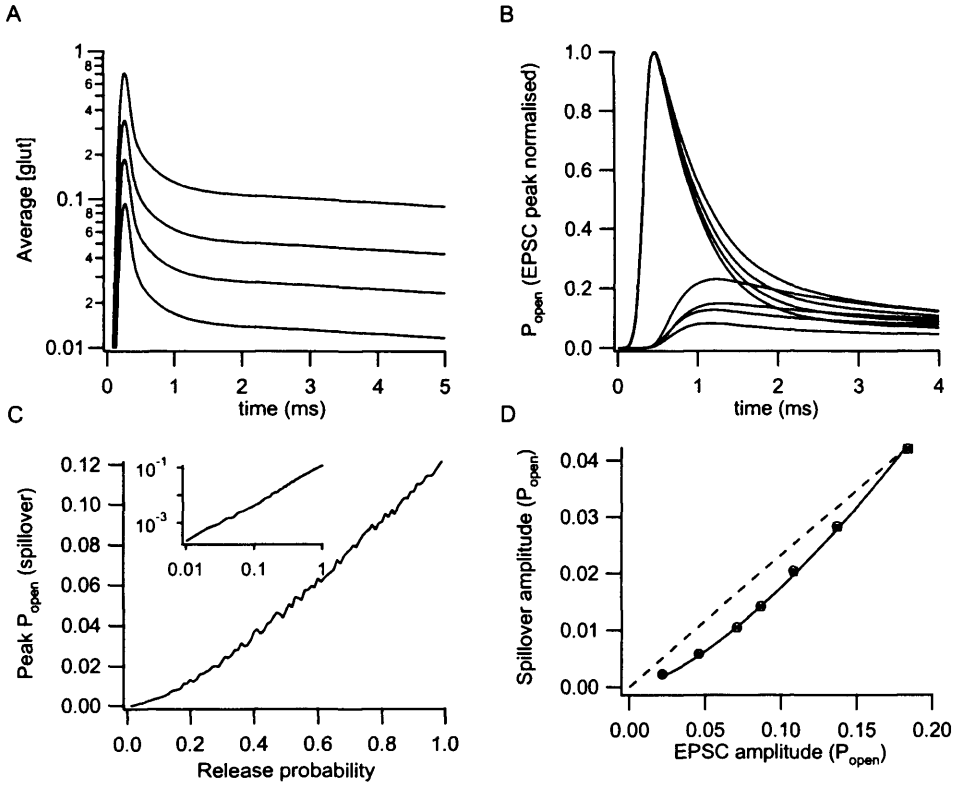

Figure 5.5: Simulations of diffusion and receptor activation at different release probabilities. **A**, average glutamate concentration from the model described in chapter three at release probabilities 0.06, 0.12, 0.22, and 0.46, including asynchronous release. **B**, Simulations of receptor activation following stochastic, asynchronous release. The P_{open} waveforms have been normalised to the peak response. Also shown, the spillover P_{open} waveforms, scaled by the same normalisation factor as the mean P_{open} waveforms. **C**, peak P_{open} for AMPAR activation by spillover following stochastic, asynchronous release, as a function of release probability. Inset, the same plot on a log-log graph indicates a power-law relationship. **D**, spillover P_{open} at various release probabilities between 0.06 and 0.46 plotted against mean P_{open} amplitude. Black line is power-law fit.

ential sensitivity to release probability, as indicated by reduction in the spillover P_{open} responses that are scaled together with the normalised mean response.

I investigated the influence of release probability on the amplitude of spillover currents by constructing a dose-response curve for spillover that averages the response to stochastic and asynchronous release over many trials for each release probability (Figure 5.5C). A double logarithmic plot (Figure 5.5C, inset) reveals that this dose-response curve fits a power law ($A(P_r)^n$) well, with A=0.12 and n=1.39 for this kinetic scheme, i.e. activation is in the supra-linear part of the dose-response curve. Finally, I plotted the amplitude of isolated spillover P_{open} against the mean P_{open} amplitude in Figure 5.5D, which shows the same non-linear profile as the experimental data (Figure 5.1E).

These simulations strongly indicate that the activation of postsynaptic AMPA receptors by spillover in the non-linear region of the dose-response curve can in principle account for the acceleration of the EPSC decay and the preferential reduction of spillover currents in low calcium.

5.2.4 Non-linearities of synaptic receptors.

Given the above findings, I explored the possibility of a quantitative interpretation of the plot of spillover against mean EPSC amplitude (Figure 5.1E). Since the concentration underlying the peak AMPAR does not depend on the release probability, changes in the release probability will be proportional to changes in the fast-rising EPSC amplitude. Therefore, the abscissa of Figure 5.1E is proportional to release probability. In addition, the lack of effect of glutamate transporter blockers on the relative amplitude of spillover currents indicates that diffusion is linear on the timescale of 1-2 ms, which includes the peak of spillover currents. Since spillover arises from many release sites from which glutamate summates

in the synaptic cleft, the $[glut]_{cleft}$ mediated by spillover is proportional to the release probability and therefore to the mean EPSC amplitude at a given synapse for a fixed set of conditions. This argument implies that it is possible to interpret Figure 5.1E as a dose-response curve for activation of AMPARs by glutamate spillover. Since the Hill equation, which is classically used to fit dose-response curves, requires a maximal response, I fit the synaptic dose-response curves with a power function instead. In addition, the spillover current was subtracted from the mean EPSC to minimise the contribution of spillover to the measured EPSC amplitude (Figure 5.6).

The average power from power-law fits to individual spillover-mean EPSC plots was 1.51±0.19 (p=0.03 different to 1; n=9). It is also possible to measure the average power by normalising both spillover and mean EPSC amplitudes to their value in 2 mM $[Ca^{2+}]_o$, and to fit a single power law to the total population of spillover-mean EPSC amplitude points (Figure 5.6, black line). This approach gives a slightly lower value of 1.41.

5.3 Discussion

I have shown that the EPSC gradually accelerates under conditions of successively lower release probabilities, and that this is accompanied by a preferential reduction in measured spillover currents. These properties are replicated in a model with simple diffusion and activation of model AMPARs. In the model, this is caused by the non-linearity of the dose-response curve for spillover. I have shown using pharmacological agents that two alternative interpretations, namely glutamate uptake and multivesicular release, cannot account for the non-linearity of the EPSC waveform at the MF-GC synapse. In addition, given that multivesicular release does not occur at this synapse, a plot of the spillover amplitude

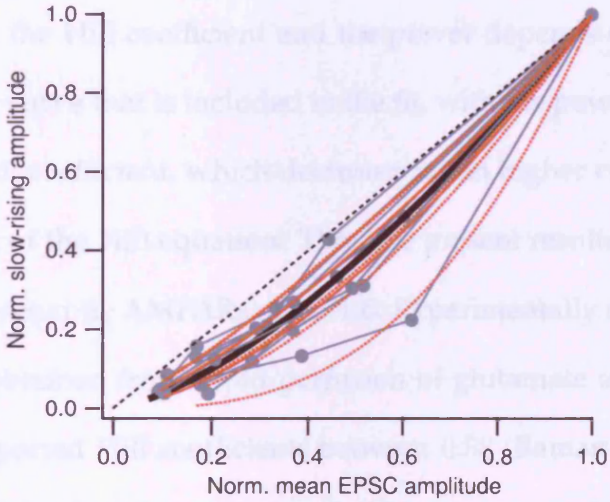

Figure 5.6: Dose-response curve for synaptically recorded slow-rising currents. Isolated slow-rising currents plotted against the peak amplitude of the mean EPSC, with the amount of slow-rising current at the time of the mean EPSC peak subtracted, for each condition in each cell, each normalised to the value in 2 mM $[Ca^{2+}]_o$. Dotted lines indicated power-law fits to curves from each cell. Black line indicated global power-law fit to all points.

against the mean EPSC can be interpreted as a dose-response curve for spillover which can be fit with a power function. This gives a power of 1.4-1.5.

The power obtained from plots of spillover vs. fast-rising EPSC amplitude (1.4-1.5) is closely associated with the Hill coefficient of AMPARs if the nonlinearity in the spillover EPSC is caused by the activation of AMPARs in the supralinear part of the dose-response curve. Fits of either power laws and Hill equations to dose-response curves obtained from simulations with AMPAR kinetic schemes indicate that both the Hill coefficient and the power depends on the portion of the dose-response curve that is included in the fit, with the power being 0.1 units lower than the Hill coefficient, which decreases when higher concentrations are included in the fit of the Hill equation. Thus the present results would predict a Hill coefficient of synaptic AMPARs of 1.5-1.6. Experimentally determined dose-response curves obtained from rapid perfusion of glutamate onto patches with AMPARs have reported Hill coefficients between 0.88 (Raman & Trussell, 1992) and 1.4 (Jonas *et al.*, 1993). When constructing dose-response-curves from simulations using AMPAR kinetic schemes using the spillover concentration waveform predicted in chapter 4, I obtain power coefficients of 1.65±0.05 (see Table 1.1). Thus, the Hill coefficient predicted by synaptic recordings fall within the range of Hill coefficients expected from the existing literature on AMPARs.

Given the absence of alternative mechanisms that can explain both the non-linearity of the slow-rising EPSC and the change in the EPSC waveform with release probability, the most parsimonious explanation for these observations is the non-linear activation of AMPARs by glutamate spillover, which is observed in a simple model of glutamate diffusion and published kinetic schemes for AMPARs. Furthermore, the quantitative predictions of the relationship between isolated slow-rising EPSC amplitude, and mean EPSC amplitude, are similar to those observed in the experiments. However, a stronger conclusion could

be reached if the dose-response curve of synaptic AMPARs could be measured directly and be shown to fit a power law similar to that predicted from the measurement of slow-rising EPSCs. Since GC AMPARs are located exclusively in PSDs on synaptic terminals, such a dose-response curve cannot be measured with conventional methods. However, novel techniques based on photolysis of caged glutamate directly in the synaptic cleft could possibly be used to investigate the kinetics of synaptic receptors. In chapter 6, I will develop a quantitative framework for predicting uncaging-evoked receptor activation, and assess whether it is possible to measure a dose-response curve with uncaging.

Not all cells tested accelerated to the same extent. Out of the 13 tested cells, 2 showed broader waveforms in low $[Ca^{2+}]_o$. It is possible that not all synapses are being activated by spillover in the supralinear region, and that high occupancy of spillover activation gives a sublinear dose-response curve. An alternative possibility is that desensitisation can form an opposing process as seen in the chick nucleus magnocellularis synapse, where without cyclothiazide, the EPSC decay does not slow in low $[Ca^{2+}]_o$ (Trussell *et al.*, 1993). At the MF-GC synapse, recordings of EPSCs in $[Ca^{2+}]_o$ that are both higher and lower than the physiological level indicate that the normalised integral of the evoked EPSC has an inverse-U shaped form with its peak at 2 mM $[Ca^{2+}]_o$ and acceleration in higher release probabilities (Sargent *et al.*, in preparation).

CHAPTER

SIX

Development of a framework for investigating synaptic receptors with photolytic uncaging of glutamate

6.1 Introduction

The previous chapters have shown that the kinetics of postsynaptic glutamate receptors play a prominent role in shaping the synaptic response. The absence of a kinetic scheme for GC AMPARs places a limit on the completeness the MF-GC synapse as a model for synaptic biophysics. Unfortunately, AMPARs are not expressed on the GC soma and thus a kinetic scheme cannot be constructed from rapid perfusion of glutamate on outside-out patches or single-channel recordings. In addition, the discovery that AMPARs can be regulated by proteins localised in the PSD (Ziff, 1997) raise the general problem for synaptic physiology that synaptic and extrasynaptic receptors may have different properties, and so far, only the kinetics of extrasynaptic receptors have been investigated in detail. The application of light-sensitive caged neurotransmitters (Matsuzaki *et al.*, 2001; Canepari *et al.*, 2001) therefore raises the possibility of activating synaptic receptors with a rapidly applied and repeatable glutamate waveform.

The $[glut]_{cleft}$ waveform evoked with uncaging is less amenable to quantitative analysis than the square waveform of glutamate during rapid perfusion. As with the $[glut]_{cleft}$ waveform evoked by synaptic release, it is difficult to predict *a priori* the shape of the uncaging-evoked waveform, which will be influenced by the synaptic geometry, the diffusion coefficient of the caged glutamate compound as well as D_{glut}, the optical point-spread function and the kinetics of photolysis. The $[glut]_{cleft}$ waveform following uncaging is difficult to measure directly, but it can be examined using diffusion-reaction simulations. Previous studies have investigated the glutamate concentration waveform following uncaging in "empty" space and without the postsynaptic activation of receptors (Pettit *et al.*, 1997; Kiskin & Ogden, 2002).

The size of the illumination volume is dependent on the optical properties of the microscope used, but can be minimised in three different ways: by using a two-photon microscope, which decreases the volume of uncaging by relying on the simultaneous absorption of two low-energy photons to evoke photolysis; by including two cages on each active molecule, thus requiring the absorption of two photons for every released active molecule; or with a diffraction-limited ultraviolet (UV) microscope, which has a more complex illumination function and achieves a high resolution due to the short excitation wavelength. At present, the caged glutamate compound with the most efficient photolysis kinetics (4-methoxy-7-nitroindolinyl–glutamate; MNI-glutamate) has a poor cross-section for two-photon absorption (Kiskin *et al.*, 2002), and large AMPAR activation cannot be achieved without the presence of cyclothiazide (Matsuzaki *et al.*, 2001), which increases the affinity of AMPARs. MNI-glutamate can, however, be efficiently uncaged with UV light (Canepari *et al.*, 2001). Present doubly caged glutamate molecules have low efficiency (Pettit *et al.*, 1997).

The purpose of the present study is to build on the diffusion model developed

in chapter 3 to predict the $[glut]_{cleft}$ waveforms and patterns of AMPAR activation evoked with diffraction-limited UV uncaging in the MF-GC synapse. I will use this model to examine which experiments are feasible using glutamate uncaging. In particular, I will address whether it is possible to use uncaging to test the predictions about D_{glut} and the shape of the dose-response curve of AMPARs from chapter 4 and 5, respectively. In addition, I will examine whether it is possible to investigate AMPAR kinetics using glutamate uncaging.

6.2 Results

6.2.1 The model

In order to examine the glutamate concentration waveforms evoked with UV uncaging of MNI-glutamate, I constructed a model of uncaging based on the geometry of the MF-GC synapse described in chapter 3 together with diffusion of both the glutamate and the caged compound, and a photolysis reaction. In general, photolytic uncaging consists of two sequential reactions (Kiskin & Ogden, 2002):

$$\text{CageR} + h\nu \xrightarrow{k_e} \text{CageR}^* \xrightarrow{k_p} \text{Cage} + \text{R} \tag{6.1}$$

where R is the released, active compound, and CageR* is an intermediate product. Recent experiments have indicated that the second reaction ("dark reaction") is very fast for nitroindoline-caged compounds (including MNI-glutamate), with $k_p = 5 \times 10^6\ s^{-1}$ (Morrison *et al.*, 2002). The dark reaction is therefore unlikely to be rate-limiting, and the rate constant of photolysis can be assumed to be proportional to the light intensity. Since the point-spread function in the diffraction-limited UV microscope is on the order of the size of a PSD, k_e cannot be assumed

to be location-independent in the synaptic geometry. I used the ideal illumination function (2.44) of the confocal microscope (Wilson, 1990), but stretched it in lateral and axial dimensions to match the full-width at half maximum (FWHM) measured in a real microscope with a 1.0NA objective with scans of fluorescent beads (resolution lateral $\times$ axial in nm: 242 $\times$ 1160 (measured; DiGregorio, Nielsen & Silver, in preparation); 242 $\times$ 926 (predicted)). The larger point spread function of the real microscope is likely to come from aberrations in the objective.

There are three principal unknown parameters in this model: the rate of cage excitation (and therefore photolysis); the orientation of the illumination spot with respect to the synaptic geometry; and the kinetic scheme mediating the P_{open} response to the uncaging-evoked $[glut]_{cleft}$ waveform. The rate of photolysis is, as stated above, proportional to the light intensity and therefore depends on the location. Because both the absolute light intensity and ratio of intensity to the rate constant are unknown, I introduced an arbitrary factor k_I, where $k_e=k_I \times I(u,v)$ (see equation 2.44). Since MNI-glutamate can be very efficiently uncaged with UV light, we will consider values of k_I in the range 10^1-10^4 ms^{-1}. If the centre of the optical spot is coincident with the centre of the PSD, the optical axis could form any angle with the orientation of the dendrites (see Figure 3.1A). I will consider the two extreme cases where the optical axis is parallel (r=0°) or perpendicular (r=90°) to the orientation of the dendrites. Illumination functions with these two orientations are shown in Figure 6.1, together with a cross-section of part of the synaptic geometry. Since I showed in chapter four that the responses of the HR AMPAR kinetic scheme to $[glut]_{cleft}$ best matches the recorded MF-GC EPSC, I will use this kinetic scheme in all figures unless otherwise stated.

D_{glut} was taken to be the weighted average from chapter 4 (0.33 $\mu m^2/ms$), and the diffusion coefficient of MNI-glutamate was calculated from D_{glut} by assuming a 1/3 power relationship between mobility and molecular weight (Weiss, 1996).

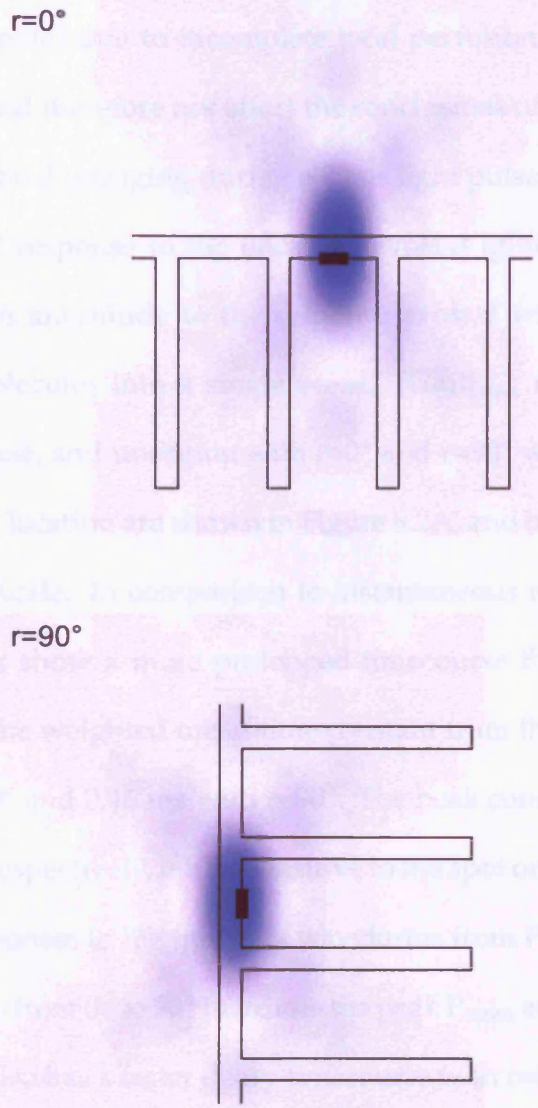

Figure 6.1: Cross-section of the point spread function along the optical axis. The synaptic geometry is superimposed on the point spread function, with orientations r=0° and r=90°.

The $[glut]_{cleft}$ waveform was averaged over a 0.2x0.2 μm square PSD, as in chapter 3. As previously, I assumed that the buffering by AMPARs is negligible and that diffusion is linear (see chapter 3 and 4). The MNI-glutamate concentration was set to 10 mM in all permeable voxels before the uncaging pulse. A different initial [MNI-glutamate] due to incomplete local perfusion will scale calculated $[glut]_{cleft}$ linearly and therefore not affect the conclusions of this chapter.

I initially simulated uncaging during a 20 μs light pulse with k_I=50 ms^{-1}, for which the AMPAR response to the uncaging-evoked $[glut]_{cleft}$ is similar in the case where r=0°, in amplitude to the response evoked with the instantaneous release of 4000 molecules into a single voxel. $[Glut]_{cleft}$ waveforms following instantaneous release, and uncaging with r=0° and r=90° with the PSD and spot centres in the same location are shown in Figure 6.2A, and in Figure 6.2A inset on a logarithmic timescale. In comparison to instantaneous release, the uncaging-evoked waveforms show a more prolonged timecourse that is sensitive to the spot orientation. The weighted mean time constant from the concentration peak is 0.19 ms with r=0° and 0.46 ms with r=90°. The peak concentration amplitude, 3.83 and 4.98 mM respectively, is also sensitive to the spot orientation. Figure 6.2B shows $P_{open}(t)$ responses to the $[glut]_{cleft}$ waveforms from Figure 6.2A. Changing the spot orientation from 0° to 90° increases the peak P_{open} amplitude from 41% to 58%. The $P_{open}(t)$ also has a faster decay timecourse with r=0° compared to r=90°, with the weighted decays being 0.71 and 1.0 ms, respectively. Nevertheless, both waveforms are slower than that evoked with instantaneous release, which has a weighted decay of 0.66 ms. It is therefore likely that glutamate uncaging under the simulated conditions will evoke a more slowly decaying $[glut]_{cleft}$ than synaptically released glutamate.

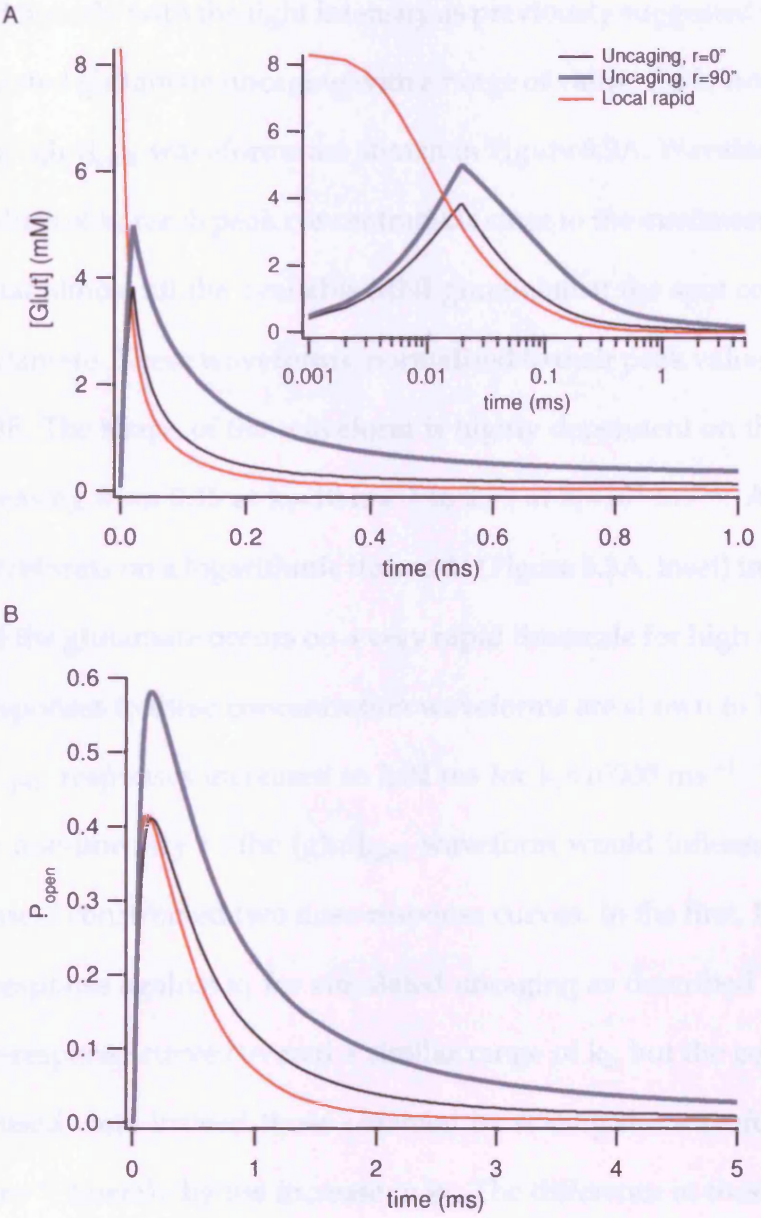

Figure 6.2: Concentration and P_{open} waveforms evoked with uncaging and instantaneous release. **A**, $[glut]_{cleft}$ waveforms following local instantaneous release and 20 μs uncaging with k_I=20 ms^{-1} and spot orientations of 0° and 90°. **B**, P_{open} responses to concentration waveforms from A, using HR kinetic scheme.

6.2.2 Saturation of the excitation reaction

In order to examine whether the concentration waveforms evoked with brief light pulses scaled linearly with the light intensity as previously suggested (Pettit *et al.*, 1997), I simulated glutamate uncaging with a range of values for k_I from 10 to 10^4. The resulting $[glut]_{cleft}$ waveforms are shown in Figure 6.3A. Waveforms evoked with high values of k_I reach peak concentrations close to the maximum of 10 mM, indicating that almost all the available MNI-glutamate at the spot centre is converted to glutamate. These waveforms, normalised to their peak value, are shown in Figure 6.3B. The shape of the waveform is highly dependent on the intensity, with τ_w increasing from 0.15 at k_I=10 ms^{-1} to 2.59 at k_I=10^4 ms^{-1}. A plot of the $[glut]_{cleft}$ waveforms on a logarithmic timescale (Figure 6.3A, inset) indicates that saturation of the glutamate occurs on a very rapid timescale for high values of k_I. The P_{open} responses to these concentration waveforms are shown in Figure 6.3C. τ_w for the P_{open} responses increased to 2.02 ms for k_I=10000 ms^{-1}. To examine whether the non-linearity in the $[glut]_{cleft}$ waveform would influence the peak P_{open} response, I constructed two dose-response curves. In the first, I plotted the peak P_{open} response against k_I for simulated uncaging as described above. The second dose-response curve covered a similar range of k_I, but the concentration waveforms used were instead those obtained by scaling the waveform evoked with k_I=10 ms^{-1} linearly by the increase in k_I. The difference in these two dose-response curves, shown in Figure 6.3D, shows that non-linearities in the $[glut]_{cleft}$ waveform affect the peak P_{open} response even at the intensities required to evoke responses of similar magnitude to the mEPSC.

These simulations indicate that high light intensities can saturate the uncaging process. Furthermore, even for relatively low light intensities, due to the saturation of the photolytic reaction, increasing intensity does not scale linearly the

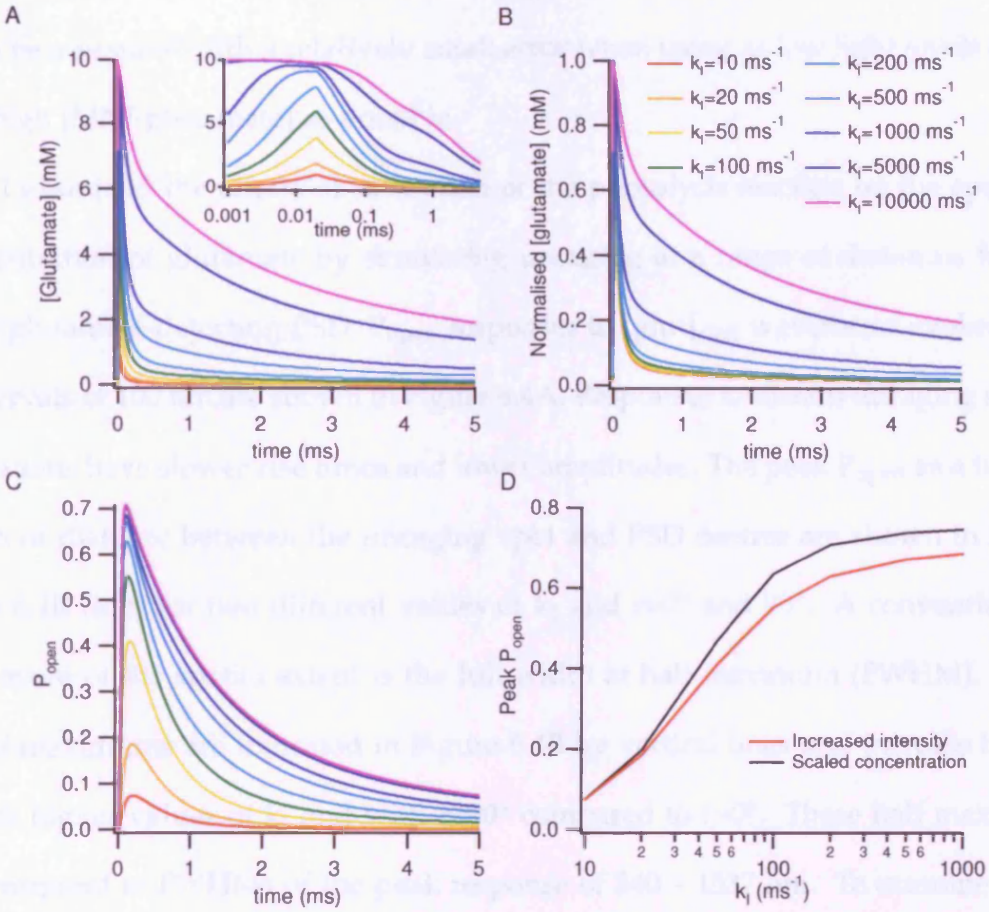

Figure 6.3: Saturation of excitation reaction following uncaging. **A**, $[glut]_{cleft}$ waveforms following 20 μs uncaging, spot orientations of 0°, and values of k_I ranging from 5 to 10000. **B**, $[glut]_{cleft}$ waveforms from A, normalised to their peak value. Inset, the same $[glut]_{cleft}$ waveforms, unnormalised and on a logarithmic time-scale. **C**, P_{open} responses (HR scheme) to $[glut]_{cleft}$ waveforms in A. **D**, red trace, relationship between the uncaging intensity and peak P_{open} amplitude for r=0°. Black trace, dose-response curve constructed by linearly scaling the $[glut]_{cleft}$ waveform evoked with k_I=10 ms^{-1} by the numerical value of k_I.

$[glut]_{cleft}$ waveform. It is therefore unlikely that the full dose-response curve for synaptic receptors can be measured accurately by changing the light intensity in an uncaging experiment. However, it is possible that the non-linearity of the foot can be measured with a relatively small error when using as low light levels and as high [MNI-glutamate] as possible.

I examined the effects of saturation of the photolysis reaction on the spatial distribution of glutamate by simulating uncaging at a range of distances from the glutamate-detecting PSD. P_{open} responses to $[glut]_{cleft}$ waveforms evoked at intervals of 100 nm are shown in Figure 6.4A. Responses to distant uncaging spot locations have slower rise times and lower amplitudes. The peak P_{open} as a function of distance between the uncaging spot and PSD centres are shown in Figure 6.4B (left) for two different values of k_I and r=0° and 90°. A conventional measure of the spatial extent is the full width at half maximum (FWHM). The half-maximums are indicated in Figure 6.4B by vertical lines and increase both with higher values of k_I and with r=90° compared to r=0°. These half maxima correspond to FWHMs of the peak response of 540 – 1537 nm. To examine the direct contribution of photolysis saturation to the degradation of spatial localisation in the absence of non-linear postsynaptic receptors, I calculated the FWHM of the glutamate distribution in the synaptic cleft at the end of a single uncaging pulse. The instantaneous glutamate concentration, as a function of distance from the uncaging spot centre, is shown in the right panel of Figure 6.4B, with the half maxima shown by vertical lines. For r=0°, the FWHM of glutamate was 363 and 419 nm for k_I of 30 and 300 ms^{-1}, respectively. For r=90°, the same FWHMs were 388 and 533 nm, respectively.

Since the FWHM depends on the uncaging intensity k_I and can be measured experimentally, it is possible that the spatial profile of glutamate can be used to calibrate k_I. In order to assess the dependence of the relationship between FWHM

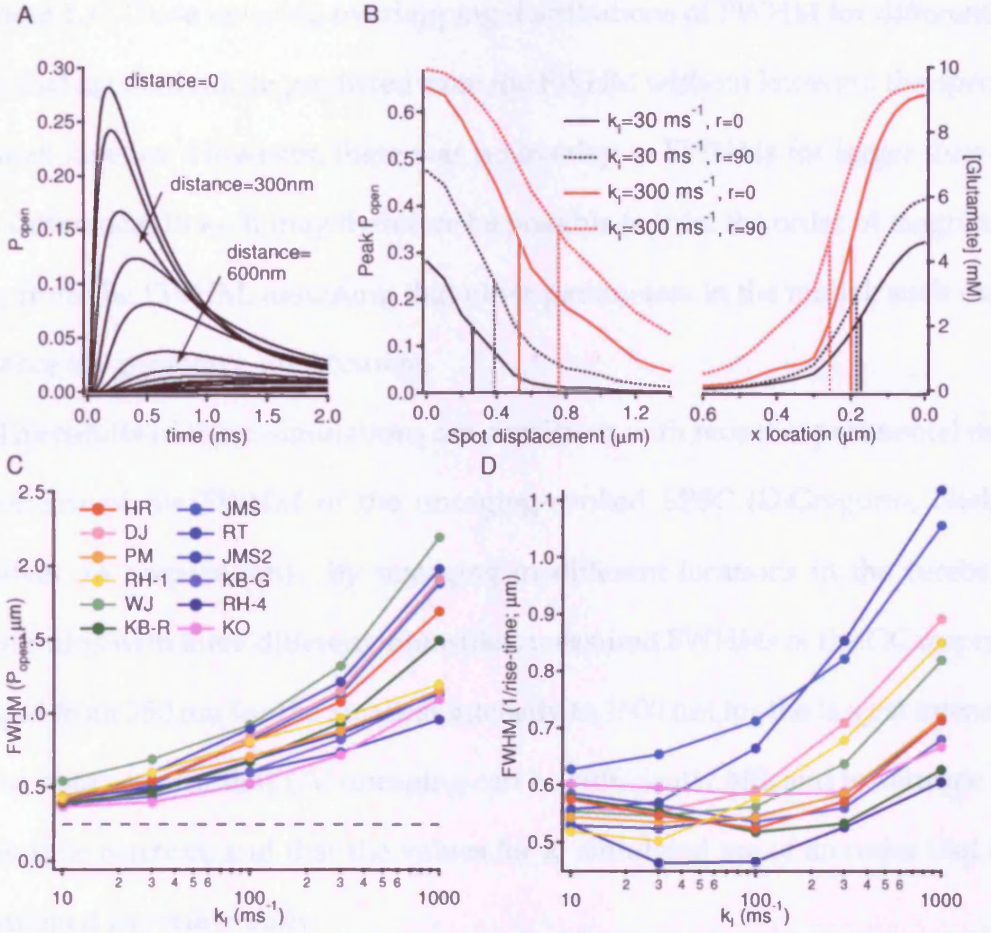

Figure 6.4: Dependence of spatial localisation on uncaging intensity. **A**, P_{open} waveforms evoked by placing the optical spot in locations with distances from the PSD of 0-1.4 μm, with k_I=30 ms^{-1} and r=0°. **B**, *left*, instantaneous glutamate concentration profile at the end of the uncaging pulse. Vertical lines indicate half maxima. *Right*, peak P_{open} amplitudes following uncaging at different distances from the PSD with k_I=30-300 ms^{-1} and spot orientations of 0° and 90°. **C**, full width at half maximum (FWHM) measured from uncaging at different distances from the PSD for different kinetic schemes and uncaging intensities (k). **D**, FWHM of the reciprocal of the 10-90% rise time of the $P_{open}(t)$, for different kinetic schemes and values of k_I.

and k_I on the postsynaptic channel kinetics, I repeated the simulations from Figure 6.4A with k_I from 10 to 10^4 and the 12 different kinetic schemes described in Table 1.1. These revealed overlapping distributions of FWHM for different k_I, such that k_I could not be predicted from the FWHM without knowing the specific channel kinetics. However, there was no overlap in FWHMs for larger than 10-fold differences in k_I. It may therefore be possible to infer the order of magnitude of k_I from the FWHM, assuming that other parameters in the model, such as for instance the geometry, are accurate.

The results of these simulations are consistent with recent experimental measurements of the FWHM of the uncaging-evoked EPSC (DiGregorio, Nielsen & Silver, in preparation). By uncaging in different locations in the cerebellar glomerulus with three different intensities, measured FWHMs of the GC response ranged from 350 nm for the smallest intensity to 1500 nm for the largest intensity. These data confirm that UV uncaging can be sufficiently efficient to saturate the photolytic reaction, and that the values for k_I simulated are of an order that can be attained experimentally.

One strategy for a direct measurement of D_{glut} is to investigate the spatial dependence of the rise time of the postsynaptic response. To investigate the influence of channel kinetics on the relationship between distance and rise time, I re-examined the simulations of P_{open} evoked by uncaging at different distances from the PSD. In order to obtain a bell-shaped curve of the spatial dependence of the P_{open} rise time, I calculated the reciprocal of the 10-90% rise time for each uncaging event, and then calculated the FWHM of this measure plotted against the distance between uncaging and PSD centres. These calculated FWHMs of the spatial dependence of the rise time are shown for different kinetic schemes and a range of values for k_I in Figure 6.4D. These relationships are more complex than the similar plots for the peak P_{open}, with some kinetic schemes show-

ing a U-shaped relationship and others monotonically increasing the FWHM as a function of k_I. However, it is clear from this graph that if neither k_I nor the kinetic scheme are known, it will be difficult to derive any information about parameters of the model, such as D_{glut}, from the spatial dependence of the rise time alone.

It is still possible, however, that uncaging can be used to investigate the kinetics of postsynaptic receptors, which I have shown are important in interpreting the change in the EPSC waveform with dextran application. The remainder of this chapter will examine, with simulations, which properties of glutamate receptors can be addressed with uncaging.

Previous studies have shown that photodamage is an important consideration in using uncaging as an experimental tool (Kiskin *et al.*, 2002). It is possible that photodamage depends both on the intensity and the duration of laser light, as would be the case assuming first-order kinetics of the photodamage reactions. It is therefore of interest to find the most efficient distribution of light for the kinetic properties of the cage, postsynaptic receptors and properties of diffusion. For the measurement of deactivation kinetics or for reproducing a mEPSC with uncaging, it is advantageous to produce a $[glut]_{cleft}$ waveform that is as rapidly decaying and spatially localised as possible. Thus, I examined how a given integral of light can best be distributed to obtain these conditions. I used an uncaging pulse with 20 μs duration, k_I=50 ms^{-1} and r=0° as a starting condition (see Figure 6.2A). I then increased the uncaging duration to 50, 100, 200 and 500 μs, and scaled the intensity down to preserve the integral of light over the uncaging duration. The resulting $[glut]_{cleft}$ waveforms, shown in Figure 6.5A, all increase in amplitude throughout the uncaging duration. The weighted decay time constants for these waveforms, measured from the peak concentration, are plotted against uncaging duration in Figure 6.5D (thick grey line). The concentration decay increases with uncaging duration. The P_{open} response amplitudes to

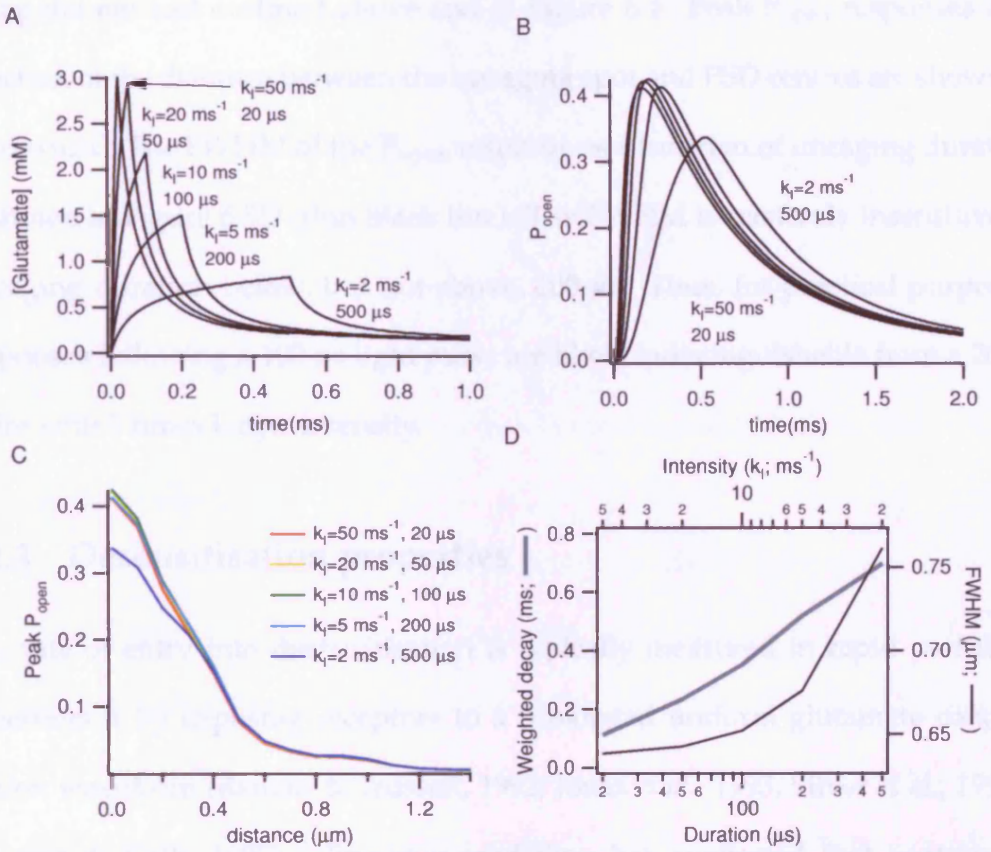

Figure 6.5: Redistribution of the light intensity to longer pulses of lower intensity increases the FWHM of the current response and the decay of the concentration waveform. **A**, $[glut]_{cleft}$ waveforms evoked with light pulses with similar products of intensity and duration. **B**, P_{open} responses (HR scheme) to $[glut]_{cleft}$ in A. **C**, Peak P_{open} responses as a function of distance from uncaging spot centre to PSD, for different combinations of k_I and duration. **D**, weighted decay time constant of the concentration waveform and FWHM of P_{open} responses plotted against uncaging duration, with k_I scaled to preserve product with duration.

these waveforms (Figure 6.5B) initially increase with longer uncaging durations before they fall again. The rise times increase and the decays slow for longer uncaging durations, as expected. I examined the spatial localisation of uncaging using the method outlined above and in Figure 6.4. Peak P_{open} responses as a function of the distance between the uncaging spot and PSD centres are shown in Figure 6.5C. The FWHM of the P_{open} response as a function of uncaging duration is shown in Figure 6.5D (thin black line). The FWHM is relatively insensitive to uncaging duration below, but not above, 100 μs. Thus, for practical purposes, responses following a 100 μs light pulse are likely indistinguishable from a 20 μs pulse with 5 times larger intensity.

6.2.3 Desensitisation properties

The rate of entry into desensitisation is typically measured in rapid perfusion experiments by exposing receptors to a prolonged uniform glutamate concentration waveform (Raman & Trussell, 1992; Jonas *et al.*, 1993; Silver *et al.*, 1996a; Hausser & Roth, 1997). Previous modelling has suggested that continuous uncaging with a two-photon laser in free solution can lead to a step-like glutamate concentration waveforms if the diffusion coefficients of the caged and uncaged glutamate are identical (Kiskin & Ogden, 2002). This is due to the diffusion of glutamate out of the uncaging volume being balanced by diffusion of caged glutamate into the uncaging volume. To investigate whether it is possible to evoke a step-like $[glut]_{cleft}$ with the difference in diffusion coefficients of glutamate and MNI-glutamate assumed here, based on their mass ratio, and in the MF-GC synaptic geometry, I simulated a 10 ms light pulse at a range of values for k_I with r=0° and r=90°. The $[glut]_{cleft}$ waveforms evoked in this manner are shown in Figure 6.6A and B. $[Glut]_{cleft}$ evoked at low uncaging intensities

increase for the first 2-4 ms, although their slope decreases with time. However, uncaging with intermediate to high intensities (>100) leads to $[glut]_{cleft}$ waveforms that are mostly flat throughout the 10 ms light pulse. These conclusions hold for both spot orientations, although the attainment of flat $[glut]_{cleft}$ waveforms occurs more rapidly and at lower intensities when r=90°. To examine the dependence of steady-state glutamate levels on the uncaging intensity, I plotted the $[glut]_{cleft}$ level attained after 10 ms uncaging against k_I for r=0° and r=90° (Figure 6.6C). The rotated spot orientation (r=90°) shows much less dependence on k_I than the upright spot orientation (r=0°). Thus, it can be difficult in some circumstances to regulate the absolute level of steady-state glutamate evoked by long uncaging durations.

Recovery from desensitisation is classically measured from the response to a test pulse of glutamate at varying time delays following a conditioning pulse that induces desensitisation. If both the conditioning pulse and the test pulse are evoked by uncaging, it is possible that the conditioning pulse may deplete MNI-glutamate such that test pulses given at short inter-pulse intervals may release a smaller amount of glutamate and thus lead to inaccuracies in estimating the amount of desensitisation induced, and the timecourse of recovery. To investigate the kinetics of MNI-glutamate recovery following an uncaging pulse, I calculated the MNI-glutamate concentration following a 20 μs uncaging pulse with k_I=50 to 1000 ms^{-1} and r=0° and 90° (Figure 6.7AB). The MNI-glutamate and glutamate concentrations at the PSD are shown in Figure 6.7A for k_I=200 ms^{-1} and r=0°, showing depletion of local MNI-glutamate on a fast timescale during the uncaging pulse. The recovery from this depletion on a logarithmic timescale is shown in Figure 6.7B. These curves indicate that for k_I=50-200 ms^{-1}, MNI-glutamate recovery is almost complete after 1-2 ms. However, for k_I=1000 ms^{-1} for both spot orientations, there can be depletion of up to 7.9% after 5 ms and

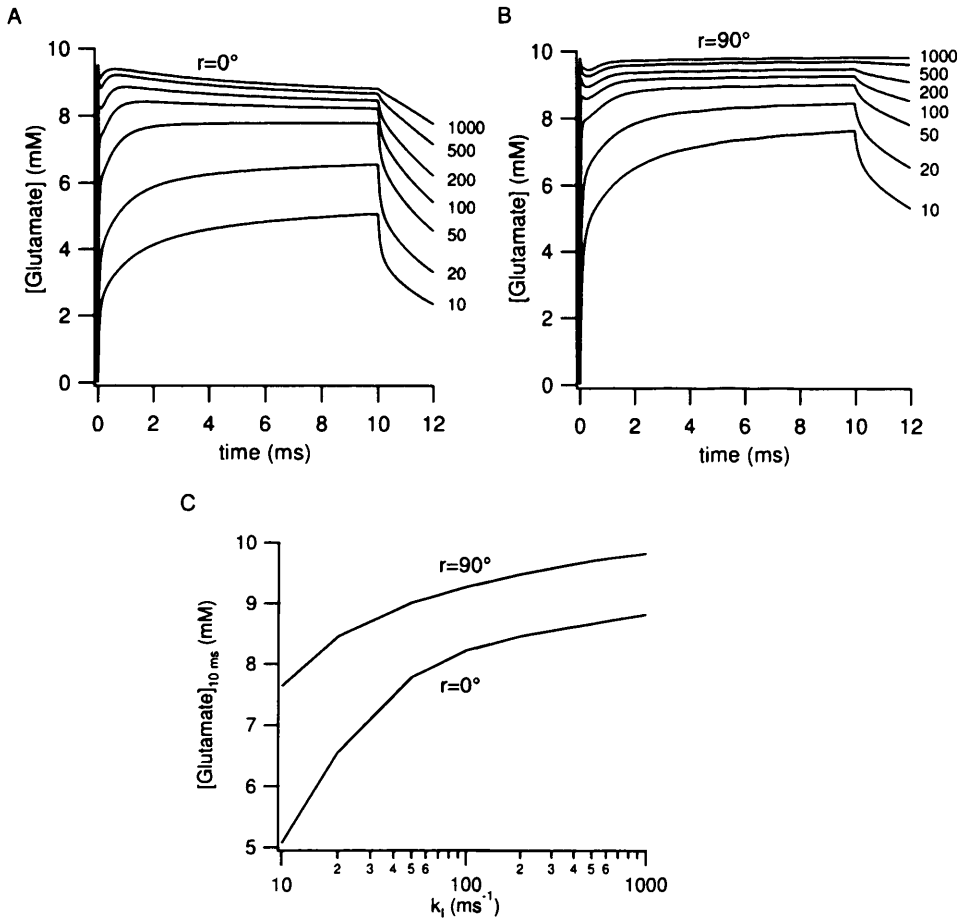

Figure 6.6: Steady-state $[glut]_{cleft}$ waveforms evoked with prolonged uncaging durations. **A**, $[glut]_{cleft}$ waveform evoked with 10 ms uncaging durations with k_I=10-1000 ms^{-1} and r=0°. **B**, as A but with r=90°. **C**, the level of $[glut]_{cleft}$ attained after 10 ms uncaging as a function of k_I for two different spot rotations.

5.5% after 10 ms. Since recovery of depression is likely to occur on a timescale of 10's of ms (Jonas *et al.*, 1993; Hausser & Roth, 1997), cage depletion is likely to introduce a minimal error.

6.2.4 Mean-variance analysis

The number of channels (N) in a PSD and P_{open} underlying the mEPSC are of special interest because they cannot be inferred from experiments on excised patches even if the kinetics properties of synaptic and extrasynaptic receptors were the same. These can be measured in the synapse using non-stationary noise analysis (Sigworth, 1980) on EPSCs (Robinson *et al.*, 1991; Silver *et al.*, 1996c), or immunogold labelling (Nusser *et al.*, 1998). The approach used by Silver *et al.* (1996c) requires a subset of synapses with saturated receptors, which may not be generally available at most synapses. Anatomical techniques only reveal N, and assume a specific antibody binding efficacy. Glutamate uncaging, in contrast, can in principle reveal the single channel conductance i, N and P_{open} from multiple trials of uncaging of a fixed amount of glutamate.

However, filtering can influence non-stationary analysis (Heinemann & Conti, 1992). For rapid perfusion techniques, the effect of filtering on estimated single-channel parameters is minimal because the patch area is small and the access resistance is small. While the granule cell acts as a single electrical compartment, the access resistance and the whole-cell capacitance still exert some filtering on recorded synaptic waveforms (Silver *et al.*, 1992, 1996c). A high quality recording with, for instance, an access resistance of 20 MΩ from a small cell (2 pF) would filter recorded currents to 4 kHz. To investigate the effect of this level of filtering, I simulated the P_{open} response to 20 μs uncaging with k_I=1000 ms^{-1} and r=90° with a Monte-Carlo algorithm (see chapter 2), and filtered individual trial to 2-4

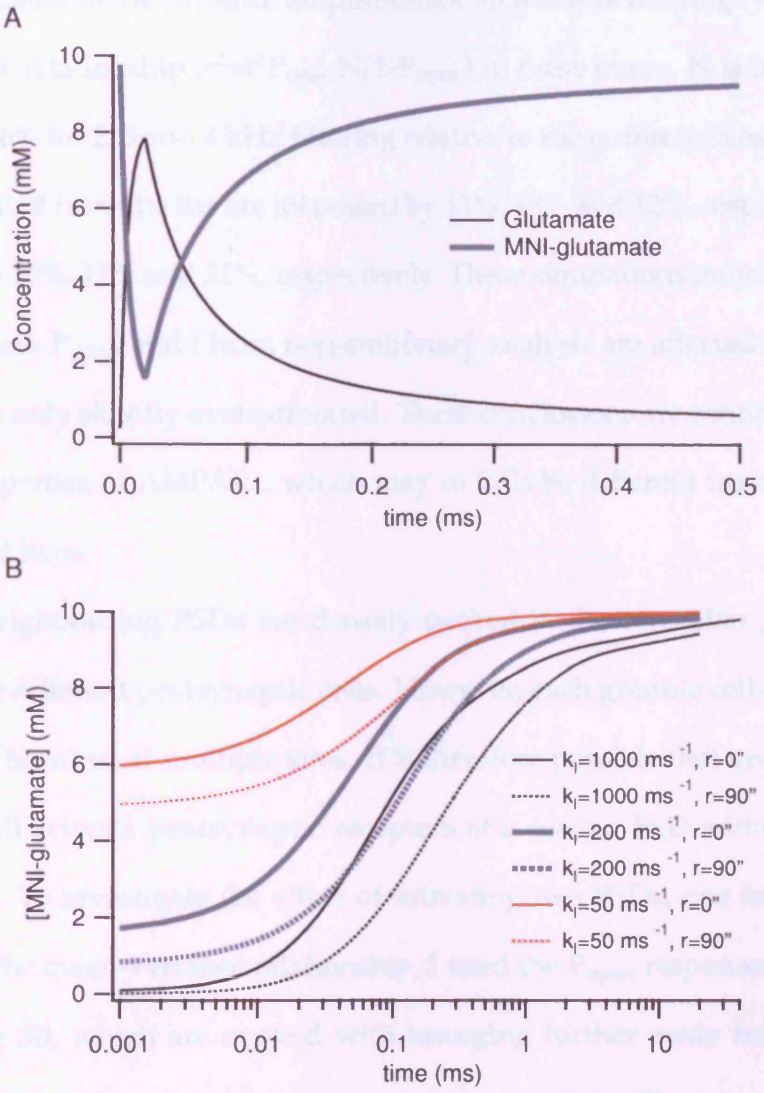

Figure 6.7: Replenishment of MNI-glutamate in uncaging spot after uncaging. **A**, MNI-glutamate and glutamate concentrations over the PSD during a 20 μs uncaging pulse with k_I=200 ms^{-1} and r=0°. **B**, recovery of [MNI-glutamate] over the PSD following a 20 μs uncaging pulse with different values for k_I and the spot rotation.

kHz before calculating the mean and variance. The mean-variance relationships before and after filtering are shown in Figure 6.8A. The rising phase of the simulated current is strongly influenced by filtering. The falling phase of the currents is also attenuated in the variance amplitude for all levels of filtering. When fitting the parabolic relationship $\sigma^2=i^2P_{open}N(1-P_{open})$ to these traces, N is increased by 4%, 3% and 6% for 2, 3 and 4 kHz filtering relative to the unfiltered case. The peak P_{open} estimated from the fits are increased by 11%, 13% and 12%, respectively and i reduced by 15%, 17% and 21%, respectively. These simulations indicate that estimates the peak P_{open} and i from non-stationary analysis are affected by filtering, but that N is only slightly overestimated. These conclusions are contingent on the kinetics properties of AMPARs, which may in GCs be different from the kinetic scheme used here.

While neighbouring PSDs are densely packed in the cerebellar glomerulus, they contact different postsynaptic cells. However, each granule cell contacts the mossy fibre terminal at multiple sites. It is therefore possible that uncaging onto one PSD will activate postsynaptic receptors at a second PSD within the same glomerulus. To investigate the effect of activating two PSDs, one local and one distant, on the mean-variance relationship, I used the P_{open} response waveforms from Figure 3B, which are evoked with uncaging further away from the PSD in steps of 100 nm, as the distant response to uncaging. These mean-variance curves were calculated with no filtering. The summed mean-variance responses to uncaging locally and distally are shown in Figure 6.8B, for k_I=1000 ms^{-1} and r=0°. These relationships indicate that at close inter-site distances, the mean-variance plot is parabolic and identical in shape to the case for the single site (compare with Figure 6.8A), although twice as large. As the second site moves further away, the mean-variance relationship takes a non-parabolic shape with a vertical rise in variance near the peak current. At longer intersite distances (>1

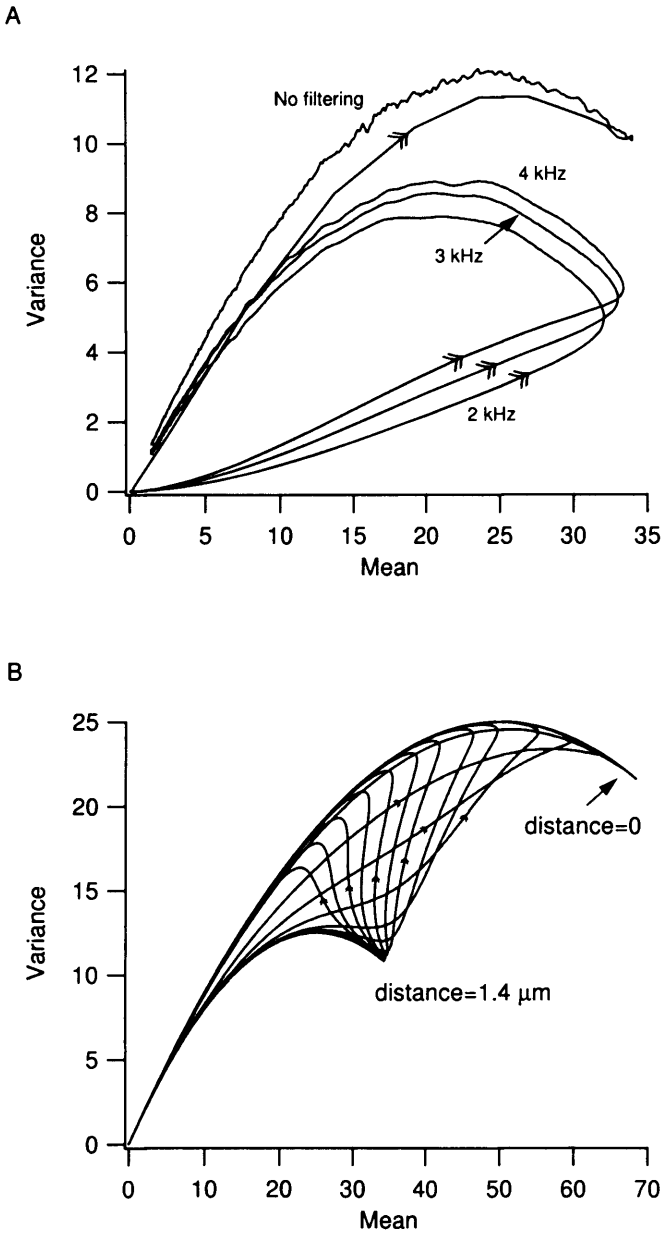

Figure 6.8: Effects of filtering and multiple glutamate-sensing PSDS on the simulated non-stationary mean-variance relationships following uncaging. **A**, Mean-variance plot following 20 ms uncaging with k_I=1000 ms^{-1} and r=0 °, with no filtering and 2-4 kHz filtering, assuming 50 receptors with a single-channel conductance of one. Double arrows indicate forward direction of time. **B**, Mean-variance plot for the sum of simulated currents from two PSDs, each with 50 receptors, with one PSD located at the uncaging spot centre and the second PSD at various distances of 0-1.4 m, in increments of 100nm.

μm), the shape is again parabolic and indistinguishable from the local uncaging alone. Thus, close neigbouring PSDs are likely either not to influence the estimation of single-channel parameters, or to be identifiable by non-parabolic mean-variance shapes.

Recent studies of single AMPA receptors indicate that multiple open states with different conductances mediate the current response to glutamate, and that the conductance depends on the number of glutamate molecules bound to each AMPA receptor. Heterogeneous conductance states may complicate the interpretation of parabolic mean-variance plots. I simulated the mean-variance relationship to a 20 μs uncaging pulse with k_I=1000 ms^{-1} and r=0°, using the kinetic scheme proposed by Robert & Howe (2003), which has three conducting states (Figure 6.9Ai), and 50 receptors. In this mean-variance relationship, shown in Figure 6.9Aii, the falling phase closely, but not exactly, mirrored the rising phase. Parabolic fits with a simple binomial model assuming one conductance state gave N=58.6 and 69.39 for the rising and falling phase, respectively, compared to the real N=50. However, there may be different representations of the configuration of the open states that more accurately describe the behaviour of single AMPA receptors. For instance, it is possible that glutamate can bind to additional subunits while the receptor is in a lower conductance state. I examined how this possibility may influence the mean variance relationship by adding direct transitions between open states with the same rate of binding as for the closed states (Figure 6.9Bi). These transitions enhanced a directionality in the mean-variance relationship (Figure 6.9Bii), such that the variance during the rising phase was higher than that during the falling phase. Parabolic fits to the rising phase gave N=49.7, close to the real value. However, fits to the decay phase gave N=84.0, 68% above the real value. The inaccuracies introduced by multiple conductance states are not, however, specific to uncaging-evoked mean-variance relationship,

and must also be considered when interpreting mean-variance plots from excised patches or synaptic connections with single release sites.

6.2.5 Rate constant fitting

Having established the conditions under which kinetic data can be obtained from uncaging, I examined the feasibility of adjusting the AMPAR kinetic rate constants to obtain a kinetic scheme for GC AMPARs. I started with the state diagram proposed by Hausser & Roth (1997), and their rate constants were likewise the starting point for the kinetic optimisation, since they best fit the MF-GC EPSC (chapter 4). The cost function for optimisation was the sum of square errors of six waveforms, weighted equally. These included the normalised quantal waveform (recorded in chapter 4; Figure 6.10A), the entry into desensitisation following a prolonged uncaging pulse (Figure 6.10B), the paired pulse depression introduced by a brief uncaging pulse with three different amplitude and 10 ms inter-pulse interval (Figure 6.10C); and paired pulse depression induced by two uncaging pulses of equal amplitude with 50 ms inter-pulse interval (Figure 6.10D; DiGregorio, Nielsen & Silver, in preparation). The paired pulse depression at 10 ms was measured with three different amplitudes for the first pulse with relative intensities of 1, 3.6 and 10, and a relative intensity of 10 for the second pulse. Entry into desensitisation and the paired-pulse depression at 50 ms was measured with a relative intensity of 10.

In order to emphasise the paired-pulse ratios as measured from the peak P_{open}, I weighted a 0.3 ms window around the peaks of the first and second pulses 10 times higher than the rest of the waveform. In addition, since a population waveform was not available for the paired-pulse depression at 50 ms, the entire weight of that waveform was in a 0.3 ms window around the peak of the second

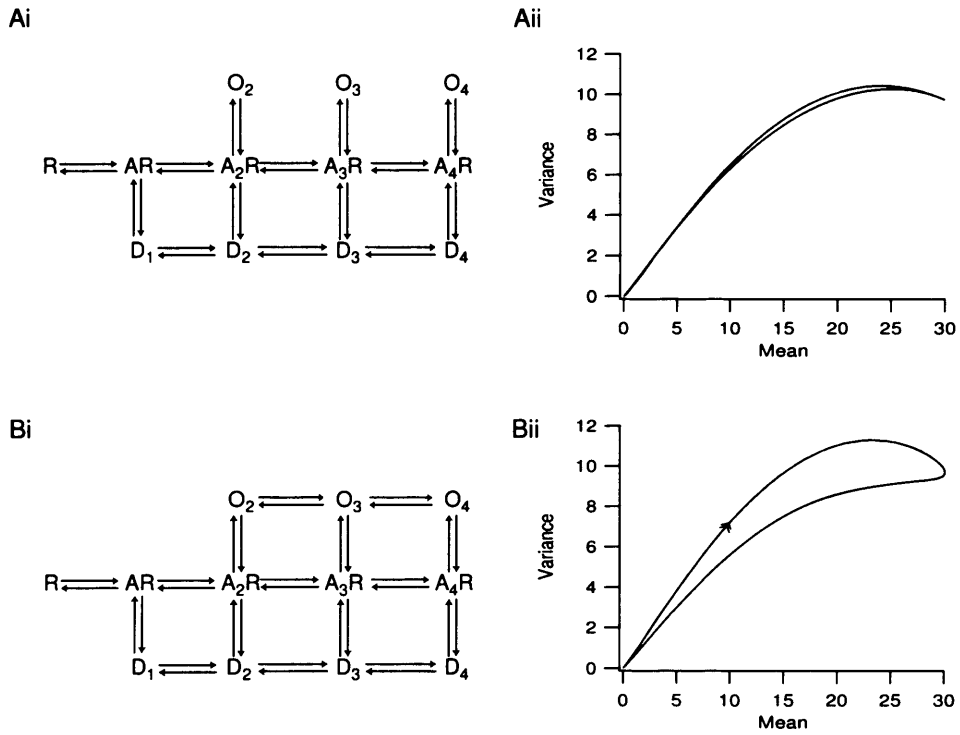

Figure 6.9: Mean-variance relationships mediated by kinetic schemes with multiple conductance states. **A**, Mean-variance plot following 20 ms uncaging with k_I=1000 ms^{-1} and r=0°, using the kinetic scheme for GluR1 (Robert et al, 2003). **B**, Mean-variance plot using the same concentration waveform as in A and a similar kinetic scheme, but with added state transitions between open states with the same rate constants at for binding between closed states.

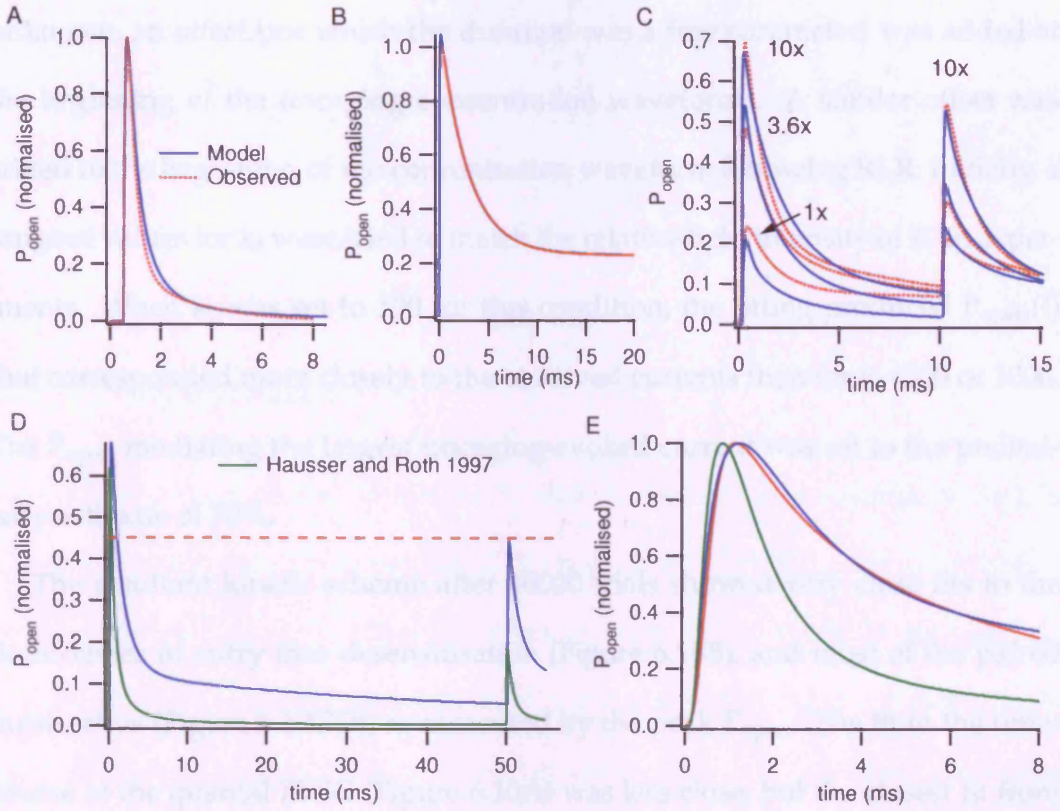

Figure 6.10: Rate constants for a kinetic scheme can be optimised to uncaging data. **A-D**, red dotted line, measured population waveforms (DiGregorio, Nielsen & Silver, in preparation) used as target for optimisation, blue solid line, response of best fit for kinetic rate constants. **A**, normalised quantal EPSC waveform (measured in chapter 4). Model simulation based on D_{glut}=0.33μm^2/ms) and instantaneous release of 4000 molecules. **B**, entry into desensitisation. Target was measured with 5 ms uncaging pulse, which gave a flat current response in cyclothiazide. The response to a 20 ms, 10 mM glutamate pulse was simulated. **C**, paired-pulse depression with 10 ms interpulse interval and with relative intensities of 1, 3.6 and 10 on the first pulse and 10 on the second pulse. Simulations with k_I=100 ms^{-1} for relative intensity of 10. **D**, paired-pulse depression with 50 ms interpulse interval and pulses of equal amplitude, with relative intensity 10 (compared to C). Also shown, response of HR scheme (green). **E**, normalised spillover $P_{open}(t)$.

pulse. Since the exact timing of laser light with respect to the recorded EPSC was unknown, an offset (for which the duration was a free parameter) was added at the beginning of the uncaging concentration waveforms. A similar offset was added to the beginning of the concentration waveform following RLR. Initially, a range of values for k_I were tried to match the relative light intensity of 10 in experiments. When k_I was set to 100 for this condition, the fitting produced $P_{open}(t)$ that corresponded more closely to the observed currents than for k_I=500 or 1000. The P_{open} mediating the largest uncaging-evoked current was set to the preliminary estimate of 70%.

The resultant kinetic scheme after 40000 trials showed very close fits to the timecourses of entry into desensitisation (Figure 6.10B), and most of the paired pulse ratios (Figure 6.10CD), as measured by the peak P_{open}. The fit to the timecourse of the quantal EPSC (Figure 6.10A) was less close, but the closest fit from the model still had two distinguishable time constants (τ_1=0.49 ms (85%) and τ_2=3.14 ms; χ^2=0.045 for exponential fit) rather than a single exponential decay (closest fit, τ=0.79; χ^2=4.97). The largest discrepancy between the optimised model and the data was in the $P_{open}(t)$ evoked with low-intensity uncaging (Figure 6.10C). Over the first 10 ms of the $P_{open}(t)$ evoked with a relative intensity of 10, the model predicted an integral that was 0.3% larger than that of the measured $P_{open}(t)$. However, for the $P_{open}(t)$ evoked with a relative intensity of 1, the predicted integral was 47% smaller than that measured.

To assess the relevance of the optimised kinetic scheme to MF-GC synaptic transmission, I used this scheme to calculate the $P_{open}(t)$ response to the average spillover $[glut]_{cleft}$ waveform calculated in chapter 4. This $P_{open}(t)$ response had a large peak amplitude, reflecting the lack of information to constrain the affinity of the AMPAR kinetic scheme. However, when normalised, it shows a timecourse that reflects the measured spillover current more closely than that mediated by

the HR scheme (Figure 6.10D). It is expected that a kinetic scheme closely mimicking GC AMPARs produce a more slowly decaying spillover $P_{open}(t)$, due to the absence of glutamate transporters in the diffusion model. It is possible that the incorrect affinity of the kinetic scheme also contributes to the slow decay of the spillover-mediated $P_{open}(t)$.

6.3 Discussion

I have shown that under conditions of high probability of uncaging, there is a non-linear relationship between the light intensity and $[glut]_{cleft}$ due to saturation of the photolysis reaction. This non-linearity changes the shape of the $[glut]_{cleft}$ waveform and the spatial distribution of glutamate with intensity, making it difficult to directly measure the full dose-reponse curve or D_{glut} using glutamate uncaging. However, uncaging can be used to obtain reliable estimates of the desensitisation of AMPARs and single-channel properties. It is therefore likely to be able to provide many constraints on a kinetic scheme for synaptic AMPARs.

The finding that glutamate profile evoked with high-intensity uncaging for 20 μs are little different from those evoked with lower intensity uncaging for 100 μs may be of interest in the choice of light sources for glutamate uncaging. If the aim of a study is to replicate the mEPSC, it may thus be adequate to choose a laser that can generate sufficient photolysis in 100 μs. Such a light source may be more economical, have a longer lifetime, or be easier to maintain than a more powerful laser. However, photodamage may be more sensitive to the peak intensity than to the laser duration (Kyagova *et al.*, 1991). In that case, it may be advantageous to use a longer uncaging duration with lower intensity even if a high-intensity light pulse is available.

The prediction that glutamate uncaging cannot replicate the waveform of

the mEPSC is not consistent with a previous study indicating that two-photon uncaging of glutamate onto cultured hippocampal neurons show the same waveform as the mEPSC (Matsuzaki *et al.*, 2001). Different studies show a two-photon-evoked EPSC that is more prolonged than the mEPSC (Smith *et al.*, 2003). It is possible that due to the enhanced axial resolution of the two-photon microscope or a difference in the synaptic geometry, $[glut]_{cleft}$ waveforms evoked by Matsuzaki *et al.* (2001) have a faster decay and are therefore indistinguishable from the mEPSC. Alternatively, the preparation used by Matsuzaki *et al.* (2001) may have slower postsynaptic receptors or poor voltage clamp, such that differences in mEPSC and uncaging-evoked EPSC waveforms are not measurable. Glutamate uptake, which is absent from the model of uncaging, may also enhance removal of glutamate after 2-3 ms at the MF-GC synapse. This process may be faster at other synapses.

Uncaging experiments are likely to tightly constrain the desensitisation properties of the kinetic scheme, since simulations indicate that flat waveforms or paired pulses of similar amplitude can be evoked with uncaging. While the prolonged presence of glutamate in the synaptic cleft following uncaging makes it difficult to evoke a step-like waveform of short duration, deactivation kinetics can be approximated by fitting the mEPSC. The fitting procedure for AMPAR rate constants can be further improved by direct measurements of the rate of cage excitation k_I *in vitro* (Canepari *et al.*, 2001) and measurement of the precise timing of laser light relative to the uncaging evoked EPSC, which will provide a better constraint of the activation kinetics. In addition, measurements of the timecourse of entry into desensitisation at different concentrations would further constrain the desensitisation kinetics (Hausser & Roth, 1997).

I have shown that changes in the absolute level of $[glut]_{cleft}$ following both short and prolonged uncaging durations are difficult to control with changes

in the light intensity due to saturation of the photolytic reaction. However, by changing the concentration of MNI-glutamate in the synapse prior to uncaging, it may be possible to change $[glut]_{cleft}$ linearly following uncaging with a fixed intensity. Since bath perfusion of MNI is often prohibitively expensive, MNI-glutamate is often applied with a local perfusion pipette, which makes it difficult to change the concentration in a controlled manner. One possible solution is to use a double-barrelled iontophoretic perfusion system with MNI-glutamate in one barrel but not the other. By calibrating this system such that the proportion of MNI-glutamate-containing solution can be regulated without changing the overall flow-rate, it is possible the regulate the MNI-glutamate concentration without risking artifact from slice movement due to different application pressures. Such a system would allow the investigator to measure the dose-response curve of synaptic receptors. Alternatively, measurement of the shape of the dose-response curve in the supralinear region may be possible using high [MNI-glutamate] and low-intensity light pulses.

CHAPTER

SEVEN

Discussion

The work presented in this thesis used a combination of electrophysiological experiments and diffusion-reaction modelling to examine diffusion of neurotransmitter in the synaptic cleft and activation of AMPARs by glutamate released locally and at a distance. The main findings are:

- Both spillover and prolonged local release of glutamate are plausible mechanisms for the slow-rising EPSC in at the cerebellar MF-GC synapse. These two mechanisms can be distinguished by lowering D_{glut}.
- Lowering D_{glut} with the macromolecule dextran reveals that spillover is responsible for the slow-rising current and the quantal EPSC is not saturated. Dextran perfusion decreases the release probability by enhancing the activation of presynaptic receptors.
- The increase in the amplitude of the quantal EPSC and in the time-to-peak of the spillover-mediated EPSC are most consistent with diffusion in the synaptic cleft being three-fold slower than in free solution. Although the estimate of D_{glut} is influenced by uncertainties in synaptic parameters, it is at least two-fold lower than in free solution.

- The fractional block of a low-affinity competitive antagonist is independent of the release probability, which indicates that at most one vesicle can be released per active zone per action potential.

- An observed acceleration of the EPSC decay at low release probabilities is likely due to non-linear activation of postsynaptic receptors at the foot of the dose-response curve, rather than saturation of glutamate transporters.

- Saturation of glutamate photolysis in an uncaging experiment can broaden the spatio-temporal profile of glutamate. Uncaging is well-suited to measure desensitisation kinetics, which can be combined with synaptic recordings to constrain a kinetic model of synaptic GC AMPARs.

In the following chapter, these findings will be discussed in a broader context of synaptic function.

7.1 How is glutamate released?

Classic studies of the NMJ have indicated that neurotransmitter is released in packets (Katz, 1969) or vesicles (Heuser & Reese, 1973), release is limited to active zones (Heuser & Reese, 1973), and released packets do not interact (Hartzell *et al.*, 1975). At central synapses, where the probability of release can be high (Gulyas *et al.*, 1993; Silver *et al.*, 2003; Dobrunz & Stevens, 1997), it is controversial whether, in response to an action potential, single (Faber *et al.*, 1985) or multiple (Wadiche & Jahr, 2001) vesicles can be released at single active zones. Experiments with low-affinity antagonists and optical measurements have led to different conclusions at different synaptic preparations (Perkel & Nicoll, 1993; Tong & Jahr, 1994; Wadiche & Jahr, 2001; Oertner *et al.*, 2002; Silver *et al.*, 2003). Previous studies of multivesicular release at the MF-GC have also come to different conclusions.

Wall & Usowicz (1998) suggested that under certain conditions, multiple release events can mediate the spontaneous EPSC. On the other hand, Silver *et al.* (1996c) found synapses in young rats where the amplitude of successes was independent of the release probability, indicating that in at least a subset of synaptic contacts, release is all-or-none. Neither of these studies directly addressed the possibility of release of multiple quanta at the same active zone across the population of GCs.

Rapidly equilibrating competitive antagonists can be used to detect whether $[glut]_{cleft}$ depends on the release probability, because they block AMPARs to an extent that depends on the agonist concentration (Diamond & Jahr, 1997). I have used the low-affinity antagonist Kyn to test whether multivesicular release occurs in 25-day old rats. The identical fractional blocks of the EPSC in different release probabilities are consistent with the univesicular release under near-physiological conditions. Several other observations support this conclusion. The linear summation of P_{open} following spillover and local release inferred in chapter 4 indicates that rapid local release activates AMPARs in the linear region of their dose-response curve, which is not the case at a synapse with multiquantal release (Foster *et al.*, 2002). MF-GC synapses with single release sites can also be found in 25-day old rats (Sargent *et al.*, in preparation), and these recordings confirm that summation of spillover and local release is linear at the peak of the EPSC. Together with the results from the fractional block of Kyn in different release probabilities, these observations indicate that at most one vesicle is released per active zone per presynaptic action potential at the MF-GC synapse. The observation that at high $[Ca^{2+}]_o$, the fractional block of Kyn does not change indicates that even at high release probabilities, multiple vesicles do not fuse at the same active zone.

This interpretation assumes that perfusion of Kyn does not in itself lead to

changes in the release probability. Wadiche & Jahr (2001) showed that γ-DGG does not change release probability by recording transporter currents from glial cells. The present experiments did not include a similar control for the effect of Kyn on release probability. Traditional indicators for release probability, such as coefficient of variation and paired-pulse ratio, are not appropriate here because Kyn changes the desensitisation characteristics of AMPARs (Wong *et al.*, 2003) and affects the proportion of current mediated by spillover, which has a different variability to the fast-rising component (DiGregorio *et al.*, 2002). It may therefore only be feasible to examine the possibility of a Kyn-induced change in release probability indirectly. Kyn could block presynaptic NMDA (Casado *et al.*, 2000), AMPA (Lee *et al.*, 2002), kainate (Delaney & Jahr, 2002) and nicotinic $\alpha 7$ (Carpenedo *et al.*, 2001) receptors. NMDA and $\alpha 7$ receptors are blocked by APV, 7-chlorokynurenic acid and strychnine in the present MF-GC experiments. The lack of change of the AMPAR-mediated EPSC waveform by a sub-saturating concentration of AMPAR antagonist GYKI 53655 (DiGregorio *et al.*, 2002) argues against control of the release probability by presynaptic AMPARs at this synapse. The recent development of specific antagonists for kainate receptors (More *et al.*, 2003) makes it possible to explore the effect of their activation on glutamate release at the MF-GC synapse, although they are typically activated poorly by single shock stimulation (Delaney & Jahr, 2002), as in the present experiments. Thus, it is not likely that Kyn changed the release probability in the experiments in chapter five.

It is unclear how to reconcile the present results with the finding of Wall *et al.* (2002) that spontaneous events recorded in sodium channel blockers can be mediated by multiple release events with distinct quantal peaks. Even if release of multiple vesicles mediate spontaneous EPSCs, it is not clear if these vesicles are released at the same or at different release sites. These events may reflect spurious activity, e.g. release of Ca^{2+} from internal stores (Emptage *et al.*, 2001) in MFs

that reflects cell death in slices and can thus coordinate several release sites in the glomerulus. Cathala *et al.* (2003) found no evidence of quantal peaks in the amplitude distribution of spontaneous events recorded in physiological $[Ca^{2+}]_o$ and temperature.

The apparent heterogeneity in the maximal number of vesicles that can be released in response to an AP at a single active zone (Perkel & Nicoll, 1993; Tong & Jahr, 1994; Auger *et al.*, 1998; Wadiche & Jahr, 2001; Oertner *et al.*, 2002; Silver *et al.*, 2003) may reflect a functional divergence in the manner in which information can be transmitted by the synapse. Activity in the cerebellar climbing fibre, where mulitvesicular release occurs (Wadiche & Jahr, 2001) reliably leads to multiple spikes in the dendritic tree of the Purkinje cell, and controls the induction of synaptic plasticity (Ito, 1989). Although glutamate release on subsequent APs is depressed following presynaptic activity (Silver *et al.*, 1998), the EPSC is depressed by a smaller magnitude than the release probability due to saturation of postsynaptic receptors following to multiquantal release, thus enhancing the reliability of the synapse (Foster *et al.*, 2002). At the MF-GC synapse, such a mechanism would decrease the effect of presynaptic modulation by e.g. mGluRs (chapter 4) and $GABA_B$ receptors (Mitchell & Silver, 2000a). It is therefore possible that synapses where the release probability is physiologically modulated and influences postsynaptic activity are more likely to show univesicular release.

7.2 What is the mechanism underlying the slow-rising current?

While the rapid rise time of AMPAR-mediated currents (e.g. Silver *et al.*, 1992) indicates that glutamate can be released very rapidly, slow-rising AMPAR-

mediated currents can also be observed at central synapses (Choi *et al.*, 2000; Renger *et al.*, 2001; DiGregorio *et al.*, 2002; Schoppa & Westbrook, 2001). Direct measurements of narrow fusion pores in neurosecretory cells (Alvarez de Toledo *et al.*, 1993; Klyachko & Jackson, 2002) led to the hypothesis that at least some of the slow-rising EPSCs at central synapses could be caused by prolonged vesicular release of glutamate. Spillover of glutamate is also likely to activate receptors on neighbouring synapses under some conditions (Otis *et al.*, 1996; Rusakov & Kullmann, 1998a), and can therefore also mediate currents with slow rise time due to the distance travelled by glutamate.

The experiments of DiGregorio *et al.* (2002) showed that the slow-rising AMPAR-mediated EPSC at the cerebellar MF-GC synapse is consistent with a spillover mechanism. Nevertheless, a model based on prolonged release from multiple vesicles can also be consistent with the results of the experimental manipulations published in DiGregorio *et al.* (2002), as described in section 1.5.4. Given the inconsistent predictions by theoretical models of the magnitude of activation of AMPARs by glutamate spillover, it is difficult to determine, based on existing literature, whether the slow-rising current is mediated by the same release mechanism as the fast-rising component, albeit at a distance, or whether a new release mechanism should be postulated. Chapter 3 describes the development of a new method for distinguishing between PLR and spillover based on slowing diffusion in the synaptic cleft.

Based on the present experiments and simulations, I found that the behaviour of the slow-rising current as a result of manipulating diffusion was best described by the spillover model, rather than the prolonged local release model. The method for distinguishing between prolonged release and spillover relies on observing a slowing in time-to-peak in currents that are mediated by spillover, but not prolonged release, when lowering D_{glut}. For very low values of initial

D_{glut} (5-fold lower than free solution), the model of prolonged release occasionally gave small increases in the time-to-peak that were smaller than 5% when lowering D_{glut} 50%. It is possible that if an even lower initial value for D_{glut} had been chosen, the increase in the time-to-peak of currents mediated by prolonged release could be larger, or perhaps even consistent with the 20% slowing observed in the experiments. Several observations indicate that this is not likely to be relevant to the MF-GC synapse. Firstly, as indicated in chapter 3, the increases in the amplitude of currents mediated by prolonged release upon lowering D_{glut} is large under these condition, which was not the case in the experimentally observed dextran-induced changes in the slow-rising EPSC. Secondly, the release timecourse derived assuming an initial D_{glut} of 0.2 $\mu m^2/ms$ was very fast and approached the estimate for the timecourse of acetylcholine release at the NMJ (Stiles *et al.*, 1996). Thus, it is unlikely that lower values for the initial D_{glut}, which would lead to faster estimates for the timecourse of glutamate release, could sustain EPSCs with both fast and slow rise times. Thirdly, increases in the time-to-peak of currents mediated by prolonged release were only observed with the scheme proposed by Jonas *et al.* (1993), which desensitises more slowly for larger glutamate concentrations. In experiments on isolated AMPARs, desensitisation occurs more rapidly (Colquhoun *et al.*, 1992; Hausser & Roth, 1997) or independently of the glutamate concentration. The increase in the time-to-peak of currents mediated by PLR may therefore be an artifact of approximations in the JMS kinetic scheme.

There may be other models based on two different release mechanisms that can account for the effect of dextran on slow-rising EPSCs. For instance, prolonged release may occur ectopically (Matsui & Jahr, 2003), such that the rise of the $[glut]_{cleft}$ is determined both by diffusion and by slow release. Since active zones are densely packed at the MF-GC synapse, ectopic release sites mediating

the slow-rising current would have to be located at most 0.32 μm from active zones and thus dextran would have to induce a large change in D_{glut} to explain the experimentally observed slowing in the slow-rising current.

In fact, the reduction in D_{glut} predicted by the dextran-induced increase in the time-to-peak of the slow-rising EPSC and in the quantal amplitude is consistent or slightly larger than an experimental estimate of this reduction (Watanabe *et al.*, 1996). The estimated reduction in D_{glut} is also in the range of predictions of the slowing based on theoretical considerations based on the volume taken up by dextran molecules (Min *et al.*, 1998; Perrais & Ropert, 2000). However, if diffusion is slower in the synaptic cleft than in free solution (see below), the dextran-induced reduction in diffusion in free solution may not translate to an equivalent fractional slowing in D_{glut}. Further evidence for the slowing of diffusion in dextran comes from a recent study showing that replenishment of Ca^{2+} depleted from the synaptic cleft following synaptic activity, which can mediate a form of synaptic depression, is reduced by dextran perfusion (Rusakov & Fine, 2003).

In addition to slowing the spillover waveform, dextran increases the $[glut]_{cleft}$ following local release. An assessment of whether this leads to an enhanced postsynaptic response provides a direct test of receptor saturation under physiological conditions. However, as it is possible that dextran changes the release probability, such a test must be accompanied by appropriate controls. One recent study interpreted a dextran-induced decrease in heterosynaptic modulation of IPSCs in the hypothalamus as the result of a reduction in spillover (Piet *et al.*, 2004). According to the simulations in chapter 3, lowering the diffusion coefficient should enhance, not reduce, postsynaptic receptor activation. The results published by Piet *et al.* (2004) may be mediated by a change in presynaptic release probability, by the masking of heterosynaptic modulation by saturation of GABA

receptors, or by desensitisation of the IPSCs during the rising phase.

The attribution of a spillover mechanism to the slow-rising EPSC, together with determination of D_{glut} and the abstract MF-GC synaptic model, provides a quantitative framework for predicting the effect of experimental and physiological modulation of the slow-rising EPSC, which contributes at least half of the AMPAR-mediated charge transfer at the MF-GC synapse (DiGregorio et al, 2002). Release through a narrow fusion pore can be regulated by for instance Ca^{2+} influx (Ales *et al.*, 1999) or synaptic plasticity (Choi *et al.*, 2000). On the contrary, spillover in a fixed geometry is much more difficult to regulate endogenously or exogenously. Although the relative contribution of spillover to synaptic transmission can be regulated by global changes in the release-probability or affinity of postsynaptic receptors, these effects on the spillover current are indirect consequences of large changes in overall synaptic efficacy.

7.3 Why is spillover so prominent at the MF-GC synapse?

The magnitude of activation of low-affinity receptors by spillover from neighbouring synapses is likely to be influenced by several factors, including the properties of diffusion in the synaptic environment, the amount of neurotransmitter released and the mechanisms whereby it can be removed from the synaptic cleft, and the kinetics of postsynaptic receptors. Several observations suggest that the MF-GC synapse is uniquely shaped to be able to detect spillover.

Some theoretical studies of glutamate diffusion into the three dimensional hippocampal neuropil suggest that glutamate is not likely to activate low affinity receptors at neighbouring synapses (Barbour, 2001; Franks *et al.*, 2002). How-

ever, when diffusion within a planar space with no diffusional sinks for glutamate is simulated, neighbouring PSDs are strongly activated (Otis *et al.*, 1996; Xu-Friedman & Regehr, 2003). I compared the peak glutamate concentration attained from the distant release of a single vesicle in the abstract MF-GC geometry with predictions from previous modelling studies, accounting for differences in vesicular content, intersite distance and release time course. Compared to simulations of the $[glut]_{cleft}$ for MF-GC geometry, a planar geometry produced a 51% greater peak concentration (Holmes, 1995), while a 3D model of parallel fiber synapses incorporating the porous neuropil (Rusakov, 2001) produced a concentration 5-fold lower than that at the MF-GC synapse. Simulations of spillover currents in hippocampus (Barbour, 2001) were nine-fold smaller than for simulations with the MF-GC geometry with the same kinetic scheme and D_{glut}. It is therefore likely that the MF-GC synaptic morphology, which is intermediate between a planar geometry and those used for simulating synapses on spines, contributes to prominent spillover.

A previous study of the MF-GC synapse at a younger developmental stage (P12) did not observe isolated slow-rising event in response to MF stimulation (Silver *et al.*, 1996c), although at this developmental stage, glutamate spillover does activate high-affinity mGluRs on inhibitory terminals in the glomerulus (Mitchell & Silver, 2000b). While it is possible that developmental changes in AMPAR affinity and kinetics contribute to the later emergence of spillover onto AMPARs, changes in the anatomy of the glomerulus may also contribute to the maturation of receptor activation. At earlier developmental stages, synaptic contacts from from each granule cells are located on same dendritic process, such that neighbouring release sites in the glomerulus are likely to contact the same granule cell (Hamori & Somogyi, 1983). Thus, while spillover may exist at this stage, for which there is indirect evidence (Silver *et al.*, 1996c), it is likely to be

intrasynaptic, and failures of all direct release sites do not lead to slow-rising currents. At later developmental stages, the dendritic process differentiates into "claws" that each contain one PSD, contacting the MF terminal at separate locations (Jakab, 1989), where neighbouring active zones are likely to contact different granule cells. Spillover may be further enhanced by the increasingly invaginated MF surface.

The large number of active zones per terminal (~191-440; Xu-Friedman & Regehr, 2003) together with the intermediate release probability (Sargent *et al.*, in preparation) ensures the spillover $[glut]_{cleft}$ is high, compared to simulations of release of single vesicles at a distance. In addition, since spillover alone activates AMPARs in the nonlinear part of their dose-response curve, the spillover-mediated P_{open} increases supralinearly with the number of vesicles released, indicating that comparisons with simulations of the release of single vesicle may also underestimate the magnitude of spillover activation relative to activation by local release. Furthermore, the inability of glutamate transporters to remove glutamate from the cleft on the millisecond timescale (Overstreet *et al.*, 1999; DiGregorio *et al.*, 2002) also contributes to prominent glutamate spillover.

The geometry used in simulations in this thesis is an abstraction of the true MF-GC synapse. For simulating $[glut]_{cleft}$ waveforms and P_{open} evoked by synaptically released glutamate, the abstraction may deviate comparatively little from a more realistic representation, because simple diffusion is insensitive to local curvatures as long as the true path length is represented correctly. For instance, in a slightly more realistic representation of the MF-GC synapse, the presynaptic membrane – here a sheet – may be represented as the surface of a hemisphere, with the dendrites oriented perpendicularly to the spherical surface. Such a change in geometry is likely to have a small impact on $[glut]_{cleft}$ and $P_{open}(t)$ because the total path length for diffusion changes little. For uncaging however,

such a model may give very different predictions from the model used in chapter 6, because the spot function, with respect to permeable and non-permeable space, would change significantly. In the ideal case, after an uncaging experiment, one would reconstruct the whole glomerulus recorded from using serial electron microscopy. Unfortunately this process is extremely time-consuming. There still is not a single full reconstruction of a whole cerebellar glomerulus, including all the GC dendrites, in the literature. An additional error is introduced in simulations of both synaptically released glutamate and uncaging in regularising the locations of release sites and dendrites, such that the nearest neighbour is always 0.64 μm instead of the distribution measured by Xu-Friedman & Regehr (2003). This inaccuracy is likely to underestimate the rise time of the spillover $P_{open}(t)$.

The role of glutamate spillover in synaptic information processing is still unclear. It has previously been proposed that averaging over more release sites gives the MF-GC response a greater reliability (DiGregorio *et al.*, 2002). However, it is difficult to predict a priori the effect of reducing synaptic variability on information processing through granule cells. Non-linear detectors, including neurons with action potentials, can display stochastic resonance, where the signal-to-noise ratio can have an inverse-U shaped dependence on the variability of the input, such that at low noise levels, additional noise can aid signal detection. It is therefore possible that spillover at the MF-GC synapse degrades the ability of granule cells to relay signals. On the other hand, it is also possible that the variability arising from stochastic release from a small number of release sites is larger than the optimal level of noise, and that reducing this variability with spillover enhances signal detection in granule cells.

Spillover may help in synchronising the granule cells that receive inputs from the same glomerulus. A recent study implemented a network model of realistic

MFs, GCs and Golgi cells without spillover at the MF-GC synapse, and found that feedback inhibition from Golgi cells caused synchronous oscillations in the granule cell layer (Maex & De Schutter, 1998). It is possible that spillover may act as an additional mechanism of GC synchronisation. However, it is also possible that the increase in synaptic reliability due to spillover is introduced at the expense of the temporal precision of the MF-GC response, which is enhanced by the fast decay of the quantal EPSC (Cathala *et al.*, 2003). The impact of glutamate spillover on timing in the GC layer is unlikely to be fully understood before existing network models are updated to include the slow-rising EPSC. The quantification of the release probability-dependence of the amplitude of this EPSC is likely to facilitate the implementation of a phenomenological description of spillover activation of AMPARs.

7.4 How does the rate of glutamate clearance influence synaptic transmission?

The timecourse of the decay of glutamate in the synaptic cleft has been the subject of intense study, because it determines the mechanisms underlying the decay of the EPSC. The rate of glutamate clearance has been experimentally estimated from synapses on cultured cells from the effect of low-affinity competitive antagonists as a dual exponential decay with τ_1=0.1 ms and τ_2=1.0-2.1 ms (Clements, 1996; Diamond & Jahr, 1997). These decays are slower than those predicted from theoretical models (Eccles & Jaeger, 1958; Wahl *et al.*, 1996), leading to the conclusion that barriers to diffusion in the micro-environment of the synapse slow the rate of clearance. Blocking buffering by glutamate transporters prolongs the measured lifetime of glutamate in the cleft, and thus buffering cannot account for the

slowed clearance (Diamond & Jahr, 1997). In fact, it is likely that this discrepancy would be even larger if experimentally measured decay rates were compared to three-dimensional simulations of the synapse rather than planar geometries.

I have presented evidence that diffusion of glutamate in the synaptic cleft at the MF-GC synapse is substantially slower than in free solution. The increase in the time to peak of the slow-rising EPSC and in the amplitude of the quantal EPSC together indicate that diffusion in the synaptic cleft is three-fold slower than in free solution. This conclusion is based the existence of a unique set of values for D_{glut} in control and in dextran that can explain the change in both the quantal and the spillover-mediated EPSC, for a given set of model parameters. The existence of a unique intersection point on the graph in Figure 4.4B is fortuitous and may not necessarily occur in the relevant range for a similar analysis, although it did for all the conditions tested in chapter 4. In addition, the change in D_{glut} was sufficiently large compared to the experimental uncertainty in measuring quantal amplitude and the time-to-peak of slow-rising EPSCs.

The largest uncertainties in estimating D_{glut} comes from the difficulty in predicting the shape of time-to-peak of the spillover EPSC and the amplitude of the quantal EPSC with respect to D_{glut} given the uncertainties in model parameters. These parameters include the channel kinetics, the number of glutamate molecules per vesicle, and details of the synaptic geometry including the possibilities of increased inter-site distances with development and a smaller cleft width outside the PSD. In order to improve the estimate of D_{glut}, I took advantage of the variability in the resemblance of predicted $P_{open}(t)$ to the measured MF-GC EPSCs. Weighting each scheme according to its ability to predict the EPSC timecourse allowed the estimates from individual kinetic schemes to be collapsed into one overall estimate for D_{glut}. A smaller variability in the estimate for D_{glut} arose from uncertainties in the MF-GC geometry or the number of molecules

in a synaptic vesicle. While these uncertainties did influence the exact estimate of D_{glut}, they did not affect the conclusion that diffusion is substantially slower in the synaptic cleft than in free solution. It is also possible that the true MF-GC synapse is best represented by a combination of two or more of the manipulations of the synaptic model presented in chapters 3 and 4. Since it is impossible to test every combination of parameter values in the model, I attempted to choose the most likely or well-characterised default values, and examine the effect of manipulations in individual parameters. The estimate for D_{glut} can be revised as new information becomes available.

The difference between the estimate of D_{glut} at the MF-GC synapse and that in free solution is not due to geometric tortuosity (Nicholson & Sykova, 1998), since the intersite distance used in the model was measured along the surface of the presynaptic membrane (Xu-Friedman & Regehr, 2003), and the model includes diffusional sinks between neighbouring dendrites, thus explicitly accounting for the full path length of diffusion. Previous measurements have shown that the bulk tissue tortuosity (λ) in the GC layer of the cerebellum is 1.77 (Rice *et al.*, 1993) corresponding to an apparent diffusion coefficient 3-fold less than for aqueous solution. This includes macroscopic geometrical factors such as diffusion around cells, which account for a slowing of 1.5 fold (λ =1.225; Kume-Kick *et al.*, 2002), leaving a 2-fold slowing by microscopic factors including D_{glut}. If the diffusion properties of the extracellular space are similar to those in the synapse this value is consistent with the upper estimate for D_{glut} of 0.5 $\mu m^2/ms$. However, the mean value for D_{glut} of 0.33 $\mu m^2/ms$ suggests that diffusion is slower in the glomerulus than in the surrounding extracellular space, which may comprise the majority of the extracellular volume in the GC layer. Although the mechanisms underlying glutamate mobility in the synapse are unknown, it is possible that macromolecules, such as ion channels and constituents of the extracellular

matrix, contribute to slowing glutamate diffusion (Sykova, 2001). However, diffusion could also be slowed by an unidentified glutamate binding protein that has a much greater capacity than AMPARs and transporters. Under these conditions the estimate of D_{glut} would reflect an effective diffusion coefficient (but see Barbour, 2001; Zador & Koch, 1994).

At the MF-GC synapse, other factors may contribute to a slow decay of the $[glut]_{cleft}$ waveform. The restriction of glutamate transporters to the periphery of the synapse (Chaudhry *et al.*, 1995; Xu-Friedman & Regehr, 2003) may limit the ability of buffering to prolong the lifetime of glutamate in the cleft, but will also limit glutamate removal. In addition, the geometry of the synapse will lead to prolonged retention of glutamate compared to synapses on spines, and the glial sheath may slow removal of glutamate over the long timescales of equilibration of glutamate within the whole glomerulus.

The simulations in chapter 4 indicate that the peak spillover $[glut]_{cleft}$ is predominantly mediated by sites that are closer than 0.9 μm from the detecting PSD. At the peak of the spillover-mediated $P_{open}(t)$, more distant sites contribute to receptor activation. Nevertheless, the most distant sites in the model, which are 2.7 μm from the detecting PSD, contribute less than 0.1% of the concentration at the time of the peak of the spillover $P_{open}(t)$. It is therefore likely that the closest sites determine the peak amplitude of activation by glutamate spillover, consistent with the estimate that three times the number of local sites mediate the slow-rising EPSC (DiGregorio *et al.*, 2002).

Based on the estimate of D_{glut} and the synaptic geometry, the diffusion model predicts three decay time constants of 20 μs, 145 μs and 3.6 ms following local release alone. The faster time constant does not exist in the previous estimates of the decay of $[glut]_{cleft}$ (Clements, 1996; Diamond & Jahr, 1997), but may be too fast to measure with low-affinity antagonists. This suggestion is consistent with

the lower peak amplitude in those estimate (1mM) compared to chapter 4 (8.3 mM), with the fast time constant accounting for 84% of the $[glut]_{cleft}$ waveform in chapter 4. The last two time constants are similar to the previously estimated time course, although slightly slower. This may reflect the MF-GC geometry, which is intermediate between a plane and synapses on spines.

A low D_{glut} has implications for the independent operation of neighbouring synaptic contacts, since the $[glut]_{cleft}$ waveform mediated by spillover slows as D_{glut} is lowered without a decrement in the amplitude. The simulations in chapter 3 show that this produces a larger spillover-mediated postsynaptic activation than would be expected for diffusion in free solution. In addition, a low D_{glut} may enhance the ability of spillover to induce AMPAR desensitisation and thus will influence short-term synaptic plasticity (Xu-Friedman & Regehr, 2003). A D_{glut} that is lower than in free solution will also produce a slower transmitter concentration waveform following rapid local release (Franks *et al.*, 2002; Rusakov & Kullmann, 1998a). This will increase the occupancy of the postsynaptic receptors and thus the amplitude of synaptic current. At the MF-GC synapse, I found no significant difference in the time-to-peak or decay time constants of quantal currents in control and dextran, indicating that the shape of the quantal current is relatively insensitive to D_{glut}. These results together with the diffusion model suggest that the decay of $[glut]_{cleft}$ is faster than the decay of the quantal current. A diffusion coefficient substantially below free solution could therefore allow this synapse to operate with fewer molecules per vesicle, without compromising the rapid kinetics associated with low-affinity receptors. The results of chapter 4 indicate that slowing diffusion with dextran enhances synaptic currents and the activation of presynaptic metabotropic receptors. The mobility of neurotransmitters is therefore an important determinant of both pre- and postsynaptic efficacy.

7.5 What do we know about the GC AMPAR kinetics?

This thesis has demonstrated that AMPAR kinetics are important determinants of the waveform of the EPSC, and are essential in linking diffusion modelling with neural function. Unfortunately, GCs do not express AMPARs somatically and so a kinetic scheme cannot be constructed from recordings from excised patches. Inferences about the kinetic properties about synaptic receptors must therefore be made indirectly.

In situ hybridisation studies have suggested that in rodents, the GC layer expresses exclusively mRNA for GluR2 (or B) and GluR4 (or D) (Fragioudaki *et al.*, 2002), although there is evidence for expression of all subunits in human granule cells (Tomiyama *et al.*, 1999). In adult rats, a mixture of flip and flop isoforms are expressed in GCs (Mosbacher *et al.*, 1994). Since inclusion of a single $GluR4_{flop}$ subunit confers rapid desensitisation properties on AMPARs, it has been assumed (Xu-Friedman & Regehr, 2003) that GC AMPARs share the properties of nucleus magnocellularis AMPARs, where $GluR4_{flop}$ is expressed (Ravindranathan *et al.*, 2000) and receptors densensitize with a time constant of 0.5 ms (Raman & Trussell, 1992).

Synaptic and patch recordings have confirmed the predictions that GC have linear IV relationships as expected for inclusion of GluR2 subunits (Silver *et al.*, 1996c), but have come to inconsistent conclusions about the timecourse of desensitisation. Silver *et al.* (1996a) found a slow timecourse of entry into desensitisation compared with the synaptic current, although Wall *et al.* (2002) recorded a faster entry into desensitisation. The interpretation of these studies is complicated by kinetic studies being confined to patches pulled from cultured cells rather than slices. Indeed, Wall *et al.* (2002) suggest that desensitisation proper-

ties may change with maturation *in vitro*. It is therefore uncertain how recordings from patches relate to the MF-GC synapse *in situ*.

By examining P_{open} waveforms simulated with the D_{glut} predicted by each scheme, I found that the channel described by Hausser & Roth (1997) best predicts the timecourse and the amplitude of both the fast-rising and the slow-rising EPSC. However, the HR model is based on recordings made at room temperature, with rate constants extrapolated to physiological temperature with the value of Q_{10} measured by Silver *et al.* (1996a) in cultured GCs. The HR model is based on patches pulled from cerebellar Purkinje cells, and AMPARs in this cell type were also investigated at higher temperature (32-35 ^{o}C) but at the same developmental stage (Wadiche & Jahr, 2001). Thus, the existence of models for the same receptors at different temperatures allows a more detailed investigation of the effect of temperature on individual rate constants. In fact, most rate constants were identical in the HR and the WJ models, including rates of association, dissociation and gating in undesensitised states, arguing that the temperature sensitivity of these rates is low. That the HR model fits GC AMPAR currents better than the WJ model argues that GC AMPARs have faster kinetics than those of Purkinje cells.

The finding that dextran enhances the quantal EPSC provides direct evidence that AMPARs at the MF-GC synapse are not saturated, which has previously been inferred at this (Silver *et al.*, 1996c) and other (Larkman *et al.*, 1991; Forti *et al.*, 1997; Liu *et al.*, 1999; McAllister & Stevens, 2000; Ishikawa *et al.*, 2002) synapses. However, non-saturation is consistent with activation in supralinear, linear and sublinear regions of the dose-response curve. The experiments described in chapters 4 and 5 have indicated that the quantal EPSC is located on the linear, and the slow-rising EPSC on the supralinear, part of the dose-response curve. While the conclusion that the quantal EPSC is in the linear region is an indirect inference from the similar increases in the quantal EPSC and the spillover-subtracted fast-

rising EPSC in dextran, it is consistent with recent recordings from synapses with single release sites in P25 rats (Sargent *et al.*, in preparation). Supralinear activation of AMPARs by spillover of glutamate will be discussed below.

Photolytic uncaging of glutamate greatly expands the range of experiments that can be performed on synaptic receptors. I have shown in chapter six that a kinetic scheme for synaptic glutamate receptors can be constructed using a combination of glutamate uncaging, mEPSC recordings, and diffusion-reaction simulations. Preliminary results indicate that desensitisation is relatively modest. This conclusion is consistent with the finding from chapter 3 that kinetic schemes with rapidly desensitising properties such as the RT scheme cannot reproduce the spillover waveform except at very low occupancies (~5-fold lower than measured). Uncaging is also likely to provide an estimate of the number of receptors in a single PSD and the occupancy following quantal release, if high receptor occupancies can be saturated with uncaging.

A full kinetic scheme is ideally constrained by the measurements of time-courses of activation, deactivation, entry into desensitisation, recovery from desensitisation, the dose-response curve and the maximal P_{open} (Diamond & Jahr, 1997). Based on the simulations from chapter 6, deactivation and the dose-response curve are the most difficult to measure using uncaging alone. Including a fit to the quantal EPSC waveform may help constraining the rate deactivation, and the dose-response curve may be more tightly constrained by measuring the value for k_I *in vitro*. It is therefore possible that a kinetic model based on uncaging data can be almost as accurate as one based on outside-out patches.

The calculation of uncaging-evoked $[glut]_{cleft}$ timecourses depends on both the synaptic geometry and D_{glut}. In the absence of better measurements, I have used the abstract geometry introduced in chapter 3 and the value of D_{glut} measured in chapter 4. Since the measurement of D_{glut} depends both on the kinetic

scheme and the synaptic geometry, it is possible that the conditions mediating the MF-GC EPSC are very different from the range I tested in chapter 4, and the D_{glut} estimate of 0.33 $\mu m^2/ms$ is grossly in error, leading to an inaccurate estimate for uncaging-evoked $[glut]_{cleft}$ waveform and thus the kinetic parameters of AMPARs. While it may be difficult to avoid the pitfalls of circularity in these experiments due to the lack of data about the MF-GC geometry and AMPAR kinetics, it may at least be possible to show internal consistency by predicting D_{glut}, using the method described in chapter 4. If future studies report a full reconstruction of the cerebellar glomerulus, including GC dendrites, the model dependence on an abstract geometry can be removed.

A full characterisation of the kinetics of GC AMPARs, together with the results of the present chapters, will constitute a significant progress in our understanding of synaptic transmission in presenting a model synapse in which all parameters necessary to reconstruct the evoked EPSC have been measured in the same preparation and under similar, near-physiological conditions. This model can then be used to further explore aspects of information processing and model synaptic disorders, such as for instance ischemia (Rossi *et al.*, 2000) or cerebellar ataxia (Hashimoto *et al.*, 1999). This model can be further extended by an appropriate model for short-term synaptic plasticity (Dittman *et al.*, 2000; Tsodyks & Markram, 1997; Magleby, 1987) and a more realistic geometry incorporating glutamate transporters. Such an extended model, by predicting the postsynaptic response throughout a train of presynaptic activity, can significantly extend our understanding of the influence of biophysical parameters on information processing (Fuhrmann *et al.*, 2002).

All the kinetic schemes tested in chapter 4 were activated to some extent by glutamate spillover, some more so than the response seen in the synapse. It is therefore not necessary to postulate that GC AMPARs have special properties

(e.g. higher affinity) that allow them to detect spillover from neighbouring release sites. However, it is still possible that the balance between rapid excitation following local release and prolonged activation following spillover is unique in the GC. For instance, the slow entry into desensitisation may allow glutamate spillover to activate AMPARs even following RLR on a single trial. It is also possible that the kinetics of GC AMPARs give a specific ratio of local-to-spillover activation that is optimised for stochastic resonance, synchronisation, or balance between reliability and precision.

7.6 Why does the EPSC waveform change with release probability?

At classic synapses where each release site acts as independent all-or-none units, changes in the release probability scale the synaptic waveform linearly. However, changes in the EPSC waveform with release probability occur at some (Trussell *et al.*, 1993; Takahashi *et al.*, 1995; Silver *et al.*, 1996c, 1998) but not at all central synapses (Isaacson & Walmsley, 1995; Diamond & Jahr, 1995). As discussed above, it is likely that some synapses do not see spillover and at most one vesicle can be released per active zones, satisfying the criteria for independent synaptic contacts (Silver *et al.*, 2003). However, at some synapses where spillover is likely to be prominent, the EPSC waveform also scales with release probability under physiological conditions (Trussell *et al.*, 1993). At the chick nucleus magnocellularis synapse, the linear scaling of the waveform is likely to be due to a balance of two opposing effects: spillover and desensitisation.

In chapter 5, I presented evidence for non-linear activation of receptors being the mechanism responsible for the release probability-dependence of both the

relative amplitude of the slow-rising EPSC and the shape of the mean EPSC waveform. In this model, diffusion of glutamate is linear, i.e. the concentration response to the release of several vesicles at different locations equals the sum of each of the concentration responses to the release of those vesicles alone. This is not the case when comparing the unitary response to release of a single vesicle to the concentration following multiple release events smeared by a latency distribution. However, when averaging over several trials, the waveform shape is independent of the release probability and therefore the number of vesicles released, provided that the distribution of latencies and release locations do not depend on the release probability. A previous study compared the $[glut]_{cleft}$ following local release of a single vesicle to the $[glut]_{cleft}$ following release of both a local vesicle and multiple additional vesicles released at a distance, and found that the $[glut]_{cleft}$ waveform is influenced by the additional distant release sites (Otis *et al.*, 1996). This situation is most likely to approximate an experiment in which the stimulation intensity is increased, thus recruiting additional fibres (Marcaggi *et al.*, 2003), but not the change of $[glut]_{cleft}$ with release probability. At a large synapse with many release sites, such as the Calyx of Held, spontaneously released glutamate will therefore reach receptors at the neighbouring synapse to the same extent as glutamate released following an action potential. This is also the case at the MF-GC synapse, but here, glutamate spillover following spontaneous release will activate receptors on dendrites from different cells. Thus, at large synapses with one-to-many connectivity, such as the MF-GC synapse, the mEPSC can be assumed to represent direct release in the absence of spillover, assuming that spillover mEPSCs cannot be resolved in the noise. At large synapses with one-to-one connectivity, this may only be true if spillover from a single vesicle produces negligible activation at postsynaptic receptors due to their non-linear dose-response.

Why do AMPARs have Hill coefficients larger than one? The classic interpretation of the Hill coefficient is that it reflects the number of binding sites per receptor. Thus, with a Hill coefficient of 1.5, synaptic AMPARs might be expected to have more than one glutamate binding sites. Clements *et al.* (1998) performed a more sophisticated analysis of the activation kinetics of excised patches stepped from antagonist to agonist solutions, and also found that the macroscopic currents were best fit by assuming two, rather than one or three, binding sites. This line of reasoning was strongly challenged by single-channel recordings of AMPARs showing that their activation involves a procession through three conductance states, of which the lowest level has a bi-exponential lifetime distribution, consistent with binding of four glutamate molecules to reach full opening. This effect could probably be accounted for by a model with only two binding states, such as for instance by changing some of the conductance levels in the three open states of the model presented by (Raman & Trussell, 1995), which has two binding sites and three open states of equal conductance. However, the finding that the average conductance level depends on the glutamate concentration (Smith & Howe, 2000) strongly argues in favour of the hypothesis that different conductance levels reflect the binding of different numbers of glutamate molecules to individual receptors. The Hill coefficient between one and two in the foot of the dose-response curve may reflect the number of glutamate molecules required to activate the lowest conductance state of the receptor, rather than the total number of binding sites per glutamate receptor.

Even in the case of a kinetic mechanism similar to the single-conductance models of AMPARs, it is unlikely that the Hill coefficient will equal the number of binding sites. This equality holds in the case of simultaneous binding which is physically implausible. The Hill coefficient may also equal the number of binding sites if binding to one site strongly increases the affinity of a second site (positive

cooperativity; Weiss, 1997). The Hill coefficient is therefore more readily interpreted as an indicator of cooperativity rather than the number of binding sites. In addition, the concentration waveform and agonist identity can also influence the Hill coefficient (Raman & Trussell, 1992; Colquhoun *et al.*, 1992).

Due to non-linear receptor activation, physiological processes that change the release probability at the MF-GC synapse will also change the shape of the synaptic conductance waveform. Long-term modifications in synaptic plasticity (D'Angelo *et al.*, 1999) and those induced by activation of presynaptic receptors (Mitchell & Silver, 2000a) will therefore alter the contribution of spillover to the EPSC, such that a given change in the release probability has a non-linear effect on the synaptic charge transfer. While the complete effect of spillover on synaptic integration is unclear (see discussion above), changes in release probability will have a knock-on effect on any role that spillover plays in reliability, precision and synchronisation.

The release probability can also be changed by the recent history of synaptic activity. Most MF-GC synapses are depressing, although a subset show facilitation (Sola *et al.*, 2004). It is therefore possible that for the majority of cells, a burst of activity in the MF leads to synaptic waveforms that are not only successively decreasing in peak amplitude, but also show acceleration of the decay. The type of behaviour might also be expected *a priori* from the cyclothiazide-treated nucleus magnocellularis synapse, which is depressing and shows the same release probability dependence of the EPSC waveform as the MF-GC synapse. In fact, the opposite is the case: at inter-pulse intervals of less than 10 ms, the response to the second pulse in a paired pulse protocol has a slower decay than to the first (Trussell *et al.*, 1993). Although the authors of this study did not interpret either this result or the release probability dependence of the EPSC waveform as non-linear receptor activation, they did suggest that the paradoxi-

cal broadening of the second pulse was due to summation of residual glutamate in the synaptic cleft from the first pulse with glutamate spillover from the second pulse. This hypothesis is, however, still feasible with non-linear receptor activation as the mechanism mediating non-linear responses to glutamate in the synaptic cleft. It is therefore possible that synaptically depressed EPSC would show the same behaviour at the MF-GC synapse.

While spillover at the MF-GC synapse may aid in information processing at the MF-GC synapse (see above), at synapses onto spines in the hippocampus, the neocortex, and the cerebellar molecular layer, spillover may degrade the storage capacity of the network (Barbour & Hausser, 1997). Indeed the geometry and more potent glutamate transporters favour smaller spillover activation at these synapses (see above). Although various mechanisms for synchronisation exists in the cortex (Singer, 1999) and hippocampus (O'Keefe & Recce, 1993), glutamate spillover from multiple presynaptic release sites is likely to be more synchronised when released from a single fibre than from multiple fibres, and thus summation of spillover from multiple vesicles is more likely to occur in the latter rather than the former case. Due to a non-linear dose-response curve, the AMPAR may act as a coincidence detector, responding to larger, more meaningful stimuli while filtering out small desynchronised responses that are likely to reflect activation of different synapses. The non-linear response to small glutamate concentrations may be a convenient activation mechanism suited to both small, tightly packed synapses where spillover is likely to degrade signal processing, and synapses with large presynaptic terminals where spillover can enhance signal processing, although the magnitude of this effect may be small.

7.7 What are the determinants of the AMPAR-EPSC synaptic waveform?

Activation of AMPARs is the principal mechanism of fast excitation in the central nervous system. The waveform of the AMPAR-mediated EPSC can be modulated by physiological processes and influences properties of synaptic integration. But do we understand at all the mechanisms that determine this waveform? Jonas & Spruston (1994) proposed a classification of central synapses based on the mechanisms of their EPSC decay: it may be determined only by deactivation in the absence of glutamate in the synaptic cleft; only by desensitisation in the prolonged presence of glutamate; or by a slower removal of glutamate, that causes a decay that is shaped by a combination of the glutamate decay, deactivation and desensitisation. As at the MF-GC synapse, a change in the EPSC waveform indicates that glutamate removal contributes to the EPSC decay. The experiments in this thesis have established that non-linear activation of AMPARs by glutamate spillover can mediate a release probability-dependence of the EPSC waveform. These findings contrast with observations at the NMJ, where it is thought that the decay of EPSC is mediated by deactivation alone (Magleby & Stevens, 1972).

The relative contributions of deactivation and desensitisation to the decay of the quantal EPSC are still unknown, in part due to the absence of sufficiently selective inhibitors of AMPAR desensitisation. The quantal EPSC at the MF-GC synapse has a dual-exponential decay as at some (Wadiche & Jahr, 2001) but not all (Hestrin, 1992; Geiger *et al.*, 1997) glutamatergic synapses. I have showed that when fitting the rate constants of an AMPAR kinetic scheme, it is possible to obtain a dual-exponential response similar to the quantal EPSC. Whether the second time constant reflects the prolonged presence of glutamate in the synaptic cleft following quantal release or is part of the intrinsic decay of the receptor may

be determined by recording quantal EPSCs in Kyn.

The EPSC rise time is likely to be determined by receptor kinetics rather than the $[glut]_{cleft}$ timecourse, for both quantal EPSCs and spillover EPSCs. The calculated spillover $[glut]_{cleft}$ has a rise time of 198 μs, which is four times faster than recorded EPSCs (DiGregorio *et al.*, 2002). This hypothesis is consistent with the similarity of activation kinetics with quantal EPSC rise time at other synapses (Trussell *et al.*, 1993). The slow rise time of spillover EPSC likely arises from a low rather than a slowly rising $[glut]_{cleft}$, although the slow decay of the spillover $[glut]_{cleft}$ may lead to accumulated receptor activation.

Several studies have stressed the importance of the EPSC waveform in synaptic integration. The rise and decay kinetics of the synaptic conductance waveform determine the magnitude of subthreshold voltage fluctuations, which in term determines whether inhibition has a subtractive or divisive effect on the firing rate (Mitchell & Silver, 2003). Synaptic conductances with rapid decays also allow a cell to charge more quickly than the membrane time constant (Koch, 1998), which may contribute to enhanced precision of the EPSPs (Harsch & Robinson, 2000; Galarreta & Hestrin, 2001). The simulations shown in Figure 4.5 indicate that despite a slow rate of glutamate clearance, the decay of quantal AMPAR EPSCs can be very rapid.

These findings indicate that specific receptor properties regulate the response to synaptically released glutamate, allowing this response to be modulated on a fast timescale. Nevertheless, development of the synaptic geometry (Hamori & Somogyi, 1983), which determines the $[glut]_{cleft}$ waveform, can contribute to maturation of the synaptic response, in particular by regulating the contribution of glutamate released at a distance to the synaptic current. Future studies are likely to clarify the mechanisms whereby modulation of the EPSC waveform can alter information processing over multiple timescales.

BIBLIOGRAPHY

Adler, E., Augustine, G., Duffy, S. & Charlton, M. (1991). Alien intracellular calcium chelators attenuate neurotransmitter release at the squid giant synapse. *J Neurosci*, **11**, 1496–507.

Albillos, A., Dernick, G., Horstmann, H., Almers, W., Alvarez de Toledo, G. & Lindau, M. (1997). The exocytotic event in chromaffin cells revealed by patch amperometry. *Nature*, **389**, 509–12.

Ales, E., Tabares, L., Poyato, J.M., Valero, V., Lindau, M. & Alvarez de Toledo, G. (1999). High calcium concentrations shift the mode of exocytosis to the kiss-and-run mechanism. *Nat Cell Biol*, **1**, 40–4.

Alvarez de Toledo, G., Fernandez-Chacon, R. & Fernandez, J.M. (1993). Release of secretory products during transient vesicle fusion. *Nature*, **363**, 554–8.

Anderson, C. & Stevens, C. (1973). Voltage clamp analysis of acetylcholine produced end-plate current fluctuations at frog neuromuscular junction. *J Physiol*, **235**, 655–91.

Aravanis, A.M., Pyle, J.L. & Tsien, R.W. (2003). Single synaptic vesicles fusing transiently and successively without loss of identity. *Nature*, **423**, 643–7.

Asztely, F., Erdemli, G. & Kullmann, D.M. (1997). Extrasynaptic glutamate

spillover in the hippocampus: dependence on temperature and the role of active glutamate uptake. *Neuron*, **18**, 281–93.

Atluri, P. & Regehr, W. (1998). Delayed release of neurotransmitter from cerebellar granule cells. *J Neurosci*, **18**, 8214–27.

Auger, C. & Attwell, D. (2000). Fast removal of synaptic glutamate by postsynaptic transporters. *Neuron*, **28**, 547–58.

Auger, C., Kondo, S. & Marty, A. (1998). Multivesicular release at single functional synaptic sites in cerebellar stellate and basket cells. *J Neurosci*, **18**, 4532–47.

Barbour, B. (2001). An evaluation of synapse independence. *J Neurosci*, **21**, 7969–84.

Barbour, B. & Hausser, M. (1997). Intersynaptic diffusion of neurotransmitter. *Trends Neurosci*, **20**, 377–84.

Batchelor, A.M., Madge, D.J. & Garthwaite, J. (1994). Synaptic activation of metabotropic glutamate receptors in the parallel fibre-purkinje cell pathway in rat cerebellar slices. *Neuroscience*, **63**, 911–5.

Bean, B. (1992). Whole-cell recording of calcium channel currents. *Methods Enzymol*, **207**, 181–93.

Bekkers, J. & Stevens, C. (1996). Cable properties of cultured hippocampal neurons determined from sucrose-evoked miniature EPSCs. *J Neurophysiol*, **75**, 1250–5.

Benke, T., Luthi, A., Isaac, J. & Collingridge, G. (1998). Modulation of AMPA receptor unitary conductance by synaptic activity. *Nature*, **393**, 793–7.

Bennett, M. (2001). *The History of the Synapse*. Taylor & Francis.

Berg, H. (1992). *Random Walks in Biology*. Princeton University Press.

Borgdorff, A. & Choquet, D. (2002). Regulation of AMPA receptor lateral movements. *Nature*, **417**, 649–53.

Bowie, D. & Mayer, M. (1995). Inward rectification of both AMPA and kainate subtype glutamate receptors generated by polyamine-mediated ion channel block. *Neuron*, **15**, 453–62.

Boyce, W. & DiPrima, R. (2000). *Elementary Differential Equations and Boundary Value Problems*. John Wiley and Sons (WIE).

Brasnjo, G. & Otis, T. (2001). Neuronal glutamate transporters control activation of postsynaptic metabotropic glutamate receptors and influence cerebellar long-term depression. *Neuron*, **31**, 607–16.

Brasnjo, G. & Otis, T. (2004). Isolation of glutamate transport-coupled charge flux and estimation of glutamate uptake at the climbing fiber-Purkinje cell synapse. *Proc Natl Acad Sci U S A*, **101**, 6273–8.

Burger, P., Mehl, E., Cameron, P., Maycox, P., Baumert, M., Lottspeich, F., De Camilli, P. & Jahn, R. (1989). Synaptic vesicles immunoisolated from rat cerebral cortex contain high levels of glutamate. *Neuron*, **3**, 715–20.

Canepari, M., Nelson, L., Papageorgiou, G., Corrie, J. & Ogden, D. (2001). Photochemical and pharmacological evaluation of 7-nitroindolinyl-and 4-methoxy-7-nitroindolinyl-amino acids as novel, fast caged neurotransmitters. *J Neurosci Methods*, **112**, 29–42.

Carpenedo, R., Pittaluga, A., Cozzi, A., Attucci, S., Galli, A., Raiteri, M. & Moroni,

F. (2001). Presynaptic kynurenate-sensitive receptors inhibit glutamate release. *Eur J Neurosci*, **13**, 2141–7.

Carter, A.G. & Regehr, W.G. (2000). Prolonged synaptic currents and glutamate spillover at the parallel fiber to stellate cell synapse E. *J Neurosci*, **20**, 4423–34.

Casado, M., Dieudonne, S. & Ascher, P. (2000). Presynaptic N-methyl-D-aspartate receptors at the parallel fiber-Purkinje cell synapse. *Proc Natl Acad Sci U S A*, **97**, 11593–7.

Cathala, L., Brickley, S., Cull-Candy, S. & Farrant, M. (2003). Maturation of EPSCs and intrinsic membrane properties enhances precision at a cerebellar synapse. *J Neurosci*, **23**, 6074–85.

Ceccarelli, B., Hurlbut, W. & Mauro, A. (1973). Turnover of transmitter and synaptic vesicles at the frog neuromuscular junction. *J Cell Biol*, **57**, 499–524.

Chaudhry, F., Lehre, K., van Lookeren Campagne, M., Ottersen, O., Danbolt, N. & Storm-Mathisen, J. (1995). Glutamate transporters in glial plasma membranes: highly differentiated localizations revealed by quantitative ultrastructural immunocytochemistry. *Neuron*, **15**, 711–20.

Choi, S., Klingauf, J. & Tsien, R.W. (2000). Postfusional regulation of cleft glutamate concentration during LTP at 'silent synapses'. *Nat Neurosci*, **3**, 330–6.

Chow, R.H., Klingauf, J. & Neher, E. (1994). Time course of ca2+ concentration triggering exocytosis in neuroendocrine cells. *Proceedings of the National Academy of Sciences of the United States of America*, **91**, 12765–9, article - journal article.

Clements, J., Feltz, A., Sahara, Y. & Westbrook, G. (1998). Activation kinetics of

AMPA receptor channels reveal the number of functional agonist binding sites. *J Neurosci*, **18**, 119–27.

Clements, J.D. (1996). Transmitter timecourse in the synaptic cleft: its role in central synaptic function. *Trends Neurosci*, **19**, 163–71.

Colquhoun, D. & Hawkes, A. (1982). On the stochastic properties of bursts of single ion channel openings and of clusters of bursts.&id. *Philos Trans R Soc Lond B Biol Sci*, **300**, 1–59.

Colquhoun, D. & Hawkes, A.G. (1995). The Principles of the Stochastic Interpretation of Ion-Channel Mechanisms. In B. Sakmann & E.e. Neher, eds., *Single channel recording*, Plenum Press, New York, 2nd edn.

Colquhoun, D., Jonas, P. & Sakmann, B. (1992). Action of brief pulses of glutamate on ampa/kainate receptors in patches from different neurones of rat hippocampal slices. *J Physiol*, **458**, 261–87.

Conn, P.J. & Pin, J.P. (1997). Pharmacology and functions of metabotropic glutamate receptors. *Annu Rev Pharmacol Toxicol*, **37**, 205–37, using Smart Source Parsing.

Connors, B. & Long, M. (2004). Electrical synapses in the mammalian brain. *Annu Rev Neurosci*, **27**, 393–418.

Crank, J. (1975). *The mathematics of diffusion*. Clarendon Press, Oxford, UK, 2nd edn., by J. Crank. Oxford science publications Includes indexes. Bibliography: p. [399]-406.

Dale, H.H. & Dudley, H. (1929). The presence of histamine and acetylcholine in the spleen of the ox and horse. *J Physiol (Lond)*, **68**, 97.

D'Angelo, E., Rossi, P., Armano, S. & Taglietti, V. (1999). Evidence for NMDA and mGlu receptor-dependent long-term potentiation of mossy fiber-granule cell transmission in rat cerebellum. *J Neurophysiol*, **81**, 277–87.

De Robertis, E.D.P. & Bennett, H.S. (1954). Submicroscopic vesicular component in the synapse. *Federation Proceedings*, **13**, 35.

Del Castillo, J. & Katz, B. (1954). Quantal components of the end-plate potential. *J Physiol*, **124**, 560–73.

Del Castillo, J. & Katz, B. (1956). Biophysical aspects of neuromuscular transmission. *Progress in Biophysics and Biophysical Chemistry*, **6**, 121–70.

Del Castillo, J. & Katz, B. (1957). Interaction at end-plate receptors between different choline derivatives. *Proc R Soc Lond B Biol Sci*, **146**, 369–81.

Delaney, A. & Jahr, C. (2002). Kainate receptors differentially regulate release at two parallel fiber synapses. *Neuron*, **36**, 475–82.

Derkach, V., Barria, A. & Soderling, T. (1999). Ca2+/calmodulin-kinase II enhances channel conductance of alpha-amino-3-hydroxy-5-methyl-4-isoxazolepropionate type glutamate receptors. *Proc Natl Acad Sci U S A*, **96**, 3269–74.

Dev, K., Nishimune, A., Henley, J. & Nakanishi, S. (1999). The protein kinase C alpha binding protein PICK1 interacts with short but not long form alternative splice variants of AMPA receptor subunits. *Neuropharmacology*, **38**, 635–44.

Diamond, J.S. (2001). Neuronal glutamate transporters limit activation of NMDA receptors by neurotransmitter spillover on CA1 pyramidal cells. *J Neurosci*, **21**, 8328–38.

Diamond, J.S. & Jahr, C.E. (1995). Asynchronous release of synaptic vesicles determines the time course of the AMPA receptor-mediated EPSC. *Neuron*, **15**, 1097–107.

Diamond, J.S. & Jahr, C.E. (1997). Transporters buffer synaptically released glutamate on a submillisecond time scale. *J Neurosci*, **17**, 4672–87.

DiGregorio, D.A., Nusser, Z. & Silver, R.A. (2002). Spillover of glutamate onto synaptic AMPA receptors enhances fast transmission at a cerebellar synapse. *Neuron*, **35**, 521–533.

Dingledine, R., Borges, K., Bowie, D. & Traynelis, S. (1999). The glutamate receptor ion channels. *Pharmacol Rev*, **51**, 7–61.

Dittman, J.S., Kreitzer, A.C. & Regehr, W.G. (2000). Interplay between facilitation, depression, and residual calcium at three presynaptic terminals. *J Neurosci*, **20**, 1374–85.

Dobrunz, L. & Stevens, C. (1997). Heterogeneity of release probability, facilitation, and depletion at central synapses. *Neuron*, **18**, 995–1008.

Dodge, F., Jr & Rahamimoff, R. (1967). Co-operative action a calcium ions in transmitter release at the neuromuscular junction. *J Physiol*, **193**, 419–32.

Eccles, J. & Jaeger, J. (1958). The relationship between the mode of operation and the dimensions of the junctional regions at synapses and motor end-organs. *Proc R Soc Lond B Biol Sci*, **148**, 38–56.

Ellis, R. (2001). Macromolecular crowding: obvious but underappreciated. *Trends Biochem Sci*, **26**, 597–604.

Emptage, N., Reid, C. & Fine, A. (2001). Calcium stores in hippocampal synaptic

boutons mediate short-term plasticity, store-operated Ca2+ entry, and spontaneous transmitter release. *Neuron*, **29**, 197–208.

Erecinska, M. & Silver, I. (1990). Metabolism and role of glutamate in mammalian brain. *Prog Neurobiol*, **35**, 245–96.

Faber, D., Funch, P. & Korn, H. (1985). Evidence that receptors mediating central synaptic potentials extend beyond the postsynaptic density. *Proc Natl Acad Sci U S A*, **82**, 3504–8.

Fagg, G. & Lane, J. (1979). The uptake and release of putative amino acid neurotransmitters. *Neuroscience*, **4**, 1015–36.

Fatt, P. & Katz, B. (1952). Spontaneous subthreshold activity at motor nerve endings. *J Physiol*, **117**, 109–28.

Finkel, A.S. & Redman, S.J. (1983). The synaptic current evoked in cat spinal motoneurones by impulses in single group 1a axons. *J Physiol*, **342**, 615–32.

Forsythe, I. & Westbrook, G. (1988). Slow excitatory postsynaptic currents mediated by N-methyl-D-aspartate receptors on cultured mouse central neurones. *J Physiol*, **396**, 515–33.

Forsythe, I.D. & Barnes-Davies, M. (1993). The binaural auditory pathway: excitatory amino acid receptors mediate dual timecourse excitatory postsynaptic currents in the rat medial nucleus of the trapezoid body. *Proc R Soc Lond B Biol Sci*, **251**, 151–7.

Forti, L., Bossi, M., Bergamaschi, A., Villa, A. & Malgaroli, A. (1997). Loose-patch recordings of single quanta at individual hippocampal synapses. *Nature*, **388**, 874–8.

Foster, K., Kreitzer, A. & Regehr, W. (2002). Interaction of postsynaptic receptor saturation with presynaptic mechanisms produces a reliable synapse. *Neuron*, **36**, 1115–26.

Fragioudaki, K., Giompres, P., Smith, A., Triarhou, L., Kouvelas, E. & Mitsacos, A. (2002). AMPA receptor subunit RNA transcripts and [(3)H]AMPA binding in the cerebellum of normal and pcd mutant mice: an in situ hybridization study combined with receptor autoradiography. *J Neural Transm*, **109**, 1115–27.

Franke, C., Hatt, H. & Dudel, J. (1987). Liquid filament switch for ultra-fast exchanges of solutions at excised patches of synaptic membrane of crayfish muscle. *Neurosci Lett*, **77**, 199–204.

Franks, K., Bartol, T., Jr & Sejnowski, T. (2002). A Monte Carlo model reveals independent signaling at central glutamatergic synapses. *Biophys J*, **83**, 2333–48.

Franks, K., Stevens, C. & Sejnowski, T. (2003). Independent sources of quantal variability at single glutamatergic synapses. *J Neurosci*, **23**, 3186–95.

Fremeau, R., Jr, Kam, K., Qureshi, T., Johnson, J., Copenhagen, D., Storm-Mathisen, J., Chaudhry, F., Nicoll, R. & Edwards, R. (2004). Vesicular glutamate transporters 1 and 2 target to functionally distinct synaptic release sites.=151. *Science*, **304**, 1815–9.

Fuhrmann, G., Segev, I., Markram, H. & Tsodyks, M. (2002). Coding of temporal information by activity-dependent synapses. *J Neurophysiol*, **87**, 140–8.

Furshpan, E. & Potter, D. (1957). Mechanism of nerve-impulse transmission at a crayfish synapse. *Nature*, **180**, 342–3.

Galarreta, M. & Hestrin, S. (2001). Spike transmission and synchrony detection in networks of GABAergic interneurons. *Science*, **292**, 2295–9.

Gandhi, S.P. & Stevens, C.F. (2003). Three modes of synaptic vesicular recycling revealed by single-vesicle imaging. *Nature*, **423**, 607–13.

Geiger, J., Bischofberger, J., Vida, I., Frobe, U., Pfitzinger, S., Weber, H., Haverkampf, K. & Jonas, P. (2002). Patch-clamp recording in brain slices with improved slicer technology. *Pflugers Arch*, **443**, 491–501.

Geiger, J.R., Melcher, T., Koh, D.S., Sakmann, B., Seeburg, P.H., Jonas, P. & Monyer, H. (1995). Relative abundance of subunit mrnas determines gating and ca2+ permeability of ampa receptors in principal neurons and interneurons in rat cns. *Neuron*, **15**, 193–204, article - journal article.

Geiger, J.R., Lubke, J., Roth, A., Frotscher, M. & Jonas, P. (1997). Submillisecond ampa receptor-mediated signaling at a principal neuron- interneuron synapse. *Neuron*, **18**, 1009–23.

Gras, C., Herzog, E., Bellenchi, G., Bernard, V., Ravassard, P., Pohl, M., Gasnier, B., Giros, B. & El Mestikawy, S. (2002). A third vesicular glutamate transporter expressed by cholinergic and serotoninergic neurons. *J Neurosci*, **22**, 5442–51.

Gulyas, A., Miles, R., Sik, A., Toth, K., Tamamaki, N. & Freund, T. (1993). Hippocampal pyramidal cells excite inhibitory neurons through a single release site. *Nature*, **366**, 683–7.

Hamill, O.P., Marty, A., Neher, E., Sakmann, B. & Sigworth, F.J. (1981). Improved patch-clamp techniques for high-resolution current recording from cells and cell-free membrane patches. *Pflugers Archiv. European Journal of Physiology*, **391**, 85–100, article - journal article.

Hamori, J. & Somogyi, J. (1983). Differentiation of cerebellar mossy fiber synapses in the rat: a quantitative electron microscope study. *J Comp Neurol*, **220**, 365–77.

Harrison, J. & Jahr, C. (2003). Receptor occupancy limits synaptic depression at climbing fiber synapses. *J Neurosci*, **23**, 377–83.

Harsch, A. & Robinson, H. (2000). Postsynaptic variability of firing in rat cortical neurons: the roles of input synchronization and synaptic NMDA receptor conductance. *J Neurosci*, **20**, 6181–92.

Hartzell, H.C., Kuffler, S.W. & Yoshikami, D. (1975). Post-synaptic potentiation: interaction between quanta of acetylcholine at the skeletal neuromuscular synapse. *J Physiol*, **251**, 427–63.

Hashimoto, K., Fukaya, M., Qiao, X., Sakimura, K., Watanabe, M. & Kano, M. (1999). Impairment of AMPA receptor function in cerebellar granule cells of ataxic mutant mouse stargazer. *J Neurosci*, **19**, 6027–36.

Hausser, M. & Roth, A. (1997). Estimating the time course of the excitatory synaptic conductance in neocortical pyramidal cells using a novel voltage jump method. *J Neurosci*, **17**, 7606–25.

Hawkins, L., Chazot, P. & Stephenson, F. (1999). Biochemical evidence for the co-association of three N-methyl-D-aspartate (NMDA) R2 subunits in recombinant NMDA receptors. *J Biol Chem*, **274**, 27211–8.

Hayashi, T. (1952). A physiological study of epileptic seizures following cortical stimulation in animals and its application to human clinics. *Jpn. J. Physiol.*, **3**, 46–64.

Heinemann, S. & Conti, F. (1992). Nonstationary noise analysis and application to patch clamp recordings. *Methods Enzymol*, **207**, 131–48.

Hestrin, S. (1992). Activation and desensitization of glutamate-activated channels mediating fast excitatory synaptic currents in the visual cortex. *Neuron*, **9**, 991–9.

Heuser, J.E. & Reese, T.S. (1973). Evidence for recycling of synaptic vesicle membrane during transmitter release at the frog neuromuscular junction. *J Cell Biol*, **57**, 315–44.

Holmes, W.R. (1995). Modeling the effect of glutamate diffusion and uptake on nmda and non-nmda receptor saturation. *Biophys J*, **69**, 1734–47.

Hrabetova, S. & Nicholson, C. (2004). Contribution of dead-space microdomains to tortuosity of brain extracellular space. *Neurochem Int*, **45**, 467–77.

Isaacson, J. & Walmsley, B. (1995). Counting quanta: direct measurements of transmitter release at a central synapse. *Neuron*, **15**, 875–84.

Isaacson, J.S. (1999). Glutamate spillover mediates excitatory transmission in the rat olfactory bulb. *Neuron*, **23**, 377–84.

Ishikawa, T., Sahara, Y. & Takahashi, T. (2002). A single packet of transmitter does not saturate postsynaptic glutamate receptors. *Neuron*, **34**, 613–21.

Ito, M. (1989). Long-term depression. *Annu Rev Neurosci*, **12**, 85–102.

Jahr, C.E. (2003). Drooling and stuttering, or do synapses whisper? *Trends Neurosci*, **26**, 7–9.

Jakab, R. (1989). Three-dimensional reconstruction and synaptic architecture of cerebellar glomeruli in the rat. *Acta Morphol Hung*, **37**, 11–20.

Jakab, R.L. & Hamori, J. (1988). Quantitative morphology and synaptology of cerebellar glomeruli in the rat. *Anat Embryol*, **179**, 81–8, using Smart Source Parsing.

Jenkinson, D. (1957). The nature of the antagonism between calcium and magnesium ions at the neuromuscular junction. *J Physiol*, **138**, 434–44.

Johnston, D., Miao-Si, S. & Gray, R. (1994). *Foundations of Cellular Neurophysiology*. The MIT Press.

Jonas, P. & Sakmann, B. (1992). Glutamate receptor channels in isolated patches from CA1 and CA3 pyramidal cells of rat hippocampal slices. *J Physiol*, **455**, 143–71.

Jonas, P. & Spruston, N. (1994). Mechanisms shaping glutamate-mediated excitatory postsynaptic currents in the CNS. *Curr Opin Neurobiol*, **4**, 366–72.

Jonas, P., Major, G. & Sakmann, B. (1993). Quantal components of unitary epscs at the mossy fibre synapse on ca3 pyramidal cells of rat hippocampus. *J Physiol*, **472**, 615–63.

Jonas, P., Racca, C., Sakmann, B., Seeburg, P.H. & Monyer, H. (1994). Differences in ca2+ permeability of ampa-type glutamate receptor channels in neocortical neurons caused by differential glur-b subunit expression. *Neuron*, **12**, 1281–9, article - journal article.

Kamboj, S., Swanson, G. & Cull-Candy, S. (1995). Intracellular spermine confers rectification on rat calcium-permeable AMPA and kainate receptors. *J Physiol*, **486 (Pt 2)**, 297–303.

Katz, B. (1969). *The release of neural transmitter substances*. Liverpool University Press, Liverpool.

Katz, B. & Miledi, R. (1967). The timing of calcium action during neuromuscular transmission. *J Physiol*, **189**, 535–44.

Katz, B. & Miledi, R. (1972). The statistical nature of the acetycholine potential and its molecular components. *J Physiol (Lond)*, **224**, 665–99.

Katz, B. & Thesleff, S. (1957). On the factors which determine the amplitude of the miniature end-plate potential. *J Physiol*, **137**, 267–78.

Kawahara, Y., Ito, K., Sun, H., Aizawa, H., Kanazawa, I. & Kwak, S. (2004). Glutamate receptors: RNA editing and death of motor neurons. *Nature*, **427**, 801.

Kiessling, V., Muller, B. & Fromherz, P. (2000). Extracellular resistance in cell adhesion measured with a transistor probe. *Langmuir*, **16**, 3517–3521.

Kinney, G. & Slater, N. (1992). Potentiation of mossy fiber-evoked EPSPs in turtle cerebellar Purkinje cells by the metabotropic glutamate receptor agonist 1S,3R-ACPD. *J Neurophysiol*, **67**, 1006–8.

Kirischuk, S., Voitenko, N., Kostyuk, P. & Verkhratsky, A. (1996). Calcium signalling in granule neurones studied in cerebellar slices. *Cell Calcium*, **19**, 59–71.

Kiskin, N. & Ogden, D. (2002). Two-photon excitation and photolysis by pulsed laser illumination modelled by spatially non-uniform reactions with simultaneous diffusion. *Eur Biophys J*, **30**, 571–87.

Kiskin, N., Chillingworth, R., McCray, J., Piston, D. & Ogden, D. (2002). The efficiency of two-photon photolysis of a "caged" fluorophore, o-1-(2-nitrophenyl)ethylpyranine, in relation to photodamage of synaptic terminals. *Eur Biophys J*, **30**, 588–604.

Klyachko, V.A. & Jackson, M.B. (2002). Capacitance steps and fusion pores of small and large-dense-core vesicles in nerve terminals. *Nature*, **418**, 89–92.

Koch, C. (1998). *Biophysics of Computation: Information Processing in Single Neurons.* . Oxford University Press Inc, USA.

Koike, M., Tsukada, S., Tsuzuki, K., Kijima, H. & Ozawa, S. (2000). Regulation of kinetic properties of GluR2 AMPA receptor channels by alternative splicing. *J Neurosci*, **20**, 2166–74.

Kolleker, A., Zhu, J., Schupp, B., Qin, Y., Mack, V., Borchardt, T., Kohr, G., Malinow, R., Seeburg, P. & Osten, P. (2003). Glutamatergic plasticity by synaptic delivery of GluR-B(long)-containing AMPA receptors. *Neuron*, **40**, 1199–212.

Korn, H., Triller, A., Mallet, A. & Faber, D.S. (1981). Fluctuating responses at a central synapse: n of binomial fit predicts number of stained presynaptic boutons. *Science*, **213**, 898–901.

Krampfl, K., Schlesinger, F., Zorner, A., Kappler, M., Dengler, R. & Bufler, J. (2002). Control of kinetic properties of GluR2 flop AMPA-type channels: impact of R/G nuclear editing. *Eur J Neurosci*, **15**, 51–62.

Kuffler, S., Nicholls, J. & Martin, A. (1984). *From Neuron to Brain: Cellular Approach to the Function of the Nervous System*. Sinauer Associates (Sunderland, MA), 2nd edn.

Kullmann, D.M., Erdemli, G. & Asztely, F. (1996). LTP of AMPA and NMDA receptor-mediated signals: evidence for presynaptic expression and extrasynaptic glutamate spill-over. *Neuron*, **17**, 461–74.

Kume-Kick, J., Mazel, T., Vorisek, I., Hrabetova, S., Tao, L. & Nicholson, C. (2002). Independence of extracellular tortuosity and volume fraction during osmotic challenge in rat neocortex. *J Physiol*, **542**, 515–27.

Kuno, M. (1994). *The Synapse: Function, Plasticity and Neurotrophism*. Oxford University Press.

Kyagova, A., Korkina, L., Snigireva, T., Lysenko, E., Tomashaeva, S. & Potapenko AYa (1991). Psoralen-photosensitized damage of rat peritoneal exudate cells. *Photochem Photobiol*, **53**, 633–7.

Larkman, A., Stratford, K. & Jack, J. (1991). Quantal analysis of excitatory synaptic action and depression in hippocampal slices. *Nature*, **350**, 344–7.

Laube, B., Kuhse, J. & Betz, H. (1998). Evidence for a tetrameric structure of recombinant NMDA receptors. *J Neurosci*, **18**, 2954–61.

Lee, C., Bardoni, R., Tong, C., Engelman, H., Joseph, D., Magherini, P. & MacDermott, A. (2002). Functional expression of AMPA receptors on central terminals of rat dorsal root ganglion neurons and presynaptic inhibition of glutamate release. *Neuron*, **35**, 135–46.

Lerma, J. (2003). Roles and rules of kainate receptors in synaptic transmission. *Nat Rev Neurosci*, **4**, 481–95.

Lester, R., Clements, J., Westbrook, G. & Jahr, C. (1990). Channel kinetics determine the time course of NMDA receptor-mediated synaptic currents. *Nature*, **346**, 565–7.

Liu, G., Choi, S. & Tsien, R. (1999). Variability of neurotransmitter concentration and nonsaturation of postsynaptic AMPA receptors at synapses in hippocampal cultures and slices. *Neuron*, **22**, 395–409.

Llinas, R., Blinks, J. & Nicholson, C. (1972). Calcium transient in presynaptic terminal of squid giant synapse: detection with aequorin. *Science*, **176**, 1127–9.

Logan, W. & Snyder, S. (1971). Unique high affinity uptake systems for glycine, glutamic and aspartic acids in central nervous tissue of the rat. *Nature*, **234**, 297–9.

Lomeli, H., Mosbacher, J., Melcher, T., Hoger, T., Geiger, J., Kuner, T., Monyer, H., Higuchi, M., Bach, A. & Seeburg, P. (1994). Control of kinetic properties of AMPA receptor channels by nuclear RNA editing. *Science*, **266**, 1709–13.

Longsworth, L.G. (1953). Diffusion measurements at 25° of aqueous solutions of amino acids, peptides and sugars. *J Am Chem Soc*, **75**, 5705–5709.

Lucas, D. & Newhouse, J. (1957). The toxic effect of sodium L-glutamate on the inner layers of the retina. *AMA Arch Ophthalmol*, **58**, 193–201.

Macek, T., Winder, D., Gereau, R., 4th, Ladd, C. & Conn, P. (1996). Differential involvement of group II and group III mGluRs as autoreceptors at lateral and medial perforant path synapses. *J Neurophysiol*, **76**, 3798–806.

Maex, R. & De Schutter, E. (1998). Synchronization of golgi and granule cell firing in a detailed network model of the cerebellar granule cell layer. *J Neurophysiol*, **80**, 2521–37.

Magleby, K. (1987). Short-Term Changes in Synaptic Efficacy. In G. Edelman, W.E. Gall & W.M. Cowan, eds., *Synaptic Function*, 21–56, John Wiley & Sons Inc.

Magleby, K. & Stevens, C. (1972). A quantitative description of end-plate currents. *J Physiol*, **223**, 173–97.

Mano, I. & Teichberg, V. (1998). A tetrameric subunit stoichiometry for a glutamate receptor-channel complex. *Neuroreport*, **9**, 327–31.

Marcaggi, P., Billups, D. & Attwell, D. (2003). The role of glial glutamate transporters in maintaining the independent operation of juvenile mouse cerebellar parallel fibre synapses. *J Physiol*, **552**, 89–107.

Marchand, P. & Marmet, L. (1983). Binomial smoothing filter: A way to avoid some pitfalls of least-squares polynomial smoothing. *Rev. Sci. Instrum.*, **54**, 1034.

Mardis, K. & Sibert, E. (1998). The Effectiveness of Newton's Method for Improving Ab Initio Force Fields with Applications to CO2 and H2CO. *J Mol Spectrosc*, **187**, 167–78.

Matsui, K. & Jahr, C. (2003). Ectopic release of synaptic vesicles. *Neuron*, **40**, 1173–83.

Matsuzaki, M., Ellis-Davies, G., Nemoto, T., Miyashita, Y., Iino, M. & Kasai, H. (2001). Dendritic spine geometry is critical for AMPA receptor expression in hippocampal CA1 pyramidal neurons. *Nat Neurosci*, **4**, 1086–92.

McAllister, A.K. & Stevens, C.F. (2000). Nonsaturation of AMPA and NMDA receptors at hippocampal synapses. *Proc Natl Acad Sci U S A*, **97**, 6173–8.

Mennerick, S. & Zorumski, C.F. (1995). Presynaptic influence on the time course of fast excitatory synaptic currents in cultured hippocampal cells. *J Neurosci*, **15**, 3178–92.

Miledi, R. (1973). Transmitter release induced by injection of calcium ions into nerve terminals. *Proc R Soc Lond B Biol Sci*, **183**, 421–5.

Min, M.Y., Rusakov, D.A. & Kullmann, D.M. (1998). Activation of ampa, kainate, and metabotropic receptors at hippocampal mossy fiber synapses: role of glutamate diffusion. *Neuron*, **21**, 561–70.

Mitchell, S.J. & Silver, R.A. (2000a). Gaba spillover from single inhibitory axons suppresses low-frequency excitatory transmission at the cerebellar glomerulus. *J Neurosci*, **20**, 8651–8658.

Mitchell, S.J. & Silver, R.A. (2000b). Glutamate spillover suppresses inhibition by activating presynaptic mglurs. *Nature*, **404**, 498–502.

Mitchell, S.J. & Silver, R.A. (2003). Shunting inhibition modulates neuronal gain during synaptic excitation. *Neuron*, **38**, 433–445.

Miyazaki, T., Fukaya, M., Shimizu, H. & Watanabe, M. (2003). Subtype switching of vesicular glutamate transporters at parallel fibre-Purkinje cell synapses in developing mouse cerebellum. *Eur J Neurosci*, **17**, 2563–72.

Momiyama, A., Silver, R., Hausser, M., Notomi, T., Wu, Y., Shigemoto, R. & Cull-Candy, S. (2003). The density of AMPA receptors activated by a transmitter quantum at the climbing fibre-Purkinje cell synapse in immature rats. *J Physiol*, **549**, 75–92.

More, J., Troop, H., Dolman, N. & Jane, D. (2003). Structural requirements for novel willardiine derivatives acting as AMPA and kainate receptor antagonists. *Br J Pharmacol*, **138**, 1093–100.

Morrison, J., Wan, P., Corrie, J. & Papageorgiou, G. (2002). Mechanisms of photorelease of carboxylic acids from 1-acyl-7-nitroindolines in solutions of varying water content. *Photochem Photobiol Sci*, **1**, 960–9.

Mosbacher, J., Schoepfer, R., Monyer, H., Burnashev, N., Seeburg, P.H. & Ruppersberg, J.P. (1994). A molecular determinant for submillisecond desensitization in glutamate receptors. *Science*, **266**, 1059–62.

Neher, E. (1992). Correction for liquid junction potentials in patch clamp experiments. *Methods Enzymol*, **207**, 123–31.

Neher, E. & Sakaba, T. (2001). Combining deconvolution and noise analysis for the estimation of transmitter release rates at the calyx of held. *J Neurosci*, **21**, 444–61.

Neher, E. & Sakmann, B. (1976). Single-channel currents recorded from membrane of denervated frog muscle fibres. *Nature*, **260**, 799–802.

Nicholson, C. & Sykova, E. (1998). Extracellular space structure revealed by diffusion analysis. *Trends Neurosci*, **21**, 207–15.

Nicholson, C. & Tao, L. (1993). Hindered diffusion of high molecular weight compounds in brain extracellular microenvironment measured with integrative optical imaging. *Biophys J*, **65**, 2277–90.

Nielsen, T., DiGregorio, D. & Silver, R. (2004). Modulation of glutamate mobility reveals the mechanism underlying slow-rising AMPAR EPSCs and the diffusion coefficient in the synaptic cleft. *Neuron*, **42**, 757–71.

Nowak, L., Bregestovski, P., Ascher, P., Herbet, A. & Prochiantz, A. (1984). Magnesium gates glutamate-activated channels in mouse central neurones. *Nature*, **307**, 462–5.

Nusser, Z. (2000). AMPA and NMDA receptors: similarities and differences in their synaptic distribution. *Curr Opin Neurobiol*, **10**, 337–41.

Nusser, Z., Lujan, R., Laube, G., Roberts, J.D., Molnar, E. & Somogyi, P. (1998). Cell type and pathway dependence of synaptic AMPA receptor number and variability in the hippocampus. *Neuron*, **21**, 545–59.

Nutt, S. & Kamboj, R. (1994). RNA editing of human kainate receptor subunits. *Neuroreport*, **5**, 2625–9.

Oertner, T., Sabatini, B., Nimchinsky, E. & Svoboda, K. (2002). Facilitation at single synapses probed with optical quantal analysis. *Nat Neurosci*, **5**, 657–64.

Ohishi, H., Ogawa-Meguro, R., Shigemoto, R., Kaneko, T., Nakanishi, S. & Mizuno, N. (1994). Immunohistochemical localization of metabotropic gluta-

mate receptors, mGluR2 and mGluR3, in rat cerebellar cortex. *Neuron*, **13**, 55–66.

O'Keefe, J. & Recce, M. (1993). Phase relationship between hippocampal place units and the EEG theta rhythm. *Hippocampus*, **3**, 317–30.

Otis, T.S., Wu, Y.C. & Trussell, L.O. (1996). Delayed clearance of transmitter and the role of glutamate transporters at synapses with multiple release sites. *J Neurosci*, **16**, 1634–44.

Overstreet, L., Westbrook, G. & Jones, M. (2002). Measuring and modeling the spatiotemporal profile of GABA at the synapse. In M. Qouick, ed., *Transmembrane Transporters*, 259–275, Wiley-liss Inc., Hoboken, NJ.

Overstreet, L.S., Kinney, G.A., Liu, Y.B., Billups, D. & Slater, N.T. (1999). Glutamate transporters contribute to the time course of synaptic transmission in cerebellar granule cells. *J Neurosci*, **19**, 9663–73.

Palay, S. & Chan-Palay, V. (1974). *Cerebellar cortex: cortex and organization.* Springer-Verlag, Germany.

Parsegian, V., Rand, R. & Rau, D. (1995). Macromolecules and water: probing with osmotic stress. *Methods Enzymol*, **259**, 43–94.

Partin, K., Fleck, M. & Mayer, M. (1996). AMPA receptor flip/flop mutants affecting deactivation, desensitization, and modulation by cyclothiazide, aniracetam, and thiocyanate. *J Neurosci*, **16**, 6634–47.

Perkel, D. & Nicoll, R. (1993). Evidence for all-or-none regulation of neurotransmitter release: implications for long-term potentiation. *J Physiol*, **471**, 481–500.

Perrais, D. & Ropert, N. (2000). Altering the concentration of GABA in the synap-

tic cleft potentiates miniature IPSCs in rat occipital cortex. *Eur J Neurosci*, **12**, 400–4.

Pettit, D., Wang, S., Gee, K. & Augustine, G. (1997). Chemical two-photon uncaging: a novel approach to mapping glutamate receptors. *Neuron*, **19**, 465–71.

Piet, R., Vargova, L., Sykova, E., Poulain, D. & Oliet, S. (2004). Physiological contribution of the astrocytic environment of neurons to intersynaptic crosstalk. *Proc Natl Acad Sci U S A*, **101**, 2151–5.

Press, W., Flannery, B., Teukolsky, S. & Vetterling, W. (1993). *Numerical Recipes in C: The Art of Scientific Computing*. Cambridge University Press.

Raman, I. & Trussell, L. (1992). The kinetics of the response to glutamate and kainate in neurons of the avian cochlear nucleus. *Neuron*, **9**, 173–86.

Raman, I. & Trussell, L. (1995). The mechanism of alpha-amino-3-hydroxy-5-methyl-4-isoxazolepropionate receptor desensitization after removal of glutamate. *Biophys J*, **68**, 137–46.

Raman, I., Zhang, S. & Trussell, L. (1994). Pathway-specific variants of AMPA receptors and their contribution to neuronal signaling. *J Neurosci*, **14**, 4998–5010.

Ravindranathan, A., Donevan, S., Sugden, S., Greig, A., Rao, M. & Parks, T. (2000). Contrasting molecular composition and channel properties of AMPA receptors on chick auditory and brainstem motor neurons. *J Physiol*, **523 Pt 3**, 667–84.

Renger, J.J., Egles, C. & Liu, G. (2001). A developmental switch in neurotrans-

mitter flux enhances synaptic efficacy by affecting AMPA receptor activation. *Neuron*, **29**, 469–84.

Rice, M., Okada, Y. & Nicholson, C. (1993). Anisotropic and heterogeneous diffusion in the turtle cerebellum: implications for volume transmission. *J Neurophysiol*, **70**, 2035–44.

Riveros, N., Fiedler, J., Lagos, N., Munoz, C. & Orrego, F. (1986). Glutamate in rat brain cortex synaptic vesicles: influence of the vesicle isolation procedure. *Brain Res*, **386**, 405–8.

Robbins, J. (1959). The excitation and inhibition of crustacean muscle by amino acids. *J. Physiol.*, **148**, 39–50.

Robert, A. & Howe, J. (2003). How AMPA receptor desensitization depends on receptor occupancy. *J Neurosci*, **23**, 847–58.

Robinson, H., Sahara, Y. & Kawai, N. (1991). Nonstationary fluctuation analysis and direct resolution of single channel currents at postsynaptic sites. *Biophys J*, **59**, 295–304.

Rosenmund, C., Stern-Bach, Y. & Stevens, C. (1998). The tetrameric structure of a glutamate receptor channel. *Science*, **280**, 1596–9.

Rossi, D., Oshima, T. & Attwell, D. (2000). Glutamate release in severe brain ischaemia is mainly by reversed uptake. *Nature*, **403**, 316–21.

Rossi, D.J. & Hamann, M. (1998). Spillover-mediated transmission at inhibitory synapses promoted by high affinity alpha6 subunit gaba(a) receptors and glomerular geometry [published erratum appears in neuron 1998 jul;21(1):527]. *Neuron*, **20**, 783–95.

Rusakov, D. & Fine, A. (2003). Extracellular Ca2+ depletion contributes to fast activity-dependent modulation of synaptic transmission in the brain. *Neuron*, **37**, 287–97.

Rusakov, D.A. (2001). The role of perisynaptic glial sheaths in glutamate spillover and extracellular ca2+ depletion. *Biophys J*, **81**, 1947–59.

Rusakov, D.A. & Kullmann, D.M. (1998a). Extrasynaptic glutamate diffusion in the hippocampus: ultrastructural constraints, uptake, and receptor activation. *J Neurosci*, **18**, 3158–70.

Rusakov, D.A. & Kullmann, D.M. (1998b). Geometric and viscous components of the tortuosity of the extracellular space in the brain. *Proc Natl Acad Sci U S A*, **95**, 8975–80.

Sakmann, B. & Stuart, G. (1995). Patch-Pipette Recordings from the Aoma, Dendrites and Axon of Neurons in Brain Slices. In B. Sakmann & E.e. Neher, eds., *Single channel recording*, Plenum Press, New York, 2nd edn.

Sargent, P., Saviane, C., DiGregorio, D., Nielsen, T. & Silver, R. (in preparation). Determinants of synaptic variability at the cerebellar mossy fibre to granule cell synapse.

Scanziani, M., Salin, P., Vogt, K., Malenka, R. & Nicoll, R. (1997). Use-dependent increases in glutamate concentration activate presynaptic metabotropic glutamate receptors. *Nature*, **385**, 630–4.

Schikorski, T. & Stevens, C. (1997). Quantitative ultrastructural analysis of hippocampal excitatory synapses. *J Neurosci*, **17**, 5858–67.

Schoppa, N.E. & Westbrook, G.L. (2001). Glomerulus-specific synchronization of mitral cells in the olfactory bulb. *Neuron*, **31**, 639–51.

Schorge, S. & Colquhoun, D. (2003). Studies of NMDA receptor function and stoichiometry with truncated and tandem subunits. *J Neurosci*, **23**, 1151–8.

Seeburg, P. (1996). The role of RNA editing in controlling glutamate receptor channel properties. *J Neurochem*, **66**, 1–5.

Semyanov, A. & Kullmann, D.M. (2000). Modulation of gabaergic signaling among interneurons by metabotropic glutamate receptors. *Neuron*, **25**, 663–72.

Shepherd, G.M. (2004). *The Synaptic Organization of the Brain*. Oxford University Press Inc, USA.

Shi, S., Hayashi, Y., Esteban, J. & Malinow, R. (2001). Subunit-specific rules governing AMPA receptor trafficking to synapses in hippocampal pyramidal neurons. *Cell*, **105**, 331–43.

Shigeri, Y., Seal, R. & Shimamoto, K. (2004). Molecular pharmacology of glutamate transporters, EAATs and VGLUTs. *Brain Res Brain Res Rev*, **45**, 250–65.

Sigworth, F.J. (1980). The variance of sodium current fluctuations at the node of ranvier. *Journal of Physiology*, **307**, 97–129, article - journal article.

Silver, R. (2003). Estimation of nonuniform quantal parameters with multiple-probability fluctuation analysis: theory, application and limitations. *J Neurosci Methods*, **130**, 127–41.

Silver, R., Colquhoun, D., Cull-Candy, S. & Edmonds, B. (1996a). Deactivation and desensitization of non-NMDA receptors in patches and the time course of EPSCs in rat cerebellar granule cells. *J Physiol*, **493 (Pt 1)**, 167–73.

Silver, R., Farrant, M. & Cull-Candy, S. (1996b). Filtering of synaptic currents estimated from the timecourse of nmda channel opening at the rat cerebellar mossy fibre-granule cell synapse. *Journal of Physiology*, **494.P**, 85–86.

Silver, R., Lubke, J., Sakmann, B. & Feldmeyer, D. (2003). High-probability uniquantal transmission at excitatory synapses in barrel cortex. *Science*, **302**, 1981–4.

Silver, R.A., Traynelis, S.F. & Cull-Candy, S.G. (1992). Rapid-time-course miniature and evoked excitatory currents at cerebellar synapses in situ. *Nature*, **355**, 163–6.

Silver, R.A., Cull-Candy, S.G. & Takahashi, T. (1996c). Non-nmda glutamate receptor occupancy and open probability at a rat cerebellar synapse with single and multiple release sites. *J Physiol (Lond)*, **494**, 231–50.

Silver, R.A., Momiyama, A. & Cull-Candy, S.G. (1998). Locus of frequency-dependent depression identified with multiple- probability fluctuation analysis at rat climbing fibre-purkinje cell synapses. *J Physiol (Lond)*, **510**, 881–902.

Singer, W. (1999). Neuronal synchrony: a versatile code for the definition of relations? *Neuron*, **24**, 49–65, 111–25.

Smith, M., Ellis-Davies, G. & Magee, J. (2003). Mechanism of the distance-dependent scaling of Schaffer collateral synapses in rat CA1 pyramidal neurons. *J Physiol*, **548**, 245–58.

Smith, T. & Howe, J. (2000). Concentration-dependent substate behavior of native AMPA receptors. *Nat Neurosci*, **3**, 992–7.

Smith, T., Wang, L. & Howe, J. (2000). Heterogeneous conductance levels of native AMPA receptors. *J Neurosci*, **20**, 2073–85.

Sola, E., Prestori, F., Rossi, P., Taglietti, V. & D'Angelo, E. (2004). Increased neurotransmitter release during long-term potentiation at mossy fibre-granule cell synapses in rat cerebellum. *J Physiol*, **557**, 843–61.

Staal, R., Mosharov, E. & Sulzer, D. (2004). Dopamine neurons release transmitter via a flickering fusion pore. *Nat Neurosci*, **7**, 341–6.

Stiles, J.R., Van Helden, D., Bartol, J., T. M., Salpeter, E.E. & Salpeter, M.M. (1996). Miniature endplate current rise times less than 100 microseconds from improved dual recordings can be modeled with passive acetylcholine diffusion from a synaptic vesicle. *Proc Natl Acad Sci U S A*, **93**, 5747–52.

Sykova, E. (2001). Glial diffusion barriers during aging and pathological states. *Prog Brain Res*, **132**, 339–63.

Takahashi, M., Kovalchuk, Y. & Attwell, D. (1995). Pre- and postsynaptic determinants of epsc waveform at cerebellar climbing fiber and parallel fiber to purkinje cell synapses. *J Neurosci*, **15**, 5693–702.

Tomiyama, M., Palacios, J., Cortes, R. & Mengod, G. (1999). Flip and flop variants of AMPA receptor subunits in the human cerebellum: implication for the selective vulnerability of Purkinje cells. *Synapse*, **31**, 163–7.

Tong, G. & Jahr, C.E. (1994). Multivesicular release from excitatory synapses of cultured hippocampal neurons. *Neuron*, **12**, 51–9.

Torri-Tarelli, F., Grohovaz, F., Fesce, R. & Ceccarelli, B. (1985). Temporal coincidence between synaptic vesicle fusion and quantal secretion of acetylcholine. *J Cell Biol*, **101**, 1386–99.

Traynelis, S. (1998). Software-based correction of single compartment series resistance errors. *J Neurosci Methods*, **86**, 25–34.

Trommershauser, J., Marienhagen, J. & Zippelius, A. (1999). Stochastic model of central synapses: slow diffusion of transmitter interacting with spatially distributed receptors and transporters. *J Theor Biol*, **198**, 101–20.

Trussell, L., Zhang, S. & Raman, I. (1993). Desensitization of AMPA receptors upon multiquantal neurotransmitter release. *Neuron*, **10**, 1185–96.

Tsodyks, M.V. & Markram, H. (1997). The neural code between neocortical pyramidal neurons depends on neurotransmitter release probability [published erratum appears in proc natl acad sci u s a 1997 may 13;94(10):5495]. *Proc Natl Acad Sci U S A*, **94**, 719–23.

Urban, N. & Sakmann, B. (2002). Reciprocal intraglomerular excitation and intra- and interglomerular lateral inhibition between mouse olfactory bulb mitral cells. *J Physiol*, **542**, 355–67.

van Harreveld, A. & Mendelson, M. (1959). Glutamate-induced contractions in crustacean muscle. *J Cell Comp Physiol.*, **54**, 85–94.

Vanier, M. & Bower, J. (1999). A comparative survey of automated parameter-search methods for compartmental neural models. *J Comput Neurosci*, **7**, 149–71.

Vignes, M. & Collingridge, G. (1997). The synaptic activation of kainate receptors. *Nature*, **388**, 179–82.

von Gersdorff, H., Schneggenburger, R., Weis, S. & Neher, E. (1997). Presynaptic depression at a calyx synapse: the small contribution of metabotropic glutamate receptors. *J Neurosci*, **17**, 8137–46.

Wadiche, J. & Kavanaugh, M. (1998). Macroscopic and microscopic properties of a cloned glutamate transporter/chloride channel. *J Neurosci*, **18**, 7650–61.

Wadiche, J.I. & Jahr, C.E. (2001). Multivesicular release at climbing fiber-purkinje cell synapses. *Neuron*, **32**, 301–13.

Wahl, L., Pouzat, C. & Stratford, K. (1996). Monte Carlo simulation of fast excita-

tory synaptic transmission at a hippocampal synapse. *J Neurophysiol*, **75**, 597–608.

Wall, M., Robert, A., Howe, J. & Usowicz, M. (2002). The speeding of EPSC kinetics during maturation of a central synapse. *Eur J Neurosci*, **15**, 785–97.

Wall, M.J. & Usowicz, M.M. (1998). Development of the quantal properties of evoked and spontaneous synaptic currents at a brain synapse. *Nat Neurosci*, **1**, 675–82.

Wang, C., Lu, J., Bai, J., Chang, P., Martin, T., Chapman, E. & Jackson, M. (2003). Different domains of synaptotagmin control the choice between kiss-and-run and full fusion. *Nature*, **424**, 943–7.

Watanabe, T., Ohtsuka, A., Murase, N., Barth, P. & Gersonde, K. (1996). NMR studies on water and polymer diffusion in dextran gels. Influence of potassium ions on microstructure formation and gelation mechanism. *Magn Reson Med*, **35**, 697–705.

Watkins, J. & Evans, R. (1981). Excitatory amino acid transmitters. *Annu Rev Pharmacol Toxicol*, **21**, 165–204.

Weiss, J. (1997). The Hill equation revisited: uses and misuses. *FASEB J*, **11**, 835–41.

Weiss, T. (1996). *Cellular Biophysics: Transport v. 1*. The MIT Press.

White, A., Kylanpaa, R., Christie, L., McIntosh, S., Irving, A. & Platt, B. (2003). Presynaptic group I metabotropic glutamate receptors modulate synaptic transmission in the rat superior colliculus via 4-AP sensitive K(+) channels. *Br J Pharmacol*, **140**, 1421–33.

Wilson, T. (1990). *Confocal Microscopy*. Academic Press.

Wojcik, S., Rhee, J., Herzog, E., Sigler, A., Jahn, R., Takamori, S., Brose, N. & Rosenmund, C. (2004). An essential role for vesicular glutamate transporter 1 (VGLUT1) in postnatal development and control of quantal size. *Proc Natl Acad Sci U S A*, **101**, 7158–63.

Wong, A., Graham, B., Billups, B. & Forsythe, I. (2003). Distinguishing between presynaptic and postsynaptic mechanisms of short-term depression during action potential trains. *J Neurosci*, **23**, 4868–77.

Wyllie, D., Traynelis, S. & Cull-Candy, S. (1993). Evidence for more than one type of non-NMDA receptor in outside-out patches from cerebellar granule cells of the rat. *J Physiol*, **463**, 193–226.

Xu-Friedman, M.A. & Regehr, W.G. (2003). Ultrastructural contributions to desensitization at cerebellar mossy fiber to granule cell synapses. *J Neurosci*, **23**, 2182–92.

Zador, A. & Koch, C. (1994). Linearized models of calcium dynamics: formal equivalence to the cable equation. *J Neurosci*, **14**, 4705–15.

Zakharenko, S., Zablow, L. & Siegelbaum, S. (2002). Altered presynaptic vesicle release and cycling during mGluR-dependent LTD. *Neuron*, **35**, 1099–110.

Zenisek, D., Steyer, J.A., Feldman, M.E. & Almers, W. (2002). A membrane marker leaves synaptic vesicles in milliseconds after exocytosis in retinal bipolar cells. *Neuron*, **35**, 1085–97.

Zhou, Q., Petersen, C. & Nicoll, R. (2000). Effects of reduced vesicular filling on synaptic transmission in rat hippocampal neurones. *J Physiol*, **525 Pt 1**, 195–206.

Zhou, Z., Misler, S. & Chow, R.H. (1996). Rapid fluctuations in transmitter release

from single vesicles in bovine adrenal chromaffin cells1 S. *Biophys J*, **70**, 1543–52.

Ziff, E. (1997). Enlightening the postsynaptic density. *Neuron*, **19**, 1163–74.